

Copyright Warning & Restrictions

The copyright law of the United States (Title 17, United States Code) governs the making of photocopies or other reproductions of copyrighted material.

Under certain conditions specified in the law, libraries and archives are authorized to furnish a photocopy or other reproduction. One of these specified conditions is that the photocopy or reproduction is not to be “used for any purpose other than private study, scholarship, or research.” If a user makes a request for, or later uses, a photocopy or reproduction for purposes in excess of “fair use” that user may be liable for copyright infringement,

This institution reserves the right to refuse to accept a copying order if, in its judgment, fulfillment of the order would involve violation of copyright law.

Please Note: The author retains the copyright while the New Jersey Institute of Technology reserves the right to distribute this thesis or dissertation

Printing note: If you do not wish to print this page, then select “Pages from: first page # to: last page #” on the print dialog screen

The Van Houten library has removed some of the personal information and all signatures from the approval page and biographical sketches of theses and dissertations in order to protect the identity of NJIT graduates and faculty.

A Comparison of Integrated and Differential
Estimates of Fluorescent Intensity Profiles Using
Digital Video Image Analysis

By
Langfang Wu

Thesis submitted to the Faculty of the Graduate School of the
New Jersey Institute of Technology in partial fulfillment of
the requirements for the degree of Master of Science in
Biomedical Engineering, 1990

APPROVAL SHEET

Title of Thesis: A Comparison of Integrated and
Differential Estimates of Fluorescent
Intensity Profiles Using Digital
Video Image Analysis

Name of Candidate: Langfang Wu

Degree: Master of Science in Biomedical Engineering, 1990

Thesis and Abstract Approval :

Dr. Arthur B. Ritter *Date*
Assoc. Professor
Physiology Department, UMDNJ

Signature of other members of the thesis committee:

Dr. David Kristol *Date*
Director
Biomedical Engineering Department, NJIT

Ms. Francine Reibman *Date*
Director
Clinical Engineering Department
University Hospital, Newark

VITA

Name: Langfang Wu

Address:

Degree and Date to be Conferred: M.S.BME., May, 1990

Date of Birth:

Place of Birth:

Secondary Education:

Collegiate Institutions Attended	Dates	Degree	Date of Degree
Chinese Culture University	Sep. 1977	B.S.E.E.	June, 1981
New Jersey Institute of Technology	Sep. 1987	M.S.BME.	May, 1990

ACKNOWLEDGEMENTS

This thesis is dedicated to my parents for their understanding and lifetime support, and my loving wife, Chuanyin, for always standing by me, encouraging me and accompanying me into foreign lands. She bravely fought loneliness, language, and postponed a personal professional career. She endured many hours of patient waiting, and the unbearable uncertainty of "how much longer it will take you to finish." To her, truly and most deservedly, I dedicate this thesis.

I would like to express my gratitude to the following people for their contribution to the fulfillment of this thesis.

I am indebted to my thesis advisor, Dr. Arthur B. Ritter, for his scientific guidance and encouragement, for having facilitated his laboratory and equipment, and for patiently reading and correcting this manuscript. The warm and kind nature will always be greatly appreciated and remembered.

I acknowledge and appreciate my graduate advisor, Dr. David Kristol, for moral and material support and for the excellent friendship he has honored me with during these years. He had put me on the track when I joined the Biomedical Engineering Program, by offering me a project with Dr. Ritter. He has been an inspiration to me all the time, and will always be. He was always there when needed most, especially dealing with the school. I will always remember him with great gratitude and respect. Thank you so much for being very nice to me.

I acknowledge Ms. Francine Reibman, for her support and understanding and for her friendship and advice in the past years.

Finally, I would also like to thank all the people I worked with at UMDNJ: Sue, Mike, Jeff, Kim, and Hiroshi for their technical assistance and kind advice.

TABLE OF CONTENTS

LIST OF TABLES	iii
LIST OF FIGURES	iv
ACKNOWLEDGMENTS	v
ABSTRACT	1
CHAPTER 1. INTRODUCTION	4
Intravital Microscopy Study	8
CHAPTER 2. EXPERIMENTAL PROCEDURE	17
Tracer and Animal Preparation	17
Characteristics of the Test molecules ..	19
Optics and Instrumentation	21
Experimental Protocol	21
CHAPTER 3 PICTURE SELECTION AND IMAGE PROCESSING ..	26
Integral Optical Density (IOD)	29
Selection of Video Frames	31
CHAPTER 4 COMPUTER PROGRAMS	37
Program IMAGE	37
Program SAGID	38
CHAPTER 5 EXPERIMENTAL OBSERVATIONS	40
Selection of Leakage Site	41
Data Observation	43
Data Treatment	44
CHAPTER 6 DISCUSSION	50

CHAPTER 7	CONCLUSION AND RECOMMENDATIONS	53
	Conclusion	53
	Recommendations	54
	Experimental Problems	55
APPENDIX A	PROGRAM SAGID	58
APPENDIX B	EXPERIMENTAL DATA	62
BIBLIOGRAPHY	vi

LIST OF TABLES

TABLE 1	Physicochemical Parameter of Test Molecules	20
TABLE 2	Average Standard Deviations for 3 different window sizes at several time points for FITC-DX 20 and FITC-DX 70	52
TABLE 5.1 - TABLE 5.24	Experimental Data	62

LIST OF FIGURES

FIGURE 2.1	Schematic Diagram of the Optical and Recording Systems	23
FIGURE 2.2	Simulated Development of A Leakage Site	25
FIGURE 3.1&2	Image Processing	28
FIGURE 3.3	Determination of "Reference Point"	36
FIGURE 5.1	Computer Mapping	47
FIGURE 5.2	Construction of Intensity Profiles	48
FIGURE 5.3 - FIGURE 5.26	Graylevel Values vs. Distance for the Selection of Six Different Frames at the Same Time ...	49
FIGURE 5.27 - FIGURE 5.58	Graylevel vs. Distance in Single Pixels and Average Graylevel vs. Distance in Windows of 5X5 and 10X10 Pixels.	49

ABSTRACT

Title of Thesis: A Comparison of Integrated and Differential
Estimates of Fluorescent Intensity Profiles
Using Digital Video Image Analysis

Langfang Wu, Master of Science in Biomedical Engineering,
1990

Thesis Directed by:

Dr. Arthur B. Ritter

Associate Professor, Physiology Department

UMDNJ, Newark, NJ

The dynamics of macromolecular transport across microvascular walls in the hamster cheek pouch have previously been studied by other investigators using fluorescence intravital microscopy. Fluorescein Isothiocyanate labeled Dextrans (FITC-Dx) of 20,000, and 70,000 molecular weight (FITC-Dx-20 and FITC-Dx-70) were used as macromolecular probes. Values of fluorescent intensity were previously recorded on videotape as a function of distance perpendicular to leaking vessels over a period of

about 2.5 hr to allow for tracer equilibration in the interstitial space. In this study, these videotapes were played back frame-by-frame and 215x130-pixel windows around each leaking vessel were selected for further analysis of the leakage patterns using digital image processing. Window areas around each leaking vessel ranging in size from 1 by 1 to 10 by 10 pixels were selected. Histograms of the light intensity distributions for the fields selected at several time points were used to construct integral optical density-position profiles of the extravasated fluorochromes.

The graylevel value of a single pixel in the middle of the window was compared with the average graylevel of 5 X 5 and 10 X 10 pixel windows. We found that the larger the window area, the less the variation is in the graylevel value. We found that, although the graylevel values for single pixels were similar in magnitude to the mean values of a pixel in the 5 X 5 and 10 X 10 windows, the standard deviation of graylevel values of single pixels, were much larger than the standard deviations calculated for the mean of the windows in 10 X 10 window areas. Thus, simple spatial filtering provides a straightforward method for smoothing the intensity profiles to estimate convective and

diffusive transport parameters from a "best fit" of these profiles to a partial differential mathematical model for blood-tissue exchange. In addition, spatial smoothing should produce more reliable estimates of the transport coefficients. The large variation in single pixel values within a small window can not be explained simply by experimental error. The data suggest that the spatial variation in intensity might be explained by the heterogeneous nature of the interstitial space. Portions of the interstitium (e.g. the intercellular compartments) might be available to the macromolecular probes used in this study, whereas other portions of the interstitium (e.g. the cellular compartments) might be exclude the macromolecules used.

CHAPTER 1

INTRODUCTION

Convection was proposed to be the dominating mechanism for macromolecular transport by Rippe et al., 1979, Arfors et al., 1979, Haddy et al., 1972, Mcnamee et al., 1979, and, Granger and Perry, 1981. Numerous other investigators, however, contend that macromolecules exchange primarily by diffusion (Renkin et al., 1977; Sejrsen et al., 1985; Garlick and Renkin, 1970; Paaske, 1982). An understanding of these contrasting conclusions requires a brief introduction into the experimental approach and respective mathematical treatment used in these studies. Two methods have been used to evaluate parameters describing macromolecular transport: a. measuring the disappearance of a radioactive or fluorescent marker from plasma or the accumulation of a marker in tissue; b. analyzing and comparing the steady state concentrations of native proteins or exogenous tracers in plasma and lymph. Determination of permeability parameters of blood-tissue exchange based on measurements

of plasma disappearance or tissue accumulation of a tracer.

Comparison of the relative concentration of the diffusible tracer to the impermeable tracer gives the proportion of the diffusible solute extravasated into the interstitium. In its classical version, this method can not be used to evaluate diffusive and convective fluxes, because only one parameter, PS (Permeability Surface area product), is calculated from the experimental data. Although recent modification of the mathematical treatment by Rippe et al., (1979) permits simultaneous determination of capillary diffusion and filtration from essentially similar experiments, (single injection indicator diffusion method), the validity of the calculated permeability parameters is still somewhat questionable. At least two criteria must be met to obtain reliable permeability data: a. the interstitial space should be homogeneous, and b. the permeability characteristics of the vascular bed should be uniform. These conditions are never fully satisfied. It is also evident that the indicator-dilution technique cannot be used to study macromolecular transport at the local level.

A steady state analysis of protein concentration in plasma and lymph has been used to determine permeability characteristics in subcutaneous tissue (Joyner, 1977; Taylor et al., 1982; Rutily and Hagander, 1979), skeletal muscle (Haddy et al., 1972; Ganrot et al., 1974; Youlten, 1969), lung (Parker et al., 1981; Blake and Staub, 1976; Brigham et al., 1979; Mcnamee and Staub, 1979), heart (Arturson et al., 1969, 1972), liver (Shannon and Lasceles, 1967; Grotte, 1956; Granger et al., 1979), stomach (Perry et al., 1981), intestine (Yablonski and lifson, 1976), and colon (Richardson et al., 1980). This is by far the most important technique to study mechanisms of macromolecular transport and most of the available experimental data have been obtained using this method. Determination of vascular permeability characteristics using lymph data is based on the assumption that lymph represents a net filtrate from microvessels in the tissue under investigation. Concentrations of the injected solute or native proteins in lymph and plasma are measured at different physiological conditions and transport parameters are calculated from the Kedem-Katchalsky equations (Kedem and Katchalsky, 1958). Because these equations have been

developed for steady state processes, a mathematical treatment of the data does not require any additional assumption and is (at least in theory) exact. Several sources of error associated with the experimental determination of steady state solute concentrations in plasma and in lymph, however, lead to contradicting results from almost identical studies (e.g. Renkin et al., 1977 and Rutili et al., 1982). These errors are : a. collected lymph may contain lymph from other organs and tissues not under study (Drake et al., 1981), b. the solute concentration in lymph can be modified during passage through lymph nodes (Adair et al., 1981); c. steady-state must be attained (in some cases it takes 4 to 6 hours to establish this condition but physiological stability of the preparation for such a long period of time is questionable). In addition, some investigators have neglected either the convective or diffusive term in the Kedem-Katchalsky equations in their calculations of the permeability parameters. Renkin (Renkin, 1964) who pioneered one of the first methods for analyzing lymphatic protein fluxes in terms of permeability-surface area product (PS), has ignored the convection term in his calculations. As a result, the PS values he has reported are overestimates of

the true PS. More than a hundred reports are available which are based on the application of Renkin's equation. It is evident that these data cannot be used to investigate mechanisms of blood to tissue exchange in terms of convective and diffusive fluxes.

All the methods described above are based on a so called "whole-organ" approach. Only phenomenological, lumped parameters can be determined using these techniques. A different approach, however, is required in order to investigate macromolecular transport across individual microvessels and also segmental differences of microvascular permeability within specified organs and tissues.

Intravital microscopy studies

Vital microscopic studies utilizing intravascularly injected dyes (Patent Blue V, Evans Blue, Trypan Blue, carbon particles, etc.) have been used to study capillary permeability in various transparent tissues for a long time (Rous et al., 1930, McMaster and

Parsons, 1939, Branemark et al., 1968). In these studies, dyes become bound to plasma proteins and are assumed to trace the movement of macromolecules across the vascular wall. Most of these tracers, however, are not biologically inert and cause serious side effects when administered in vivo. Moreover, the degree of binding of these compounds to plasma proteins is not known precisely and can lead to substantial overestimation of microvascular permeability (Levitt and Michel, 1973).

The transport of macromolecules through the intercellular junction in postcapillary venules has been reported by several investigators in several different organ systems and has become an active research area especially for those investigators studying chemical mediators of inflammation (Svensjo et al., 1978; Hulstrom and Svensjo, 1979; Gawlowski et al., 1982; Boric et al., 1987; Dillon and Duran, 1988). At the present time, it is generally accepted that there are two principal transport mechanisms by which macromolecules are transported between blood and tissues; hydrostatic pressure gradient (Convection) and, concentration gradients across the wall and within the interstitium (Diffusion) are the major physical

driving forces for the two mechanisms.

In general, quantitative information on blood-tissue transport of large solutes has resulted from two major approaches: macroscopic and microscopic. In the macroscopic approach, blood-tissue transport of solutes in whole organs or tissues is monitored using several different techniques. For example: Renkin et al., (1977) studied plasma-to-lymph exchange of albumin and dextran 110, while Perl (1975) used the osmotic transient method to study transport of albumin between plasma and interstitium. In the microscopic approach, the transport of molecules is studied in and around a single vessel or segment of a vascular bed (Curry, 1984; Crone et al., 1984). An effective permeability-surface area product is calculated from either of the two approaches. The physicochemical interactions between the solutes and the constituents of the transport pathway cannot be directly evaluated from either of these approaches.

Quantitative assessment of macromolecular transport became possible with the introduction of the Silicon Intensified Target (SIT) TV cameras and high

sensitivity photometric devices. Using these instruments, Nakamura and Wayland (1975) and Fox and Wayland (1979) have evaluated interstitial diffusion coefficients for various FITC-Dextrans and Fluorescein labeled Bovine Serum Albumin (BSA) in the cat and rat mesenteries. The introduction of digitized fluorescein angiography helped to further characterize the blood-tissue transport pathway for macromolecules. Apparent interstitial diffusion coefficients for macromolecular tracer were determined using this methodology (Nakamura et al., 1975; Fox and Wayland, 1979). Nugent and Jain (1982,1984) later developed a photometric technique and a digitizing procedure for localized measurements of fluorescent intensity-time relationships in both intravascular and interstitial regions of the rabbit ear. Ley and Arfors (1986), using a digital image analysis of fluorescein angiograms developed by Aslund et al., 1979, determined permeability parameters for sodium fluorescein and FITC-Dx-3 using a one-dimensional mathematical model of microvascular blood-tissue transport in the hamster cheek pouch.

Although these measurements should be considered as a beginning of a new era in the

application of intravital fluorescence microscopy to study vascular permeability, reported diffusion coefficients should be judged only as descriptive parameters which satisfy the selected one-dimensional model. Several possible sources of errors have been discussed by these authors. They are: a. the mathematical model did not include a convective component of the overall transport (convective transport is the result of a net movement of macromolecules from the vascular system through the interstitium and into the lymphatics), b. data was taken from the leading edge of the diffusing tracer (considering that dextran fractions contains a range of molecular weights, calculated diffusion coefficients are overestimated), and c. tissue hydration is greater than normal. In view of the above discussion, it is evident that a quantification of macromolecular transport in microvascular beds in term of convective and diffusive fluxes requires a mathematical model which contains parameters describing both convective and diffusive fluxes. Subsequent comparison of the experimentally determined and theoretically predicted amounts of extravasated solute will allow estimation of the parameters responsible for

extravasation. It can be shown that in a homoporous membrane, convective flux is related to the average linear velocity of a solute in a pore and, that the permeability coefficient is a function of solute dispersion.

New discoveries in the life sciences are often linked to the development of unique optical tools that allow experimental material to be examined in new ways. Computer processing can be used to obtain numerical information from a microscope image that is more accurate, less time-consuming, and more reproducible than the same operations performed by other methods. Digital image processing techniques can be used to produce information about the optical image that cannot be obtained in any other way. The first step in digital image processing is the conversion of the optical image into a form that can be stored in computer memory. This conversion is performed by a light-sensitive system known as an optical digitizer, which produces coded numbers that are a measure of light intensity. This system which in our case incorporates an S.I.T. (Silicon Intensified Target) TV camera, samples the optical image over regular intervals,

and the electronic output is converted into a string of discrete numerical values that represent the distribution of intensity in the optical image. This process is called "digitizing", and the stored numerical representation of the original optical image is called a digital image.

From frame-by-frame playback of each experiment, particular discrete leakage sites can be observed over the course of time. The digitizer provides graylevel distributions for a selected field (215 * 130 pixels) around each leakage site. Graycolor levels during control are subtracted from subsequent frames to yield the spatial changes in graycolor distribution in the interstitial space (The extravasated FITC-Dextran 20K and 70K) as a function of time. Since the TV camera is set to a fixed gain and pedestal when the experiment is recorded, graylevels at each pixel are related to changes in the local amount (or Concentration) of flurochrome present. Graycolor values can be converted to normalized concentration by dividing each graycolor value by the graycolor which corresponds to the measured venous concentration of flurochrome. Mixed venous

concentration of flurochrome is measured periodically during each experiment by withdrawing a sample of blood from a catheter in the femoral vein and analyzed for the flurochrome using a spectroflurometer. Distance along each vessel and in the interstitial space are measured using a video image shearing device, calibrated with a stage micrometer. From these measurements, concentration profiles as a function of both time and distance can be determined for each leakage site.

Measured concentration profiles as a function of distance and time can then be compared with similar profiles generated by a partial differential equation model for blood-tissue exchange. A "best-fit" (in the least-squares sense) of the model to the data yields estimates for the model parameters. A convection-diffusion partial differential equation model was used and best-fit estimates of a diffusion coefficient and a velocity coefficient were obtained from the model and the data (Bekker, et al., 1988; Dumrong Siri). Changes in the values of these parameters with molecular size and experimental conditions can yield the relative contributions of convective and diffusive mechanisms to the blood-tissue transport of

macromolecules and their alterations in health and disease.

Since estimates of the transport parameters are obtained from the best-fit of a mathematical model to the experimental intensity profiles, the uncertainty in the parameter estimates will, to a certain extent, be determined by the experimental variation in the measured intensity profiles.

The objective of this study is to compare the variation in point estimates of concentration (intensity) with a single spatial filter (spatial average) to assess the improvement possible in estimation of the transport parameters.

CHAPTER 2

EXPERIMENTAL PRODEDURE

Tracer and Animal Preparation

The hamster cheek pouch was used as an experimental model for study of the microcirculation. Several factors make this preparation well-suited for the present study, namely:

(1) The hamster cheek pouch is highly vascularized and thin enough to accomodate both epi- and transillumination studies.

(2) Microvascular fields may be readily traced from their arteriolar origin, through the capillaries, to their venous confluence.

(3) It is believed that the lymphatic drainage of the cheek pouch is practically absent; a situation that simplifies mathematical treatment of the experimental data.

(4) Finally, a cheek pouch preparation is relatively non-traumatic and can be used for experimentation for up to 4 hours.

Syrian Hamsters weighing 80 to 100 g were initially anesthetized by interaperitoneal injection of 6 mg/100 g body wt of pentobarbital. Body temperature was maintained at 37°C with a heating pad regulated by a thermistor probe coupled to a temperature controller. Tracheotomy was performed (PE 90) to facilitate spontaneous respiration. The carotid artery and jugular vein were cannulated (PE 10) for obtaining blood samples and injecting the tracer and additional doses of sodium pentobarbital, respectively.

The cheek pouch was prepared for fluorescent intravital microscopy in a manner similar to that described by Mayhan and Joyner (1984) and Gawlowsky and Duran (1986). Briefly, an oval shaped lucite plate with two small pegs at each end was inserted into the pouch through the mouth. The skin overlying the pouch and plate was incised along the midline of the cheek and the epithelium cleared of connective tissue. A lucite chamber containing a 1 ml reservoir was attached to a single layer of the pouch and secured to the base by means of the pegs. The seam was sealed externally with a purse string suture and petroleum jelly to prevent leakage from the reservoir. The

preparation was subsequently placed on a lucite board and mounted on a microscopic stage. Figure 2.1 shows the design of the lucite chamber and a scheme of the working preparation (reprinted from M. Boric, 1985; with permission).

Following surgical dissection and mounting, the preparation was suffused with 35°C bicarbonate buffer solution (composition in mM: 151.8 NaCl, 4.69 KCl, 2.00 CaCl₂, 1.17 MgSO₄, 20.00 NaHCO₃). The buffer was adjusted to pH=7.35 and equilibrated with 95% N₂ and 5% CO₂ (Duling and Staples, 1976). After ten to fifteen minutes of equilibration, the buffer solution was replaced by continuous superfusion with 35°C mineral oil. Mineral oil was selected to prevent swelling of tissue and the escape of tracer molecules into the superfusate (Fox and Wayland, 1979).

Characteristics of the Test Molecules

The FITC-Dextran were prepared as a 5% solution in bicarbonate buffer and administered through a

cannula in a jugular vein. Peak absorption of FITC-Dextran solution occurs at 488nm and the emission peak lies at 515 nm.

Table 1. Physicochemical Parameter of FITC-DX 20 and FITC-DX 70

Physicochemical Parameter of Test Molecules					
TRACER	M_w^a	M_n^b	DEGREE OF SUBSTITUTION	$E^c(\text{Å})$	$D^d(@37^\circ\text{C}) \text{ CM}^2/\text{S}$
FITC-DX 20	19400	17400	0.006	31.2	10.5
FITC-DX 70	71600	62300	0.004	56.8	5.6

where,

M_w^a - Weight Average Molecular Weight.

M_n^b - Number Average Molecular Weight.

E^c - Einstein-Stoke Radius.

D^d - Free Diffusion Coefficient in Water.

Optics and Instrumentation

Observations were made with an Olympus BH microscope equipped for both bright-field transillumination and epi-illumination studies using a 10X long working distance objective with a 10X ocular. Light was delivered to the pouch via a fiber optic lightguide equipped with a 45° angled mirror and a small lens designed to reflect and condense light onto the surface of the cheek pouch. Epi-illumination was provided by a 100-W mercury DC lamp source in conjunction with an Olympus FITC exciter filter(488 nm), an Olympus dichroic mirror (DM-500), and an Olympus-515 barrier filter . The recording system was comprised of a DAGE SIT-TV camera coupled to an RCA real time generator, a V0-2800 Sony video recorder and a Sony video monitor. A schematic diagram of the optical and recording system is depicted in Figure 2.1

Experimental Protocol

A few connective tissue free fields with a well developed vascular net were located and, a site

selected with two or three prominent post-capillary venules separated by at least 50 μm . At this time the intravascular tracer (FITC-Dextran 70K Daltons) was injected (10mg/100 g body wt.) intravenously and a slow continuous infusion of the FITC-Dextran was begun and continued for the duration of the experiment to maintain a constant concentration of FITC-Dextran in the plasma. The infusion rate was 10 $\mu\text{l}/\text{min}$ and the concentration was 1 mg/ml for the 70K. Arterial blood samples were obtained at 5, 15, 30, 60, 90, and 120 minutes.

Immediately after fluorochrome injection, the selected fields were recorded on videotape. Recording was repeated at 3-5 minute intervals for approximately 3 hours. This mode of videotaping was preferred over continuous recording to avoid tissue damage by constant UV irradiation. The videotapes obtained were analyzed off line using digital image processing.

SCHEMATIC DIAGRAM OF THE EXPERIMENTAL SYSTEM

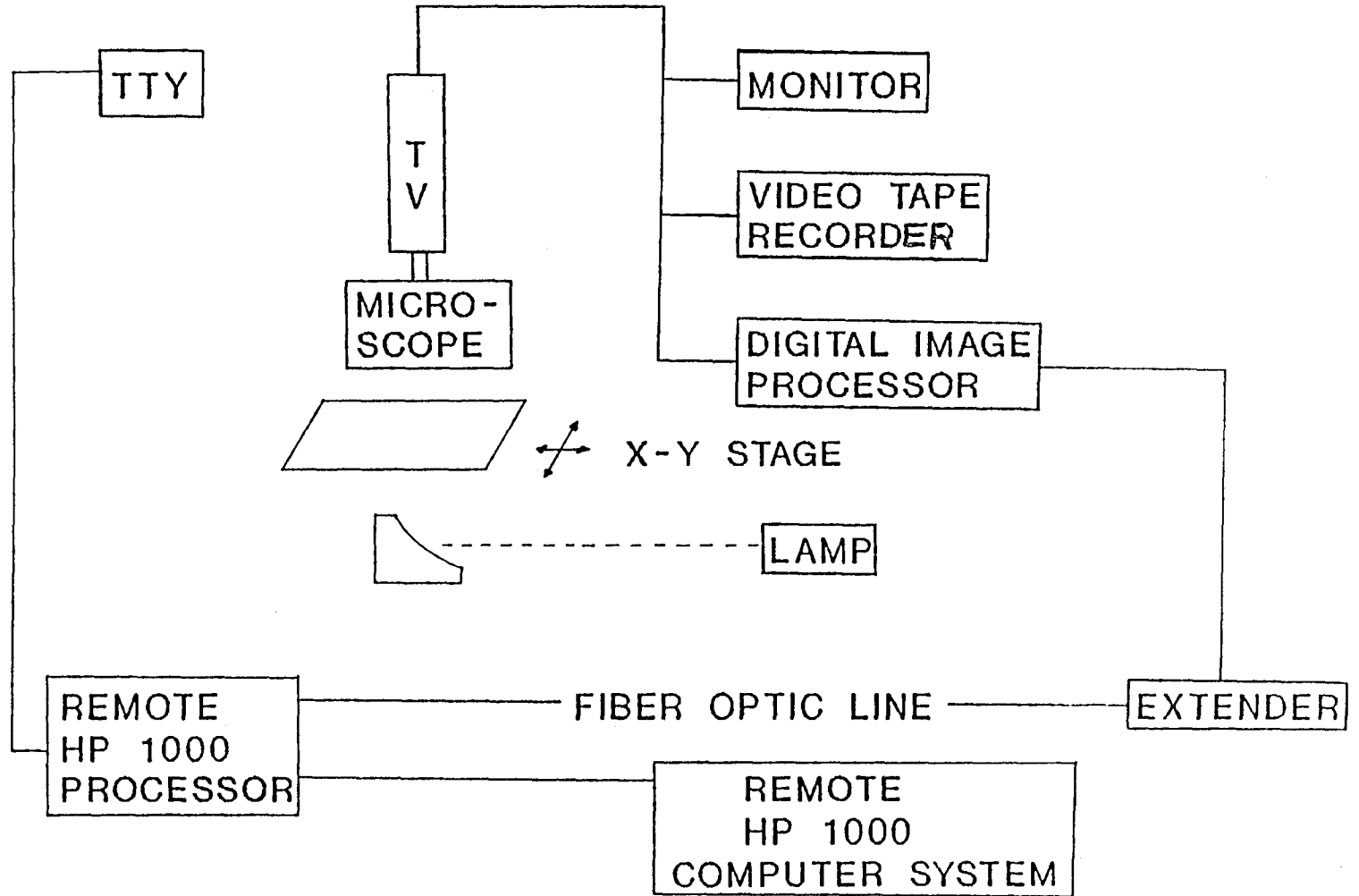


FIG. 2.1 A schematic diagram of the optical and recording system)

An example of time development in the leakage sites is shown in Figure 2.2 (A through C). During the control period (just before the injection of FITC DXs) each preparation was inspected for the maintenance of tissue integrity. The preparation was discarded if red blood cells were detected outside the microcirculation. The preparation was also discarded if blood flow was sluggish or spontaneous leaking sites were observed immediately after FITC DXs administration. For large molecules, it is believed that the immediate appearance of the tracer in the interstitium is a result of surgical trauma, rather than a characteristic of the microcirculation. To prevent damage to the tissue, only a minimal amount of loose connective tissue was dissected away. Consequently the contrast in the recorded images was poorer than is usually accepted for hamster cheek pouch preparations. The quality of the picture, however, is not a major issue in our method of image digitization. The level of the tracer concentration in the plasma was monitored by analyzing blood samples obtained from an arterial cannula. A procedure to determine plasma concentration of the FITC DXs using flurometry is described by Gawlowski et. al., (1984).

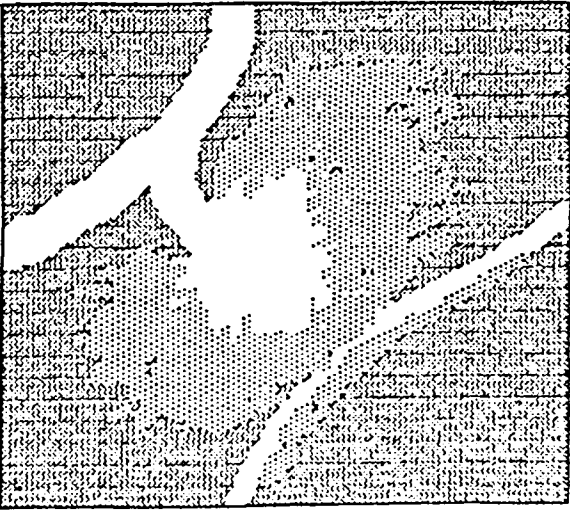
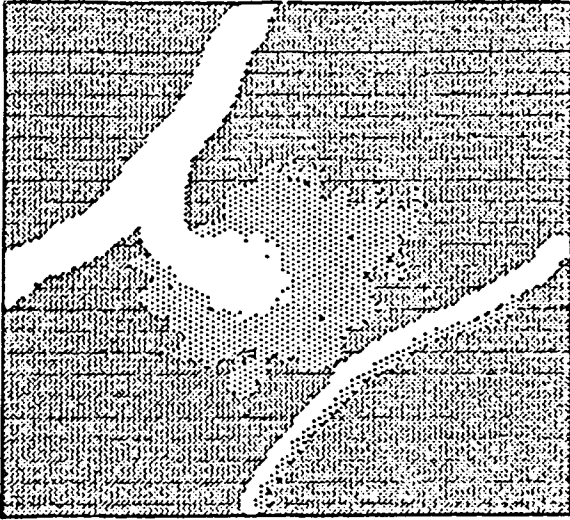
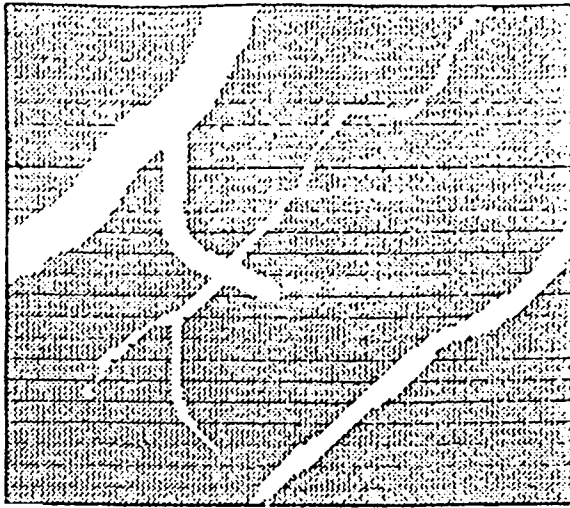


FIG. 2.2 A-C

Simulated development of a leakage site-made by SAGID

CHAPTER 3

PICTURE SELECTION AND IMAGE PROCESSING

A frame-by-frame playback of the video-record of each experiment permits the selection of frames for detailed analysis. In their original form, however, images are not directly amenable to computer analysis and, thus, must be converted to numerical form before processing. This conversion process is called *Digitization* and a common form is illustrated in Figure 3.1. Each frame was digitized into x,y arrays of 512 by 512 picture elements, called "*pixels*" using a real time video image digitizer (Quantex DS20F). Each pixel had associated with it an 8 bit gray scale (a number between 0 and 255), and the most common subdivision scheme is the rectangular sampling grid shown in Figure 3.2. The image is divided into horizontal lines made up of adjacent pixels. At each pixel location, the image brightness is sampled and quantified. This step generates an integer at each pixel representing the brightness or darkness of the image at that point. When this has been done for all

pixels, the image is represented by a rectangular array of integers. Each pixel has a location or address and an integer value called the *Gray Level*. This address and integer value can be varied in 2^n fashion, basically depending on the available memory of the computer and/or digitizer. In our case, we have defined an array of 256 by 256 integers. If we define the threshold intensity (black) as 0 and maximum intensity as 255 (white), the relative light intensity of any pixel can be represented by a graycolor number between 0 and 255.

IMAGE PROCESSING

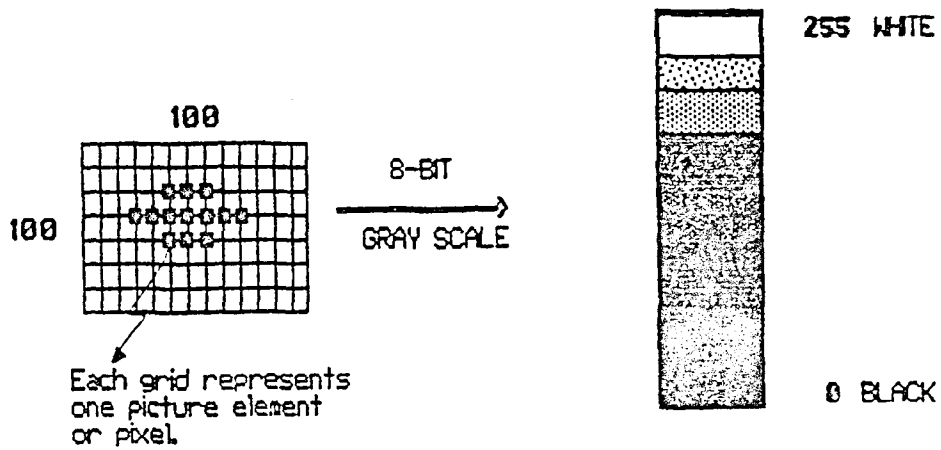
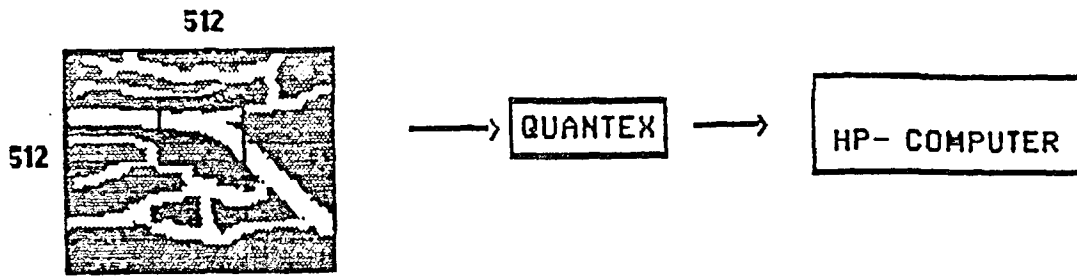


Fig. 3.1 & Fig. 3.2 IMAGE PROCESSING

The gray values were read from the digitizer memory using a computer program called "IMAGE" (details of the program are given in Ritter et al., 1985). After digitizing a video frame, the IMAGE program allows the user to either display the digitized video frame or a part of it on the TV monitor or store the digitized data in a file on an HP-1000 computer for subsequent image analysis.

Integral Optical Density (IOD)

A measure of the "mass" of an image is called the integrated optical density (IOD) and is defined by:

$$IOD = \int_0^a \int_0^b h(i,j) dx dy = \sum_{i=1}^{NC} \sum_{j=1}^{NR} h(i,j)$$

where $h(i,j)$ is the intensity (gray level) of a pixel at position x and y , and a and b delimit the region of the image and NC and NR are total number of

columns and rows of pixels chosen from the selected frame. A. Bekker et al. (1989) have shown that, with proper calibration, the Δ IOD (after background subtraction) can be used as a quantitative measure of the total amount of fluorescent tracer which has extravasated into the interstitium.

If fluorescent light intensity is linear with FITC-Dextran concentration, the IOD of the selected video field after background subtraction would be proportional to the total amount of the tracer molecules within the tissue:

$$I_{\text{tot}}(t_i) = K \left[\text{IOD}(t_i) - \text{IOD}(t=0) \right]$$

where K is a proportionality constant. Linear dependence of IOD on the amount of extravasated dextrans was confirmed using a calibration procedure developed by Nugent and Jain(1982).

Selection of Video Frames

Since flow in these small postcapillary venules was difficult to observe with a 1 % hematocrit perfusate, the IOD of selected areas at different time steps were used to confirm the selection of suitable leaking vessels. The IOD of the interstitial area adjacent to each leaking vessel must increase with time, if the plasma concentration of fluorescent label is kept constant (Bekker et al., 1989).

Selection of a particular area on a time-stamped frame requires careful consideration, since at subsequent times the same area or window of the video frame must be selected in order to perform the image processing.

After a leaking vessel was selected for study, the same subregion of the video frame which contained this vessel was read from different video frames at different time steps. This presents a problem, since small excursions of the vessel in the video field occurred over time. To compensate for these excursions and to assure reproducibility of the spatial coordinates from frame-to-frame, an easily

identifiable anatomical reference point (e.g. a branch point) was located, this "reference point" was a well-defined morphological landmark such as a bifurcation which could be precisely located (± 1 pixel) in each subsequent video frame, so that subsequent frames could be lined-up precisely. For example, in Figures 3.3a, and b, the two subregions of 100 x 100 pixels had to be positioned so that they coincided exactly. Since the branching points A1 and A2 (Figures 3.3a, and 3.3b), in different video frames are common to both fields, points A1 and A2 were selected as a "reference point". The "CURSOR" subroutine in the IMAGE program was used to define the relative positions of point A1 and A2 ($A1(x,y), A2(x,y)$) in both frames. Then the position of point X2 in the second frame could be located exactly by adding or subtracting the deviations along the x- and y- axes which were measured in the first frame.

A leakage site was observed during the control period and for an hour to an hour and a half after the control period. To calculate the amount of FITC which extravasated from a leakage site in a given time period, subtraction of frames was employed. A frame of 215 by 130 pixels was selected at time $t = 0$, i.e. the time at which

FITC was just injected. At any subsequent time, (e.g. at time $t=t_i$), we again selected a 215 by 130 pixel window of the same area. A pixel-by-pixel subtraction of the window selected at $t = 0$, from the window selected at $t = t_i$, yields the increase in graylevel at each x,y location over the time period 0 to t_i . A summation of the increment in graylevel over the entire spatial region of interest gives the Δ IOD over the selected time period. The Δ IOD is thus proportional to the amount of FITC which has extravasated in the time period. The experimental data for all the leakage sites was determined in this manner.

Bekker et al (1987) used the Δ IOD and a partial differential equation for blood-tissue exchange to estimate diffusion and velocity coefficients for a range of macromolecules. A further analysis of the coefficients estimated from the model provided insights into the relative contribution of convective and diffusive transport mechanisms for the range of molecular sizes studied.

The Δ IOD is, in effect, a spatial filter and the integrated spatial average is expected to be a more stable estimate of the concentration profile than those

obtained by point estimates of the intensity. Previous investigators (Fox and Wayland, 1979; Baxter and Jain, 1988) have used point estimates of intensity to fit their models. The question addressed by this thesis is : Do spatial averages yield more stable estimates of intensity profiles than do point estimates?

Video tapes of the Bekker experiments just described were used in this thesis. The tapes were played back frame-by-frame and areas around leaking vessels were selected for analysis.

Five different time periods were chosen for study. At each time point, nine spatial points were chosen in the interstitium along a line perpendicular to a particular leaking vessel. The same vessel was followed for at least two time points. At each spatial location, pixel intensities for windows of 1 by 1, 5 by 5, and 10 by 10 pixels were recorded and IOD's calculated. Average pixel intensity was also calculated for each window.

Paired and non-paired t-statistics were used to compared the variation of the intensities of

individual pixels with the different spatial averages and ΔIOD values.

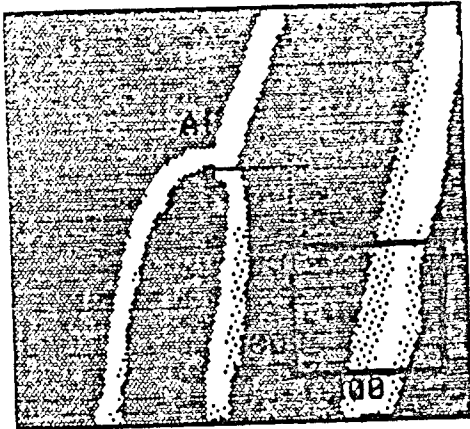


Fig. 3.3a

POSITION OF A1 = (190,200)
 POSITION OF X1 = (260,260)
 HORIZONTAL DEVIATION = +70
 VERTICAL DEVIATION = +60

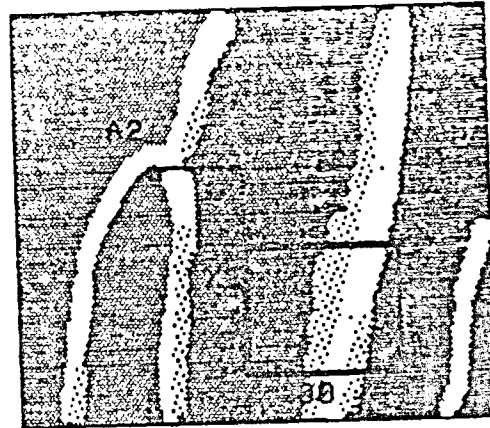


Fig. 3.3b

POSITION OF A2 = (150,210)
 POSITION OF X2 = 150+70, 210+60
 = (220,270)

CHAPTER 4

COMPUTER PROGRAMS

Program *IMAGE*:

Figure 4.1 shows a block diagram for the program *IMAGE*. The selected frame from a particular video tape is digitized into 512 by 512 array of pixels using a video image digitizer (QUANTEX DS 20f). The 215 by 130 pixel window which is selected from each digitized frame is then read from the digitizer memory and stored in a file in digital form on a hard disk, using the *IMAGE* software. Once we have the digital data file the software in *IMAGE* allows us a number of operations. To highlight a few: one can employ different types of digital filtering operations in order to improve a blurred picture. The *IMAGE* software also has options such as Histogram equalization, to improve contrast. Signal averaging to improve signal to noise ratio. Edge detection using a Kirsch operator, and several other features. The options we used most in this study were Histogram equalization and the subtraction of two windows. In

the option of subtraction, a pixel-by-pixel subtraction is carried out using previously stored windows of the same pixel size. Since the subtraction is carried out pixel by pixel, both frames must be of same size and shape. For this reason locating a reference point is as important as selecting a leakage site, since we have to use the same reference point in each frame. The IMAGE software is menu driven and interactive. Once an option is selected, the software guides the user through each operation by asking for all necessary information. For example, each of the windows chosen, as well as the results of the pixel-by-pixel subtraction can be converted to analog form and displayed on a TV monitor through the digitizer memory.

Program SAGID:

The program SAGID enables one to transform the digital data obtained by IMAGE into a hard copy, via a digital 4-pen plotter. SAGID takes the 0 - 256 graylevel span of a digitized image and sorts these into 4 ranges, each range corresponding to one of the four different colors available on the plotter. Since each window may not have the entire 0 - 256 range of graycolors present, SAGID allows the

user to select the graylevel ranges which correspond to each color. A complete description of the SAGID program and its operations including inputting a data file and getting a plot is listed in Appendix A.

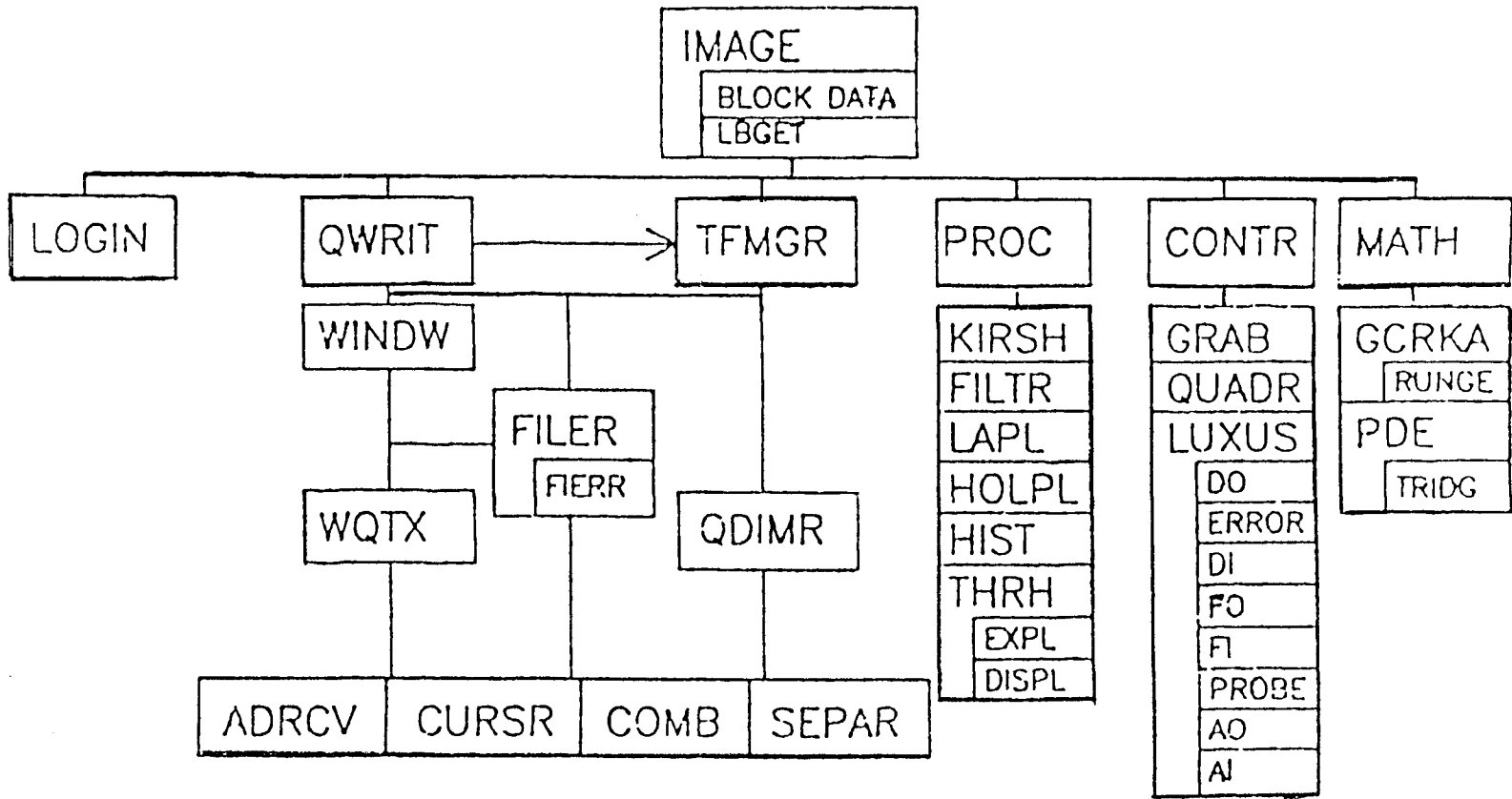


Figure 4.1: Program Image

CHAPTER 5

EXPERIMENTAL OBSERVATIONS

Methods

Four different leakage sites were studied at five different times. Two leakage sites with FITC DX-70 as the macromolecular species and two leakage sites with FITC DX-20 as the micromolecular species. All the video tapes of the hamster cheek pouch macromolecular extravasation studies used in this thesis were prepared by Alex Bekker ("*Transient Analysis of Macromolecular Blood-Tissue Exchange in Microvascular Bed*", 1987). In the hamster cheek pouch preparation the FITC DXs all appeared in the microcirculation within 40 seconds after injection and were seen simultaneously in all vessels in the field of view. Visible leakage sites developed within 5 to 25 minutes after the injection depending on the molecular weight of the tracers. The leakage sites were observed at post-capillary venules with luminal diameter between 30 to 35 μm (Sevensjo et al. 1978; Gawlowski et al., 1982).

Selection of Leakage Site

A number of considerations went into choosing a leaking site to study the time course for the extravasation of tracer. The important aspects were as follows:

(1) *Time Period* : The leaking site has to be remain active for at least an hour to draw any meaningful conclusions. There were a few occasions when an excellent leaking site was found but it stopped leaking within 30 to 45 minutes. In some cases a particular site could not be followed beyond about 45 minutes, due to numerous practical limitations, such as: burning the microvessel with UV light at epi-illumination; sluggish of blood flow.

(2) *Interference* : This factor was really difficult to overcome. Flurochrome from nearby leaking sites with variable magnitude interferes with the observation. These interferences are unpredictable and one never know when interference from a nearby leaking site will force one to stop the observation on the current leaking site. For this reason alone, five leaking sites were abandoned.

(3) *Reference Point* : Though it looks straightforward to locate a reference point, in reality, this problem also forces us to give up one or two excellent leaking sites. In these cases, interference from nearby leaking sites caused the marked reference point to become ambiguous after some time. The size and shape of the windows must remain the same in order to carry out the pixel by pixel subtraction. Choosing a reference point far away from a leaking site is not recommended, since the size or shape of the vessel may change during the course of the experiment.

Some other small, but significant, problems which were encountered were: a, change in the size or shape of the vessel itself during the course of the time. Minute changes may not be discernible to the eye but are significant during Digital Image Processing. The leaking sites which were selected for analysis were close to 'perfect'. Before going into details of the analysis, a brief explanation of these data gathering would be helpful.

The IMAGE software computes the I.O.D. and Histogram for each digitized window around each leakage site. The software SAGID, reconstructs the frame, pixel by pixel.

This reconstructed image allows one to nearly exactly locate each leakage site. The software GRAFIT statistically analyzes the graylevel data and computes Standard Deviation values. The intensity of an individual pixel in an image which was reconstructed by SAGID, can really be found on the corresponding digitized frame. In other words, once a leakage site is located in a reconstructed image, it is easy to follow this particular site during the entire course of time. In this fashion Graylevel Vs. Radial Distance was experimentally evaluated over time.

Data observation

Table 5.1 through Table 5.24. (in Appendix B) show graylevel, mean, and standard deviation vs. perpendicular distance for each of five *different* times at the same leaking site. Then two *different* times were arbitrarily chosen and six frames taken at the same time were each analyzed. Windows comprising 1 by 1 pixels, 5 by 5 pixels, and 10 by 10 pixels were chosen from each frame in a straight line perpendicular to the leaking site. All intensity profiles were measured in the interstitial space.

An important practical problem in these studies is converting the measured graylevel intensity to concentration of FITC DXs. The camera and digitizer are calibrated in such way that the plasma concentration of FITC DXs corresponds to a graylevel intensity of 255 in a large vessel (Dumrongsiri). A mathematical relationship between concentration of FITC DXs and the graylevel intensity *inside* the vessel was reported by Nugent and Jain (1984). Their relationship is a linear one. From our observations, the relationship between FITC DXs and graylevel intensity is not linear *outside* the vessel.

Data Treatment

A 215x135 pixel window around each leaking site was digitized and stored in a digital image file on the computer. The digitized data was then processed as follows:

1. Computer software was used to provide a hard copy of each image from a 4 pen (Green, Red, Blue and Black color) digital plotter. The graycolor range corresponding to each of three available colors was selected by the user, and a "Computer Mapping" similar to that shown

in Figure 5.1 was plotted. This computer mapping helps to accurately determine direction perpendicular to the leaking vessel.

2. The intensity of each pixel starting from the nearest point outside of the leaking vessel ($x=0$) was plotted against distance perpendicular to the vessel as shown in Figures 5.2A and 5.2B. The graph shown in Figure 5.2B is called an "intensity profile". The nearest point outside of each leaking vessel analyzed was used as the starting point ($x=0$) for all intensity profiles.

3. A Digital Image Shearing Device and a recorded stage Micrometer (Nikon Micron Optics, Inc.) allowed calibration of the interpixel distance (in μm). This calibration was used to determine the interpixel distance in the reconstructed image. A comparison between the original video image and reconstructed image gave the horizontal/vertical distance between each pixel (e.g. If a vessel with a diameter of 30 μm horizontally contains 20 pixels in a reconstructed image, then the horizontal distance between each pixel is $30/20 = 1.5 \mu\text{m}$). Through this method, we determined that 20 pixels equals 50 μm for the

magnification used in these experiments.

4. Figure 5.3 through figure 5.26 shows the selection of six different frames at the same time in which graylevel values are decreasing with distance away from the leaking microvessel. Figure 5.27 through figure 5.58 shows graylevel vs. distance in single pixels (which are more variant) and average graylevel vs. distance in windows of 5 X 5 and 10 X 10 pixels (which are smoother).

The experimental data for figures 5.3 through 5.58 are located in tables 5.1 through 5.24 in appendix B.

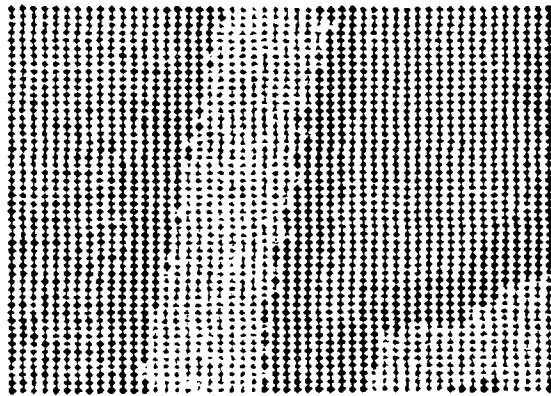
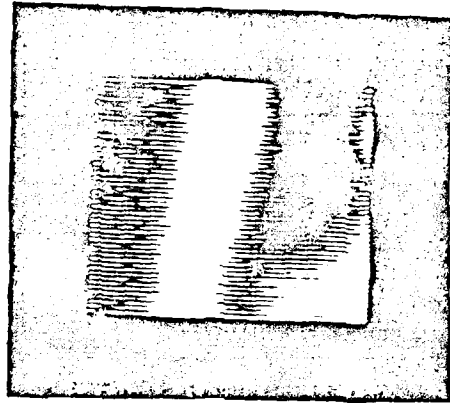


Fig. 5.1 Example of "computer mapping" of a 50x50 pixel window. Pixels with intensity range 0-40 were represented by blue. Red represented pixel intensity ranges from 41 to 70. Green represented pixel intensity ranges from 71 to 255.

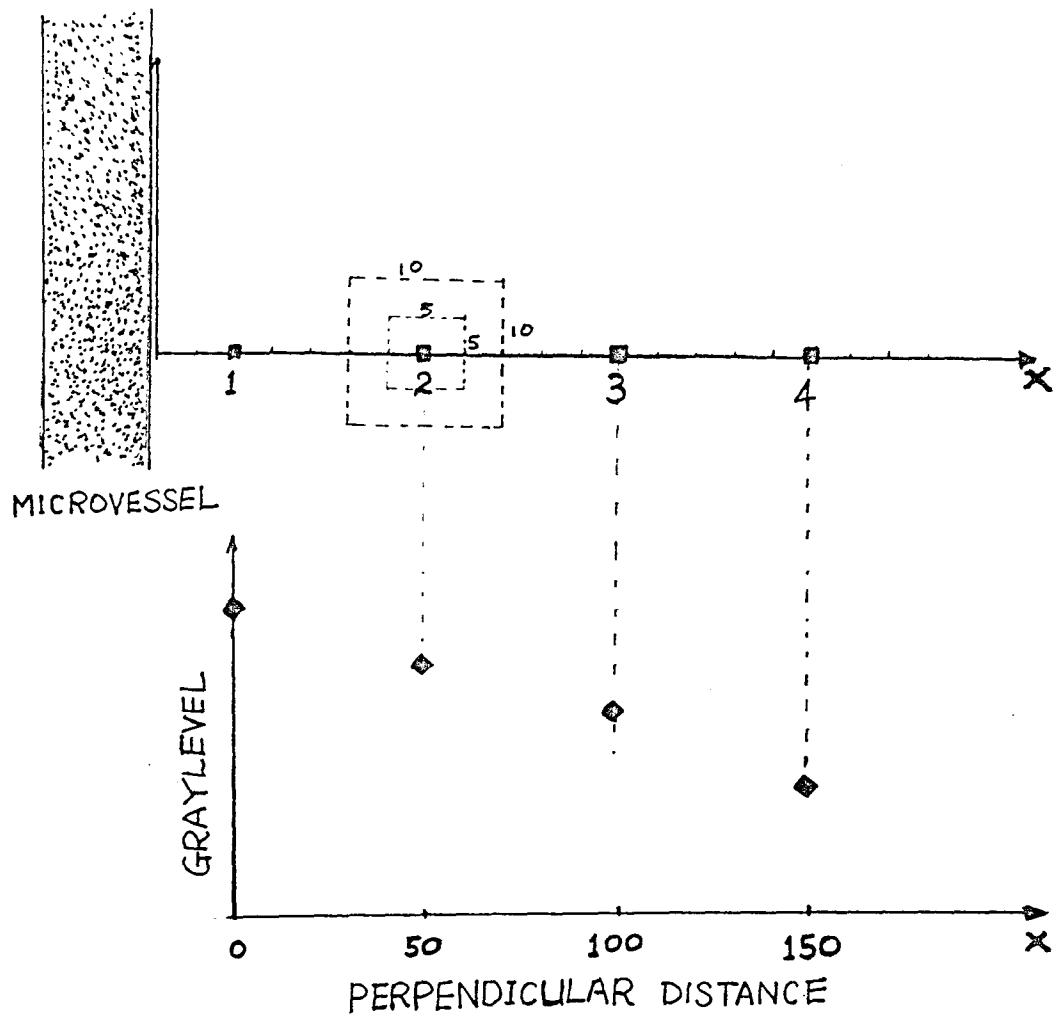


Fig. 5.2 Construction of "Intensity Profiles". Point #1 was defined as the nearest point to the microvessel on the x-axis. An intensity profiles is the graph of graylevel of each pixel plotted against distance perpendicular to the vessel.

Following pages are Figure 5.3 through Figure 5.58

FIG.5.3 FITC-20 FIRST LEAKING SITE
TIME(sec)= 2711 PIXEL 1X1

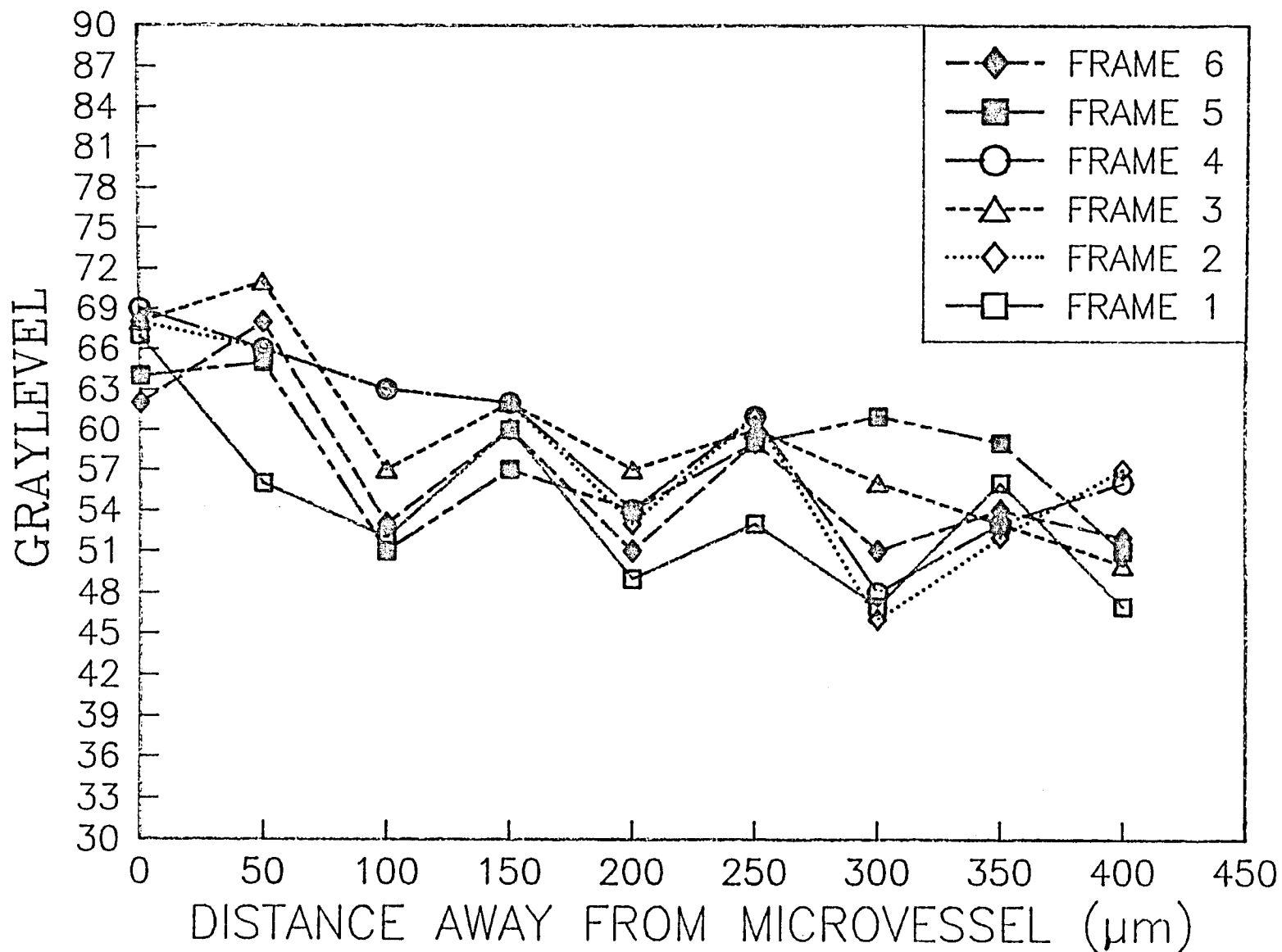


FIG.5.4 FITC-20 FIRST LEAKING SITE
TIME(sec)= 2711 PIXEL 5X5

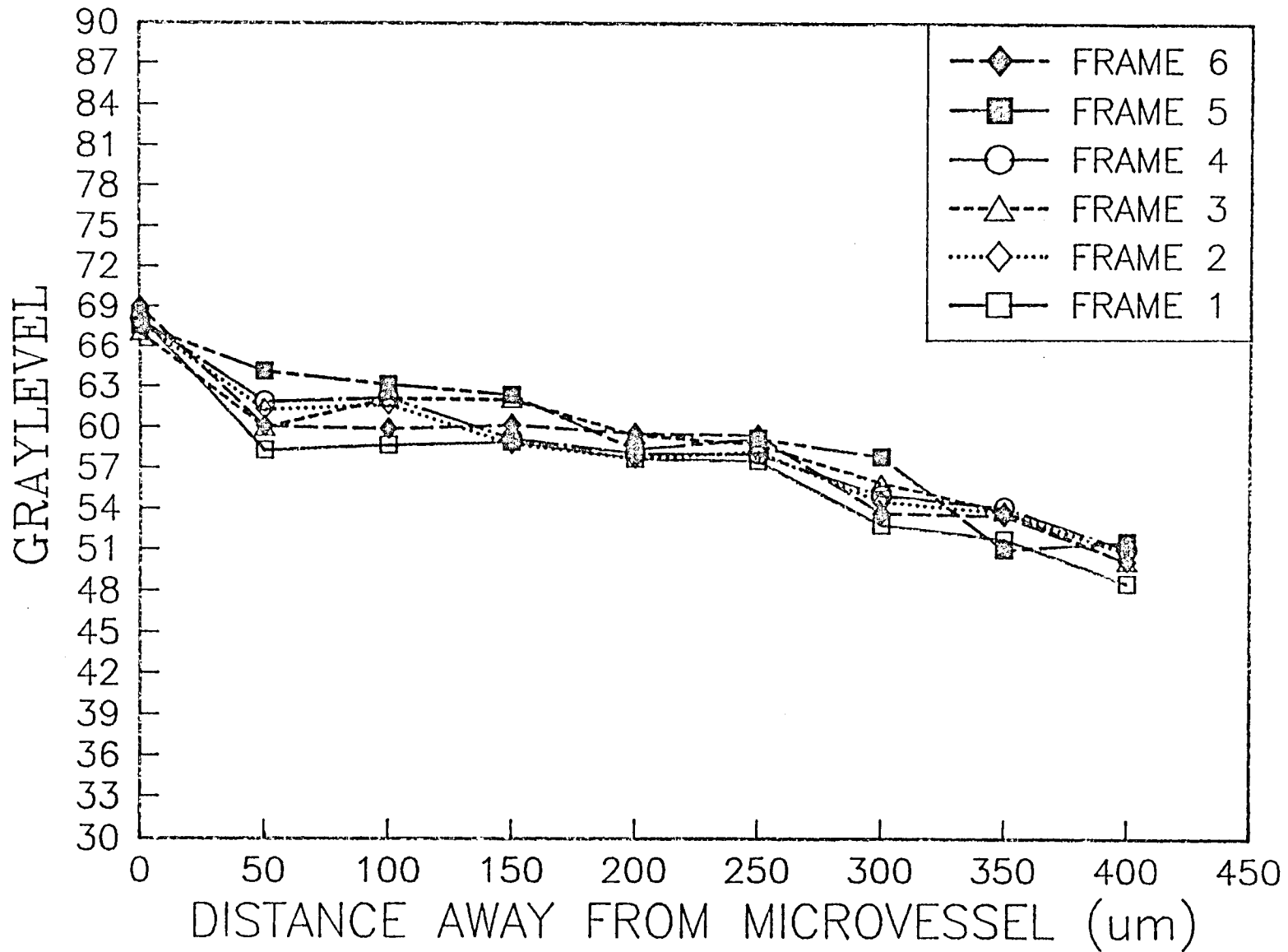


FIG.5.5 FITC-20 FIRST LEAKING SITE
TIME(sec)= 2711 PIXEL 10X10

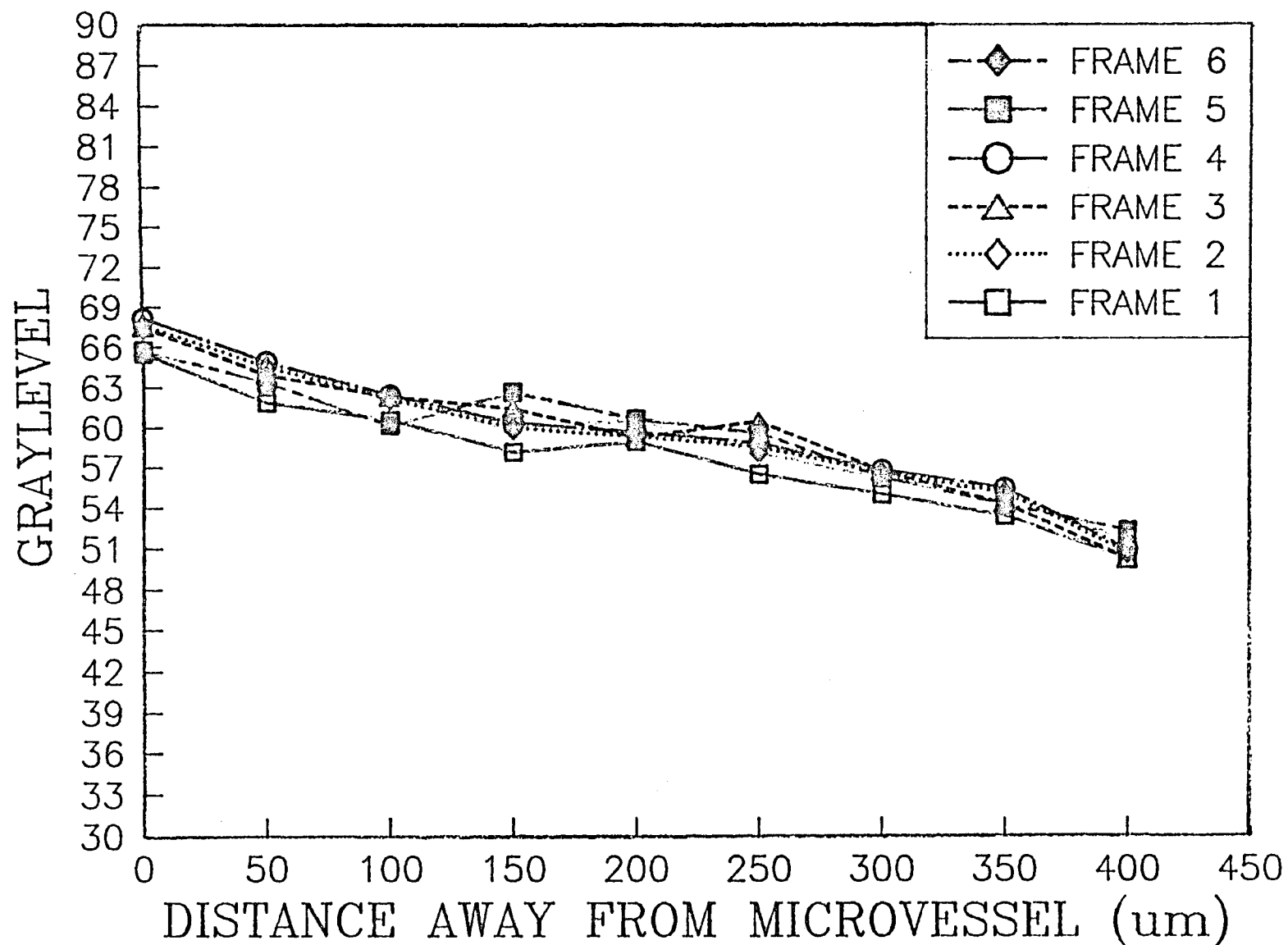


FIG.5.6 FITC-20 FIRST LEAKING SITE
TIME(sec)= 4401 PIXEL 1X1

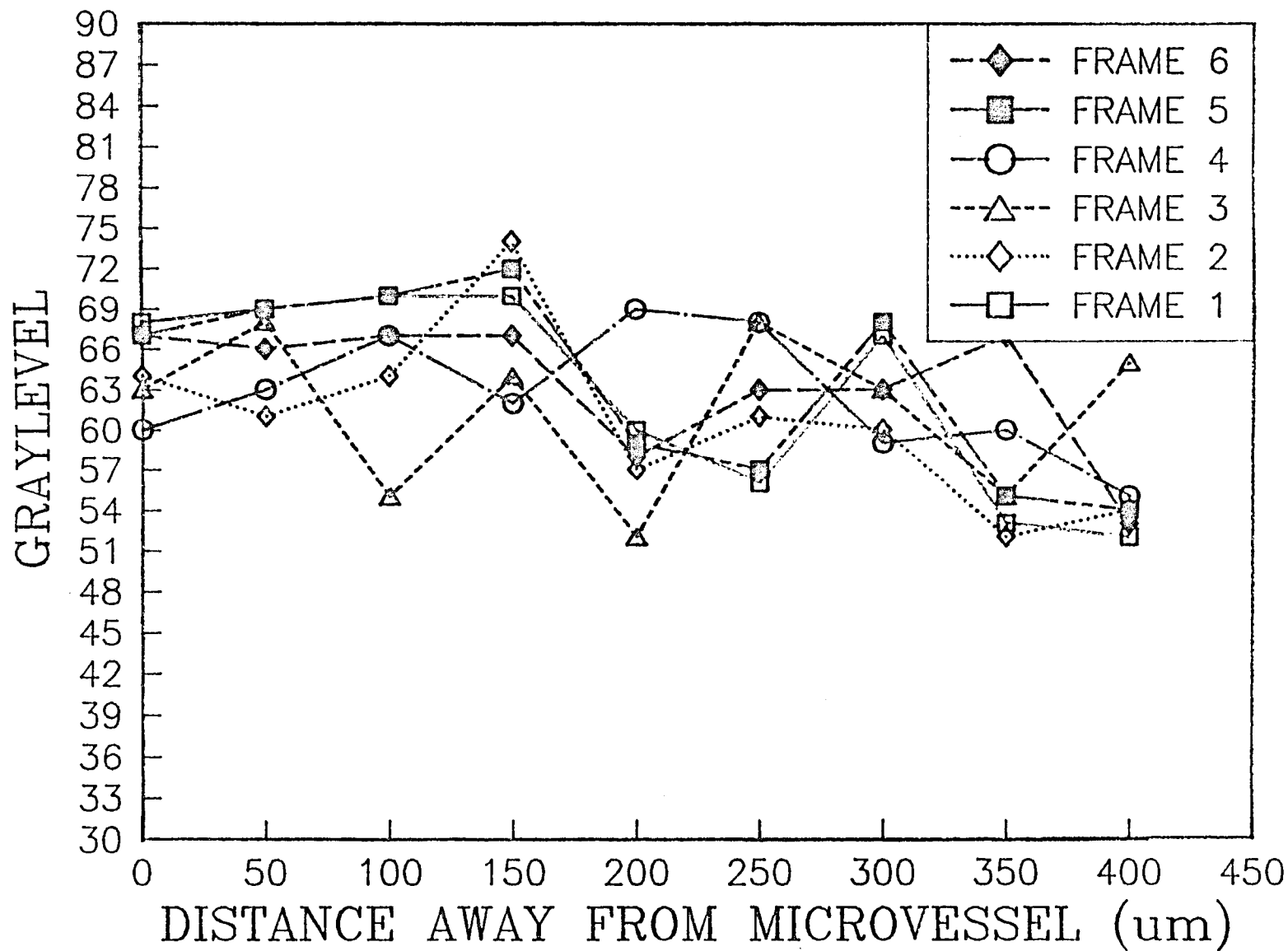


FIG.5.7 FITC-20 FIRST LEAKING SITE
TIME(sec)= 4401 PIXEL 5X5

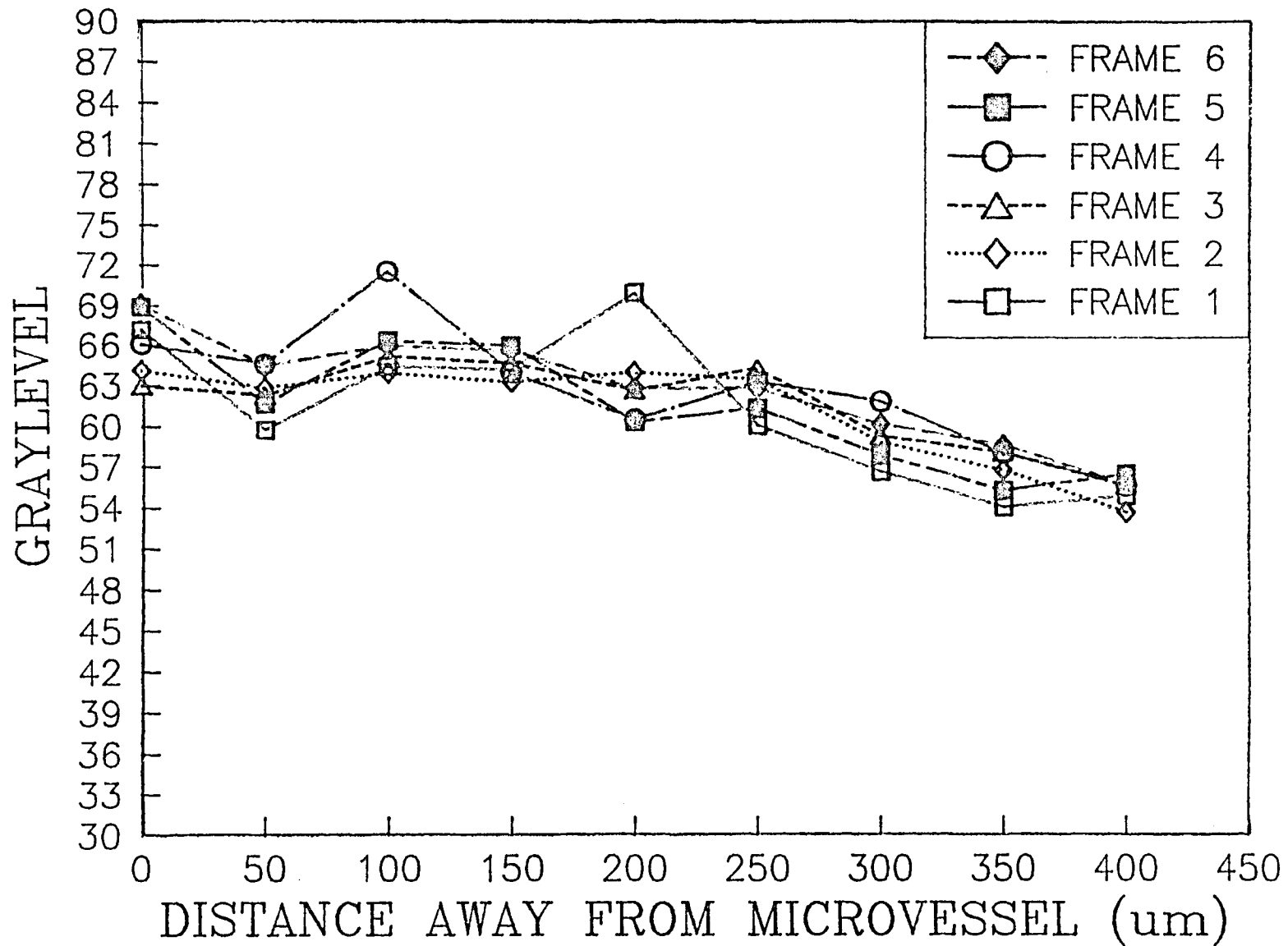


FIG.5.8 FITC-20 FIRST LEAKING SITE
TIME(sec)= 4401 PIXEL 10X10

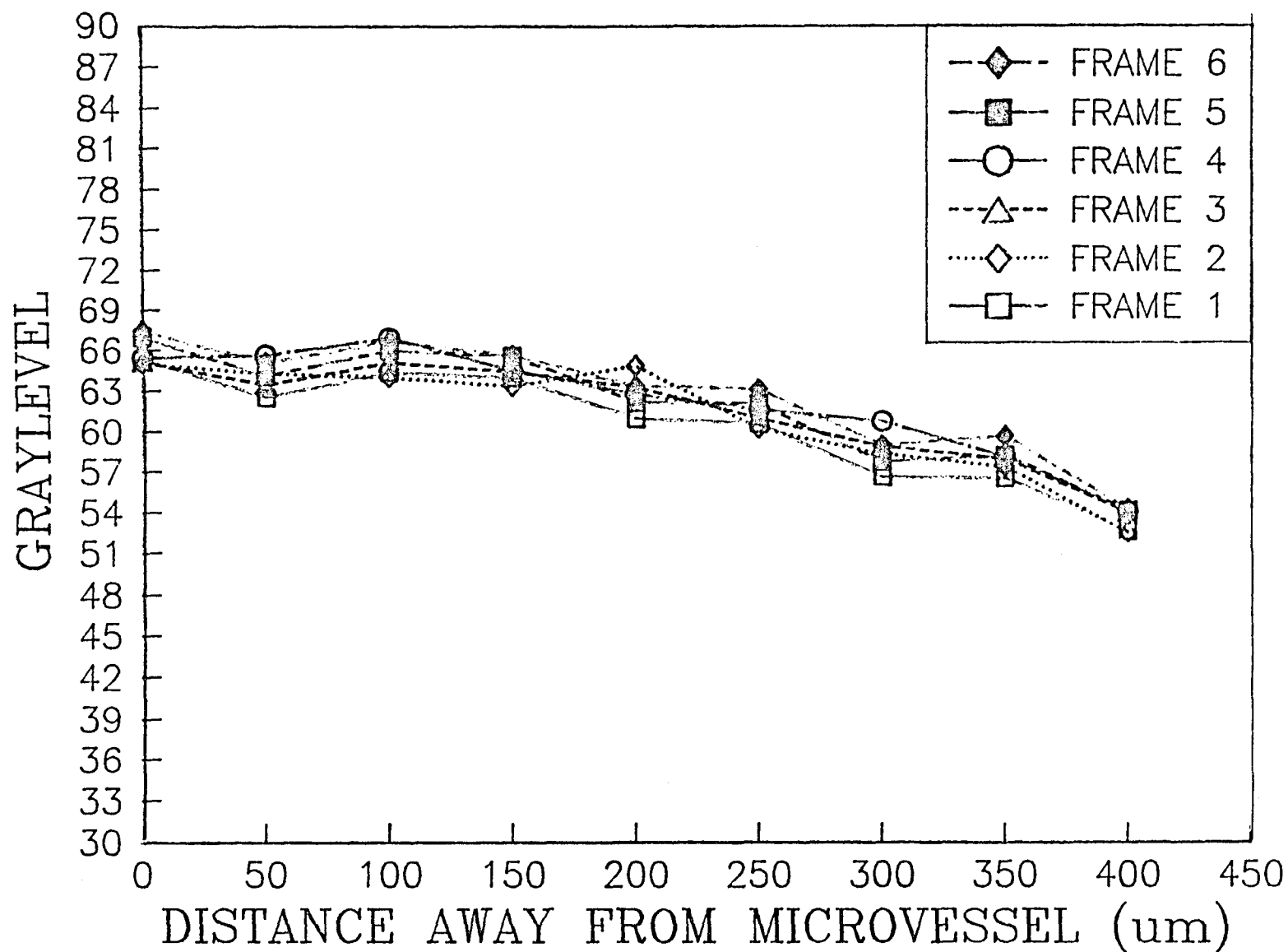


FIG.5.9 FITC-20 SECOND LEAKING SITE
 TIME(sec)= 4446 PIXEL 1X1

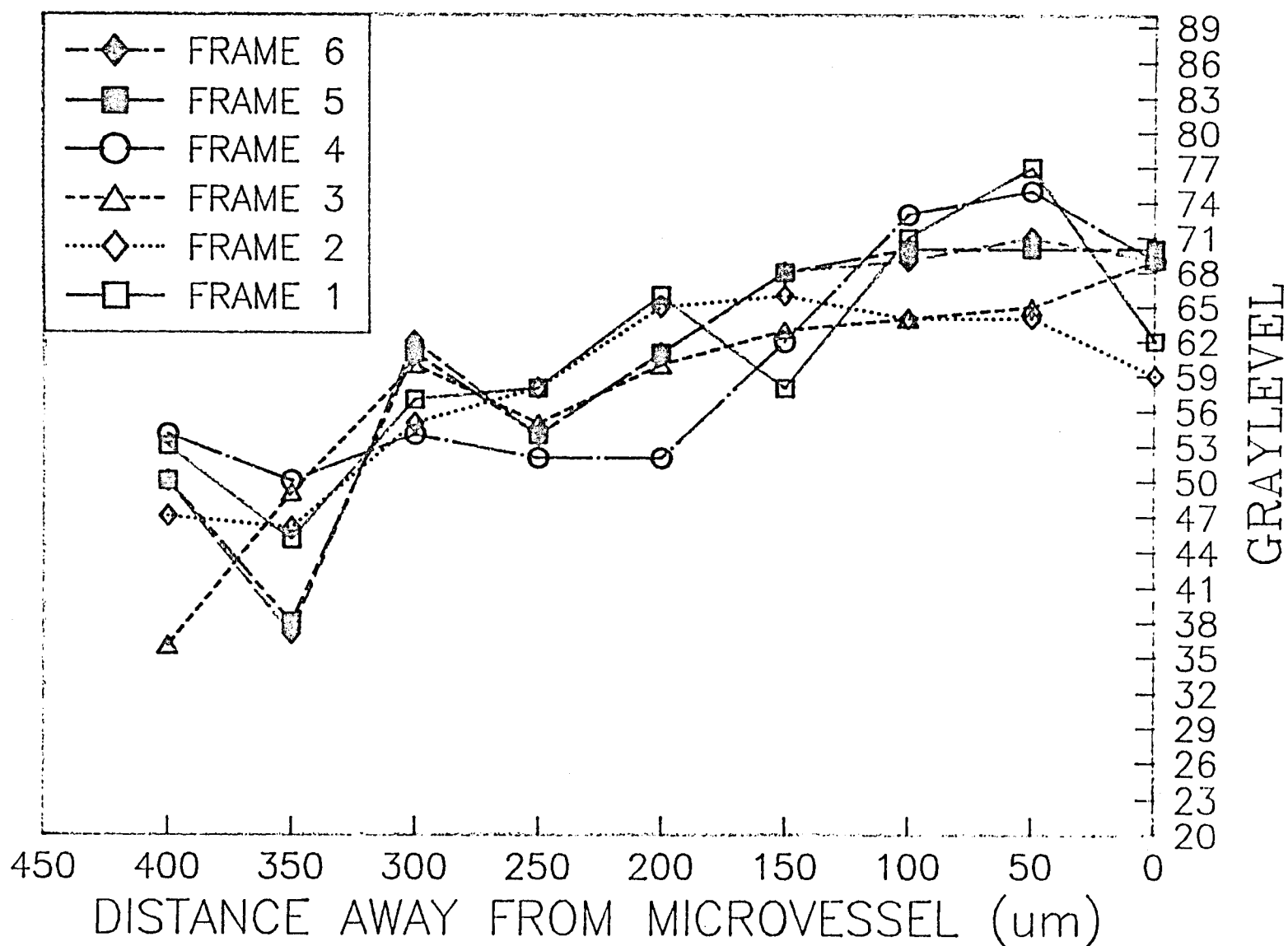


FIG.5.10 FITC-20 SECOND LEAKING SITE
 TIME(sec)= 4446 PIXEL 5X5

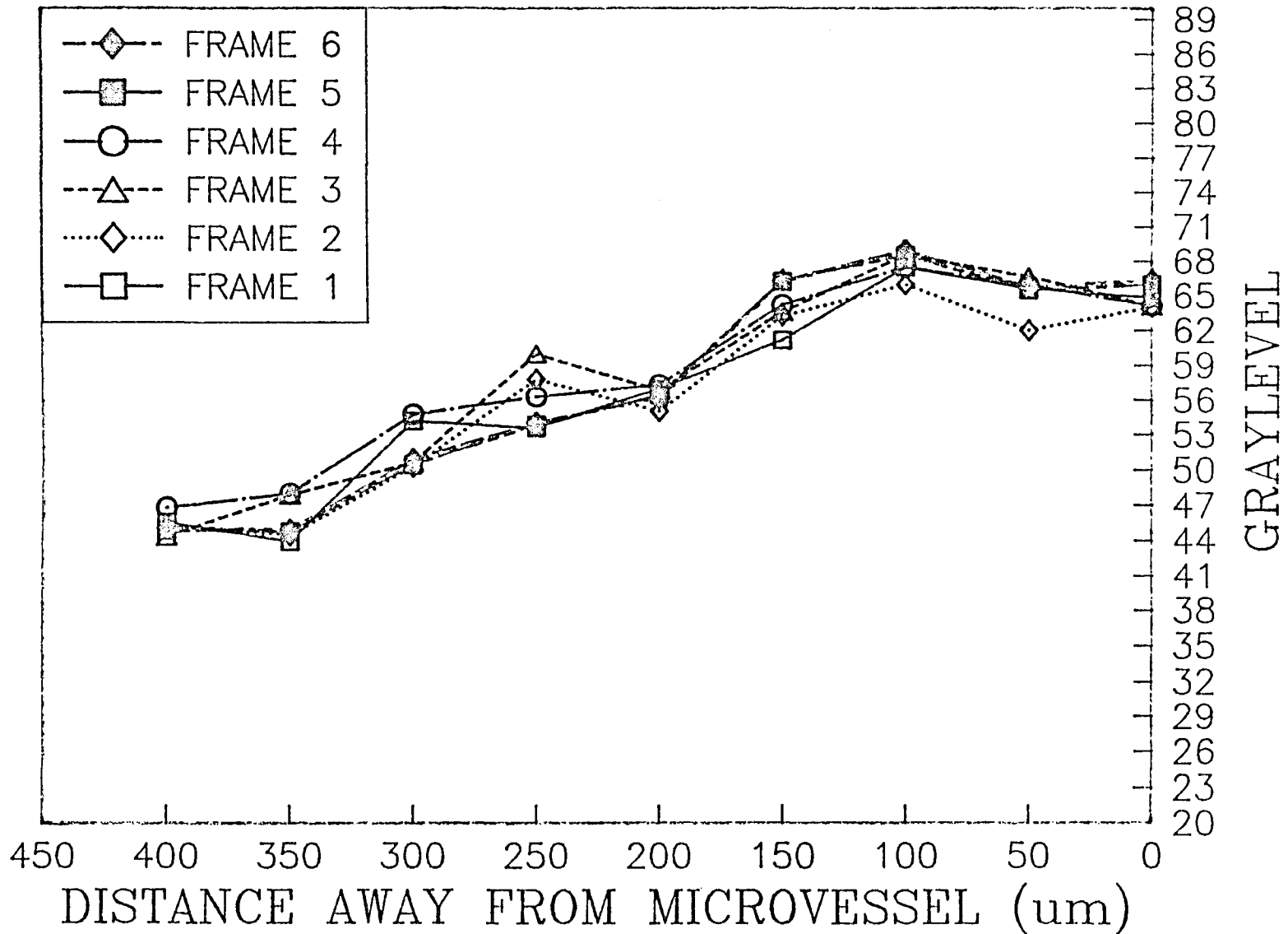


FIG.5.11 FITC-20 SECOND LEAKING SITE
 TIME(sec)= 4446 PIXEL 10X10

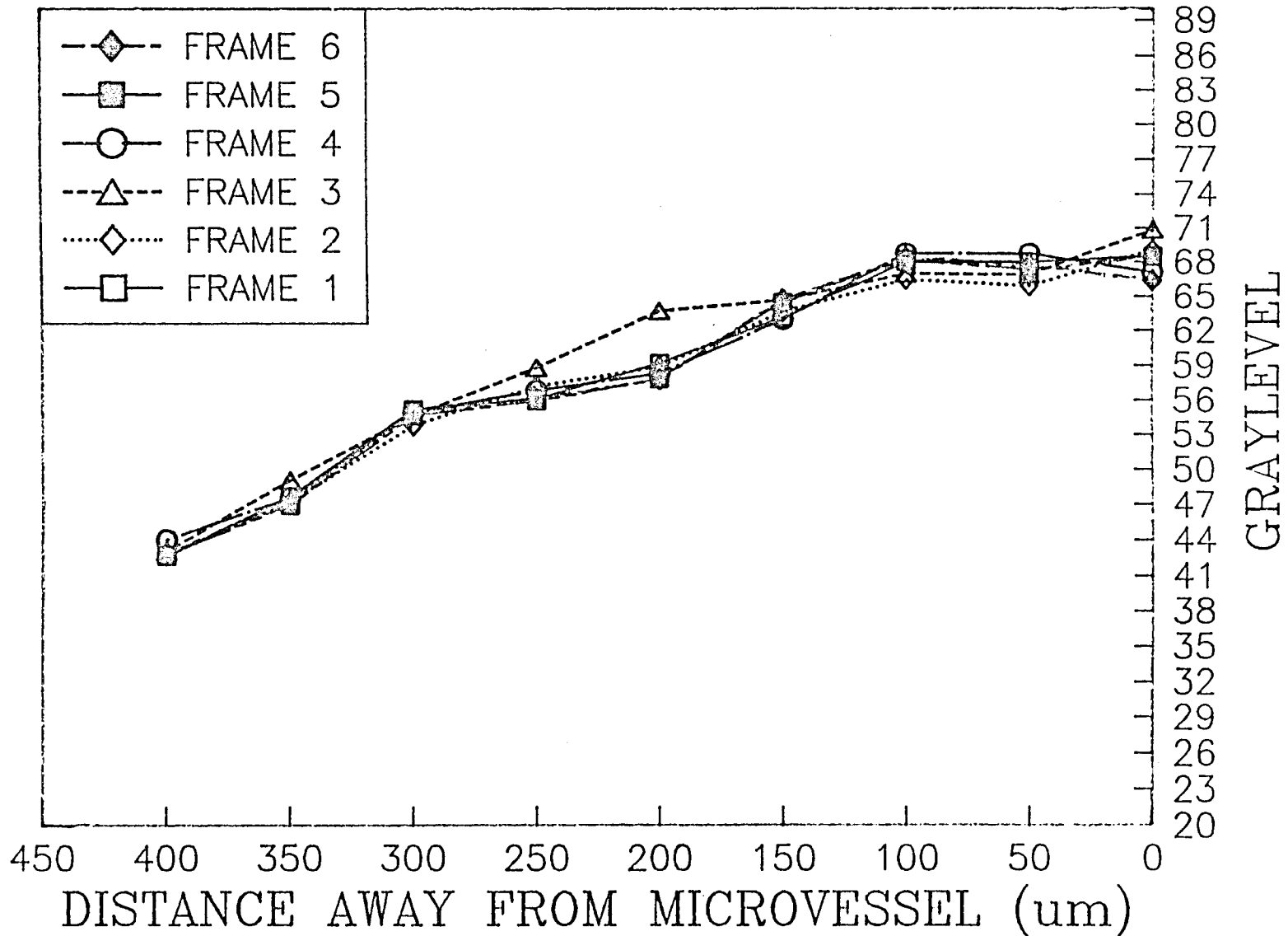


FIG.5.12 FITC-20 SECOND LEAKING SITE
 TIME(sec)= 5591 PIXEL 1X1

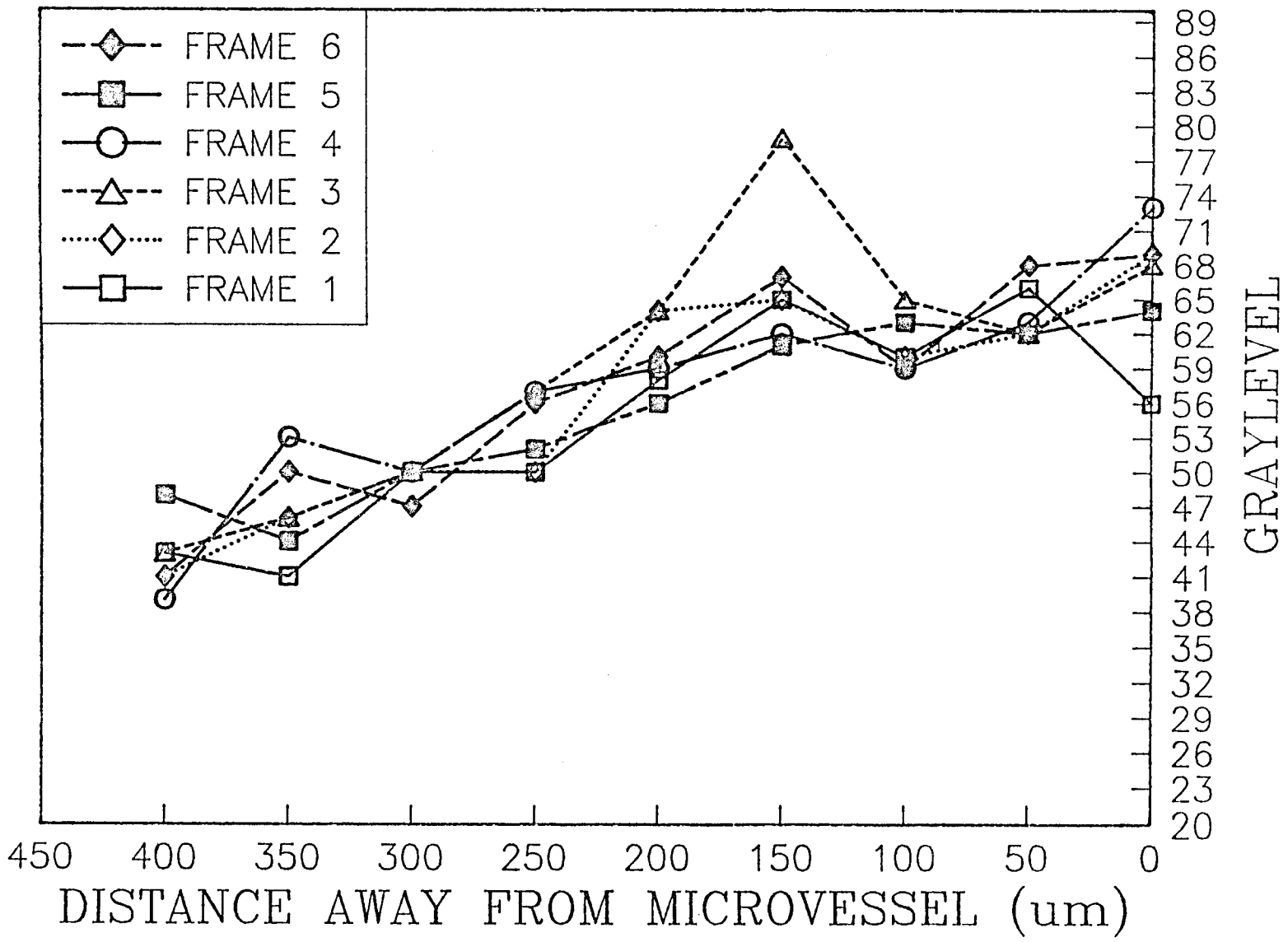


FIG.5.13 FITC-20 SECOND LEAKING SITE
TIME(sec)= 5591 PIXEL 5X5

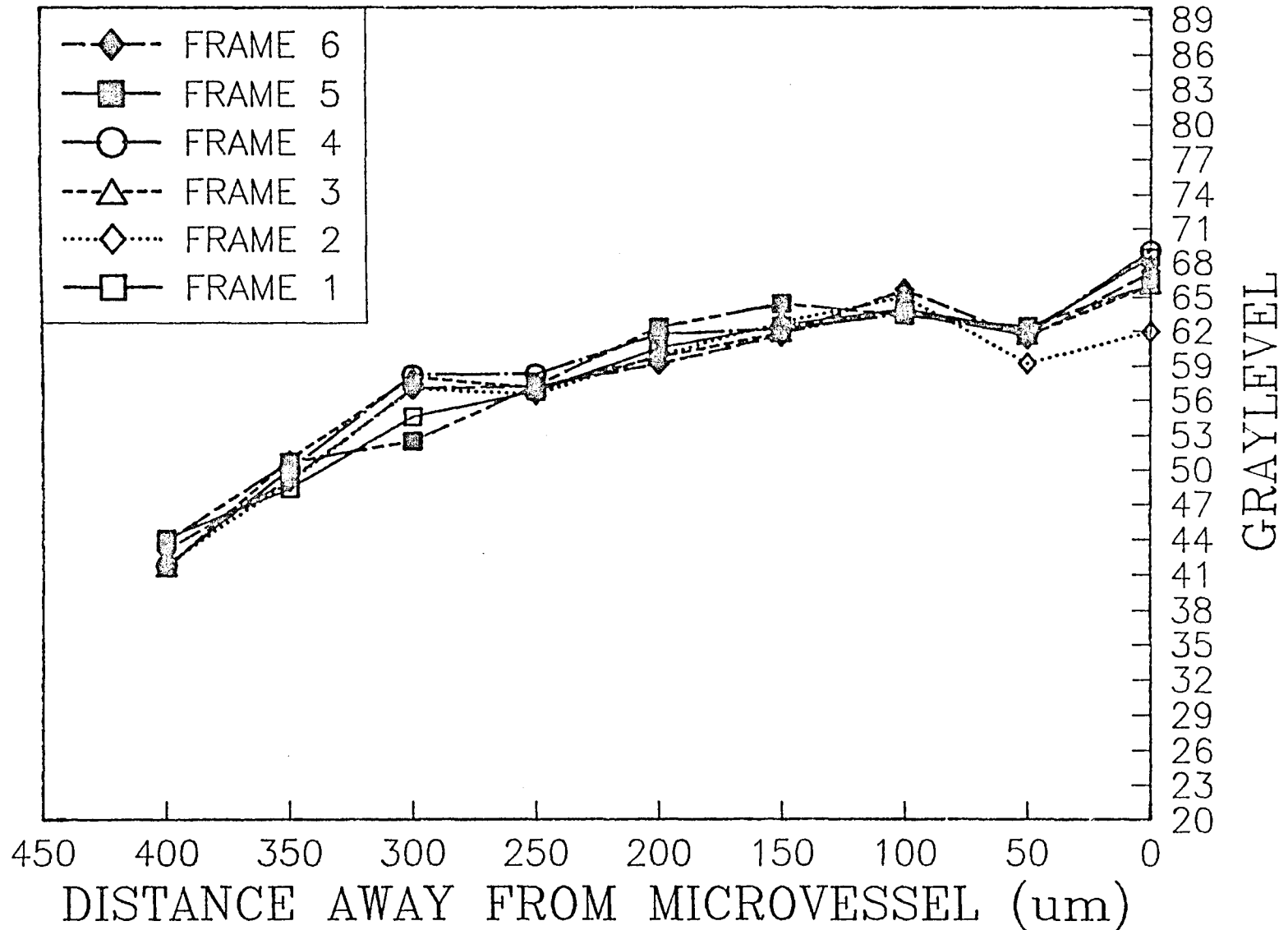


FIG.5.14 FITC-20 SECOND LEAKING SITE
TIME(sec)= 5591 PIXEL 10X10

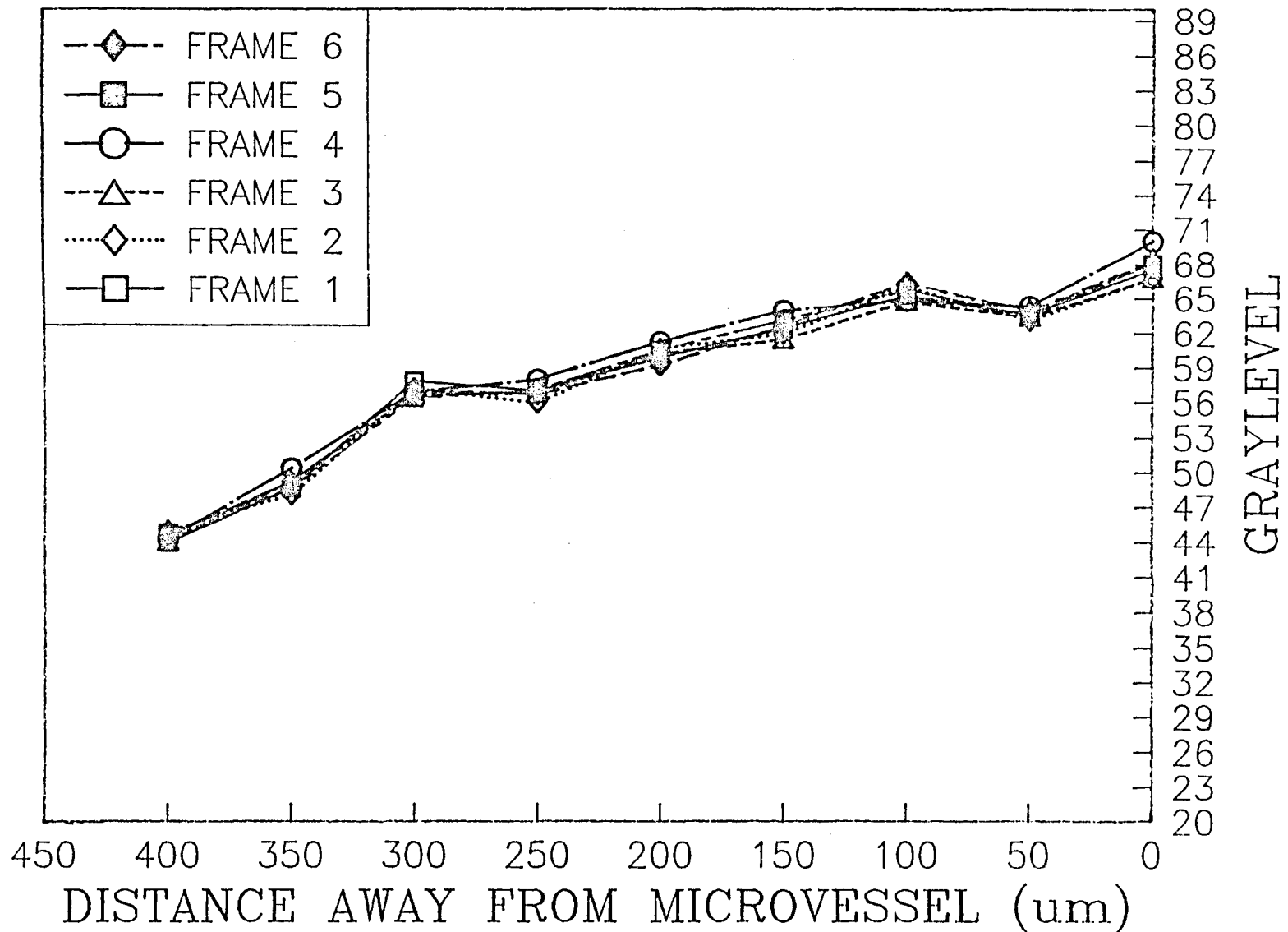


FIG.5.15 FITC-70 FIRST LEAKING SITE
TIME(sec)= 5895 PIXEL 1X1

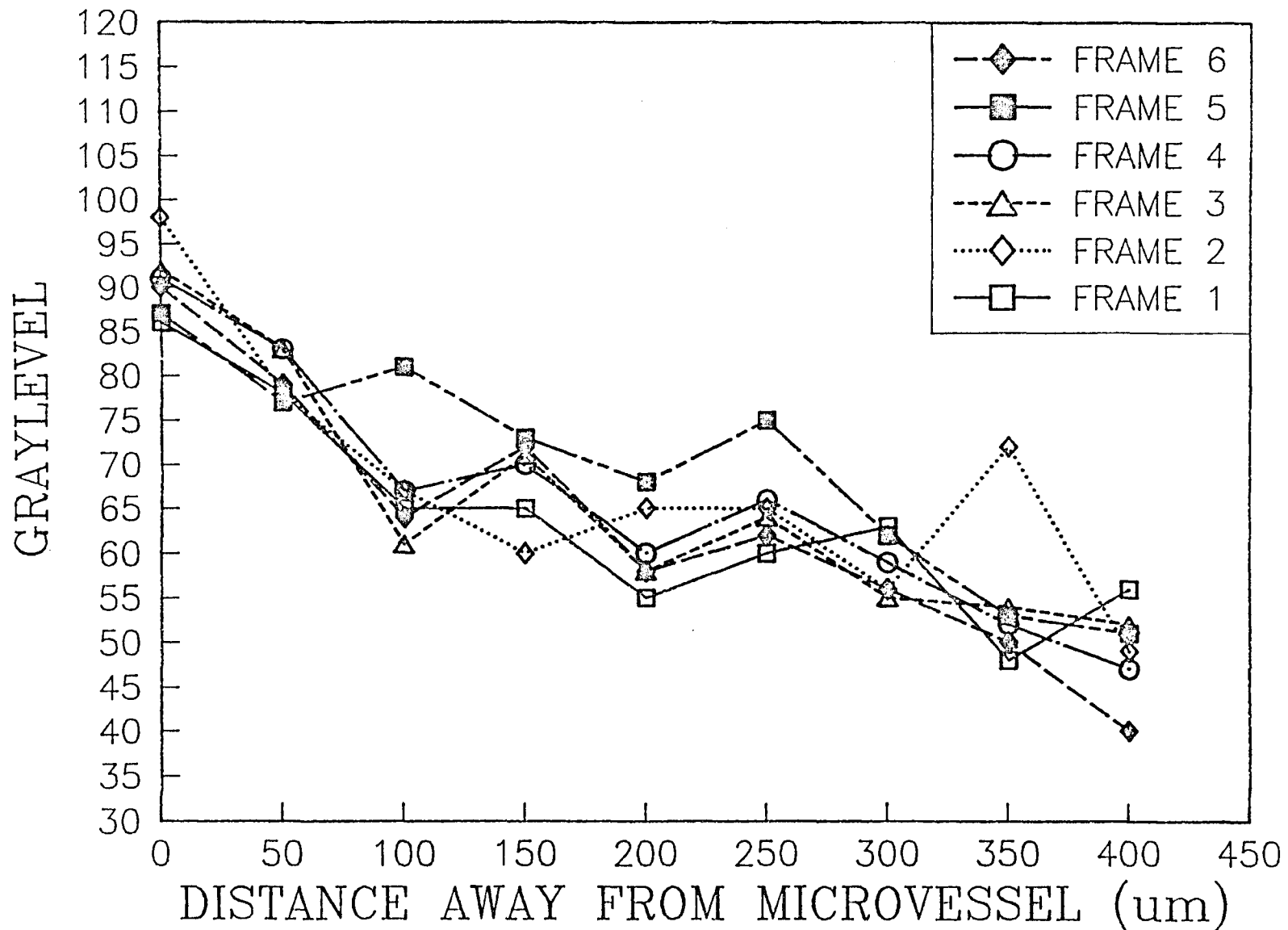


FIG.5.16 FITC-70 FIRST LEAKING SITE
TIME(sec)= 5895 PIXEL 5X5

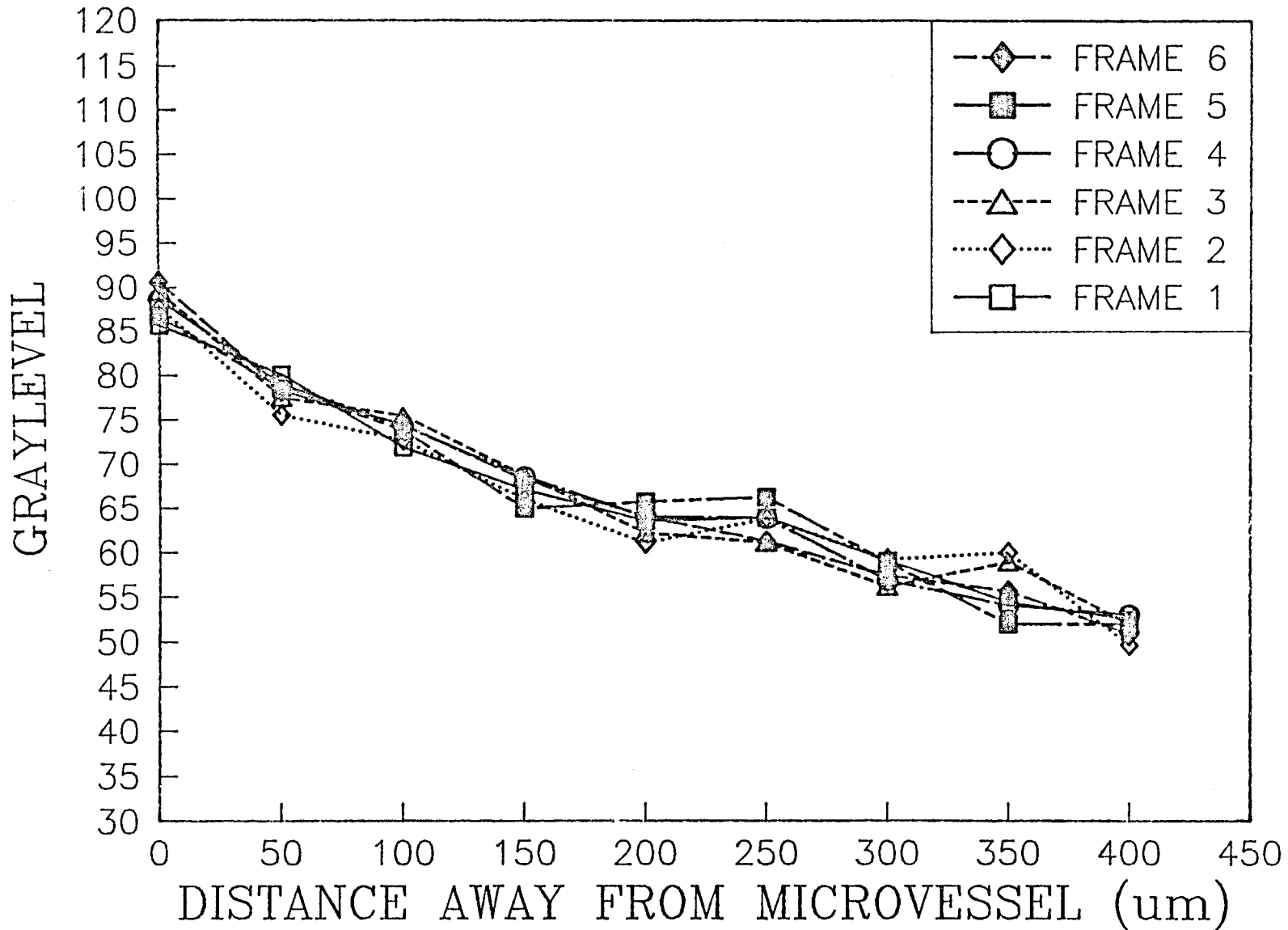


FIG.5.17 FITC-70 FIRST LEAKING SITE
TIME(sec)= 5895 PIXEL 10X10

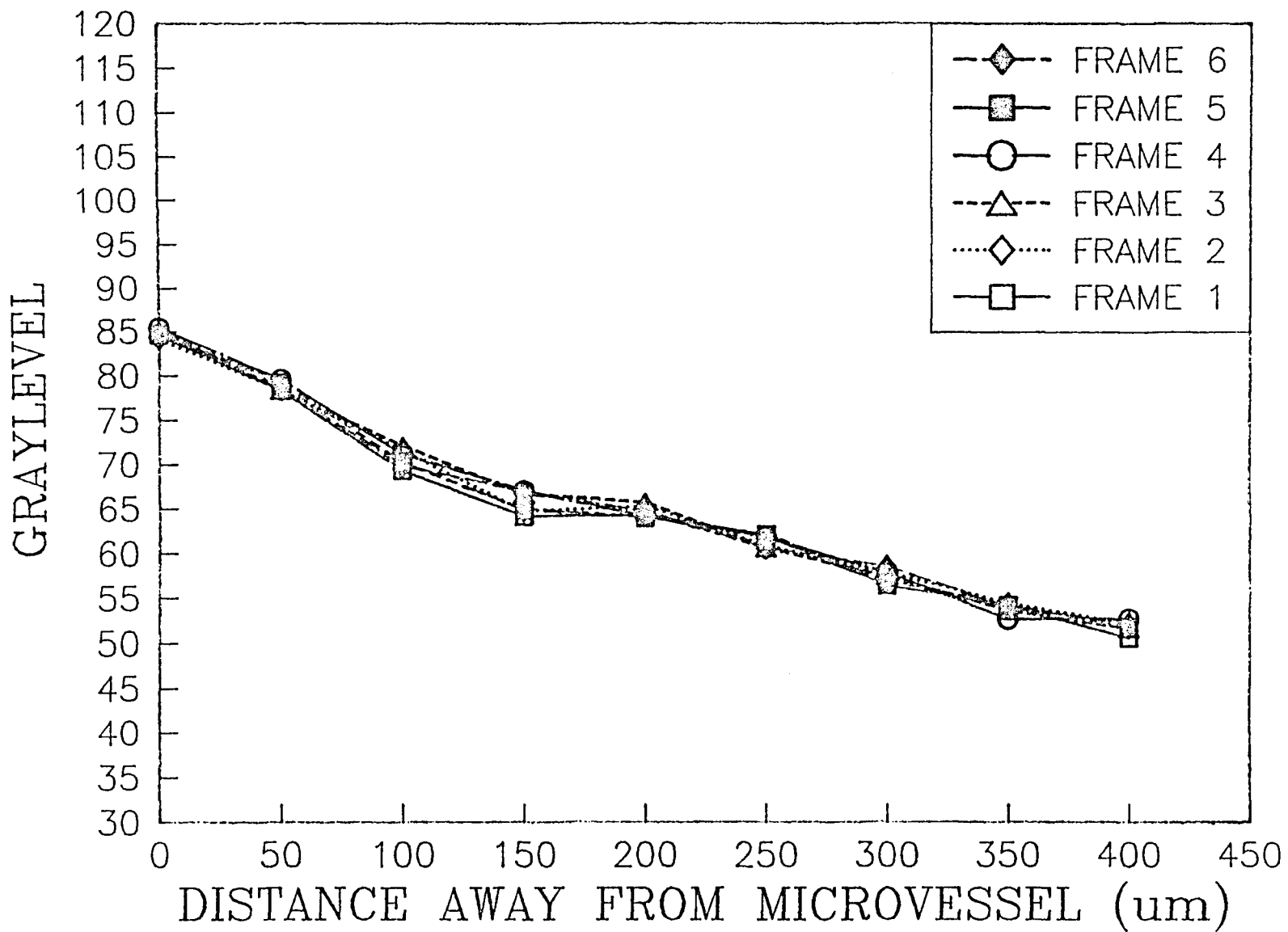


FIG.5.18 FITC-70 FIRST LEAKING SITE
TIME(sec)= 7950 PIXEL 1X1

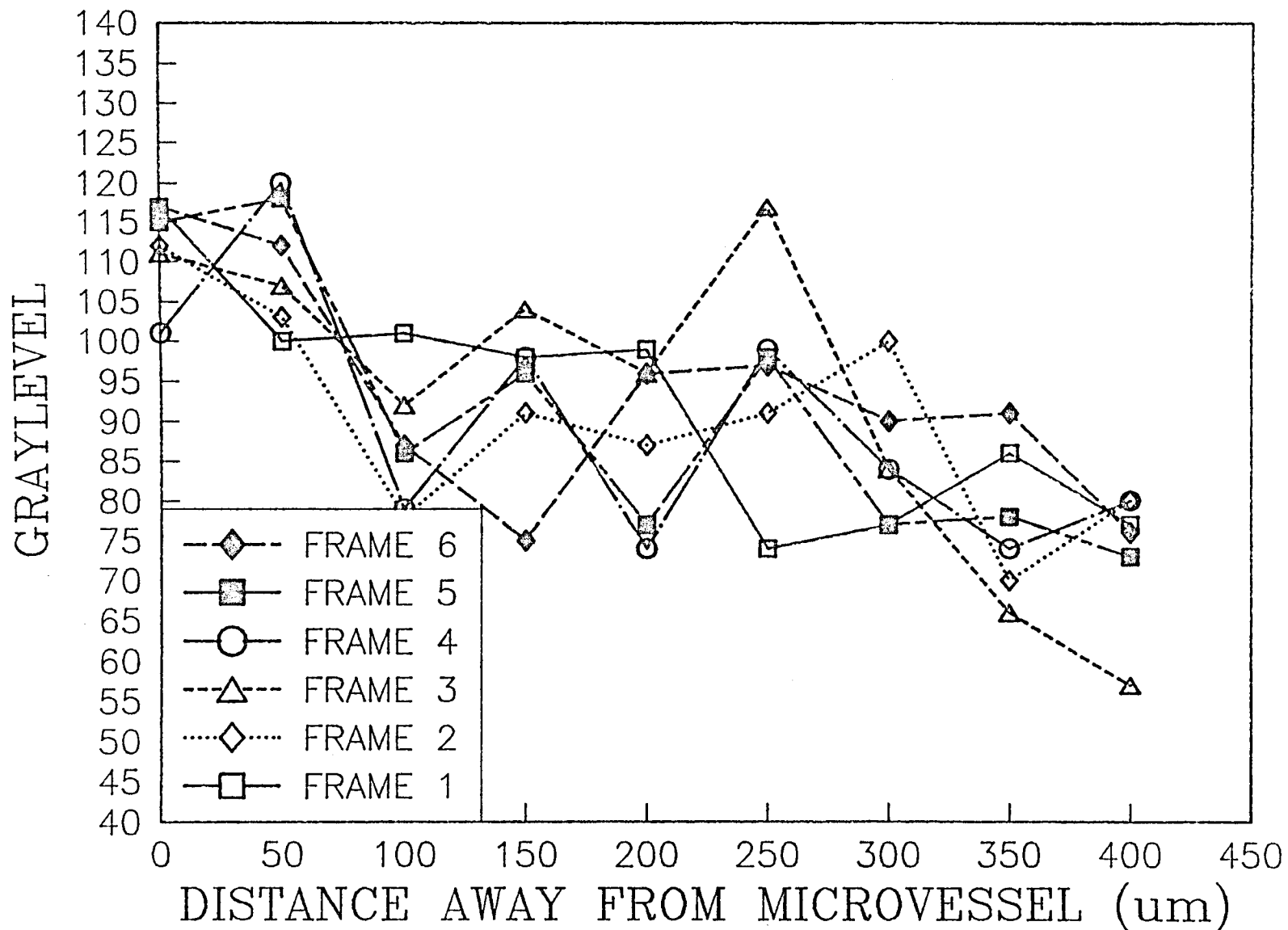


FIG.5.19 FITC-70 FIRST LEAKING SITE
TIME(sec)= 7950 PIXEL 5X5

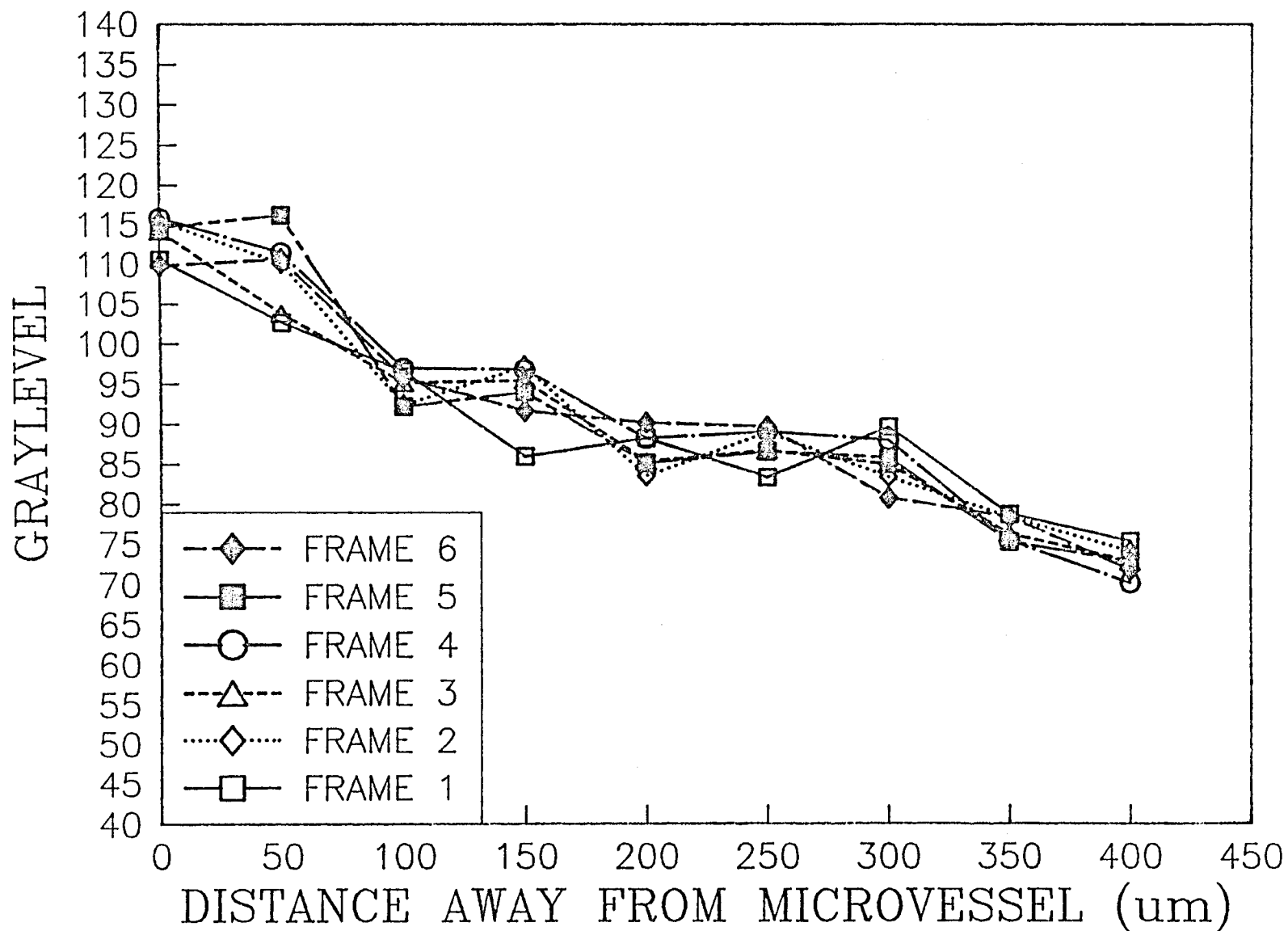


FIG.5.20 FITC-70 FIRST LEAKING SITE
TIME(sec)= 7950 PIXEL 10X10

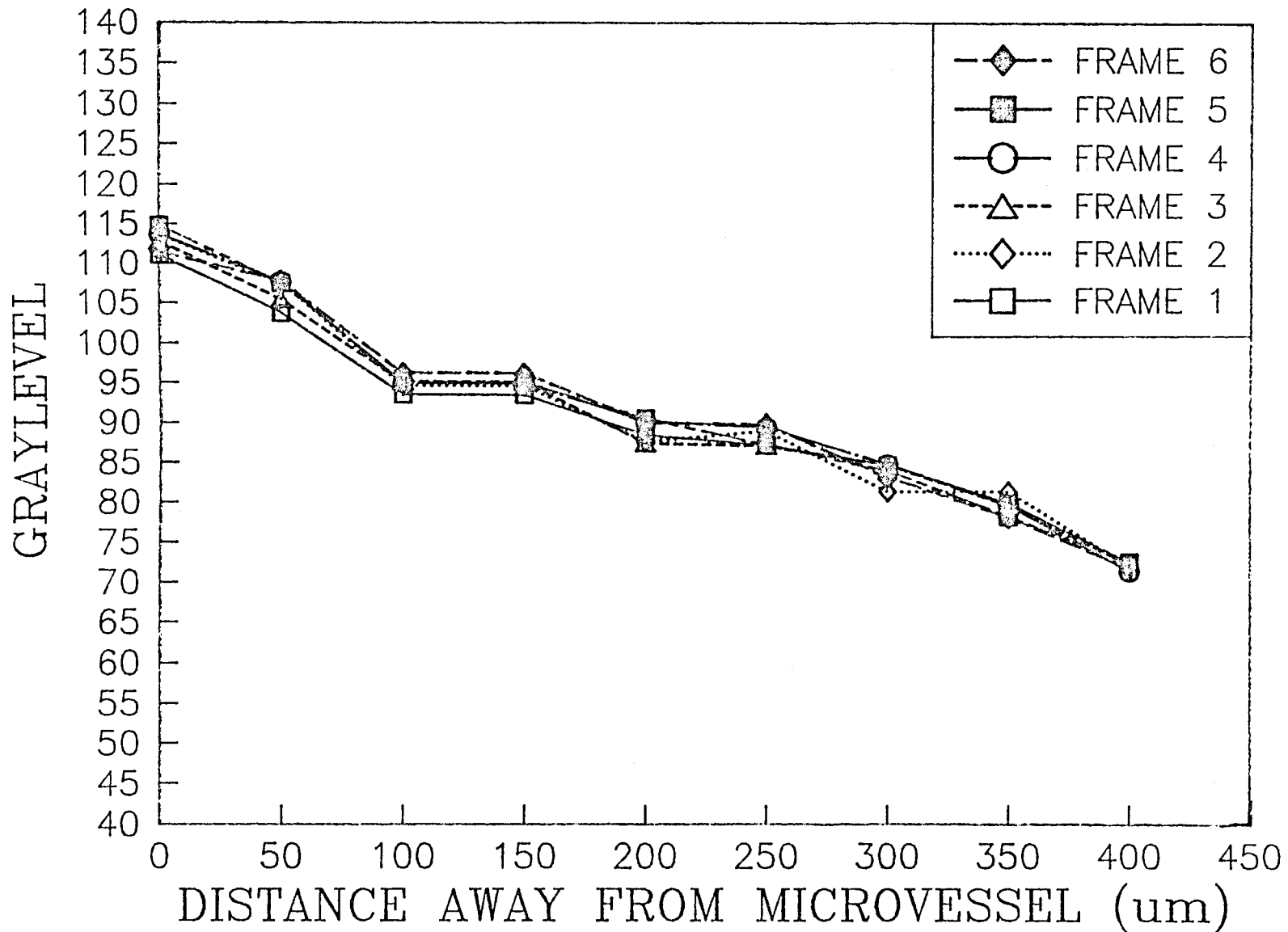


FIG.5.21 FITC-70 SECOND LEAKING SITE
TIME(sec)= 4320 PIXEL 1X1

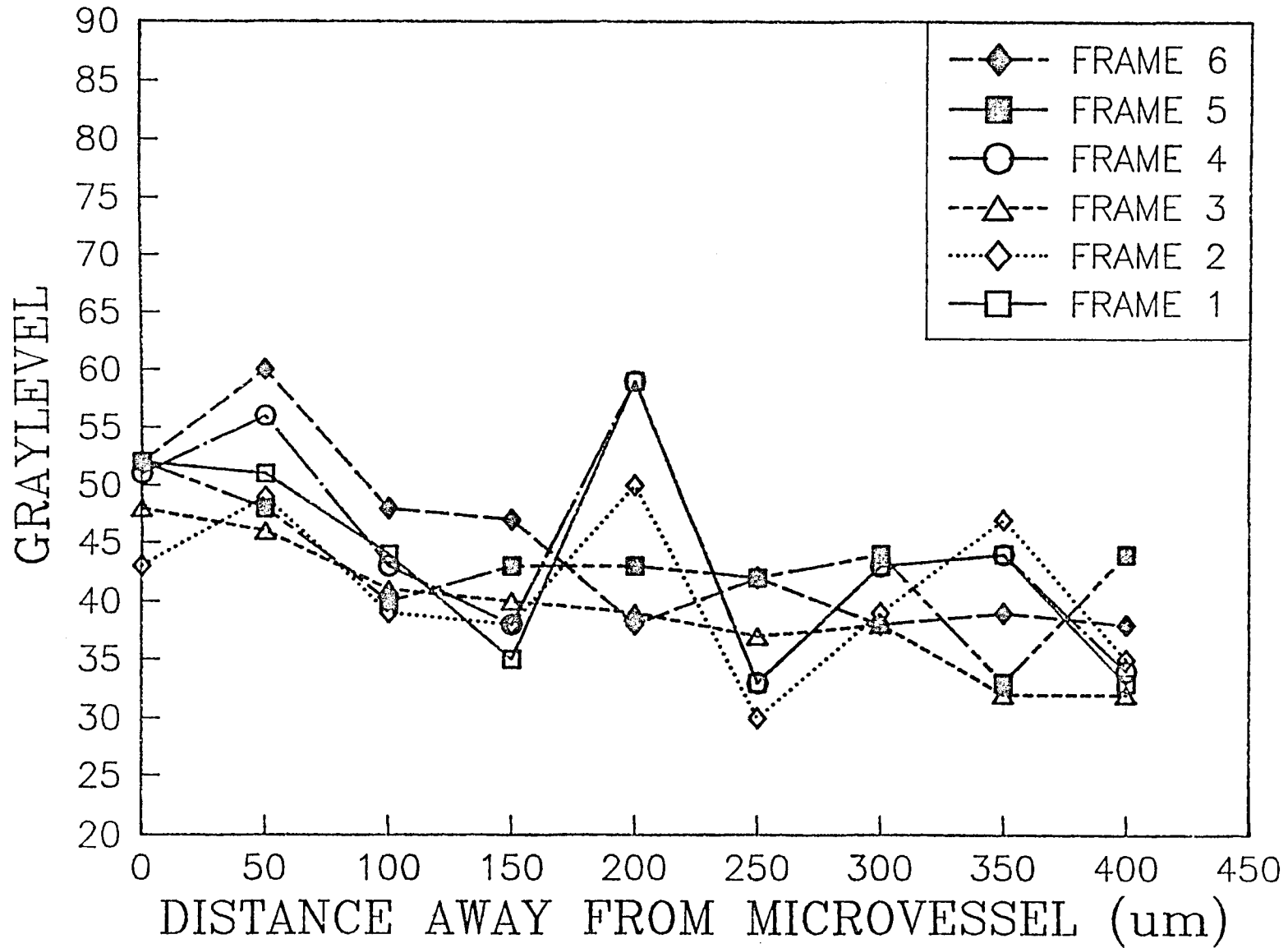


FIG.5.22 FITC-70 SECOND LEAKING SITE
TIME(sec)= 4320 PIXEL 5X5

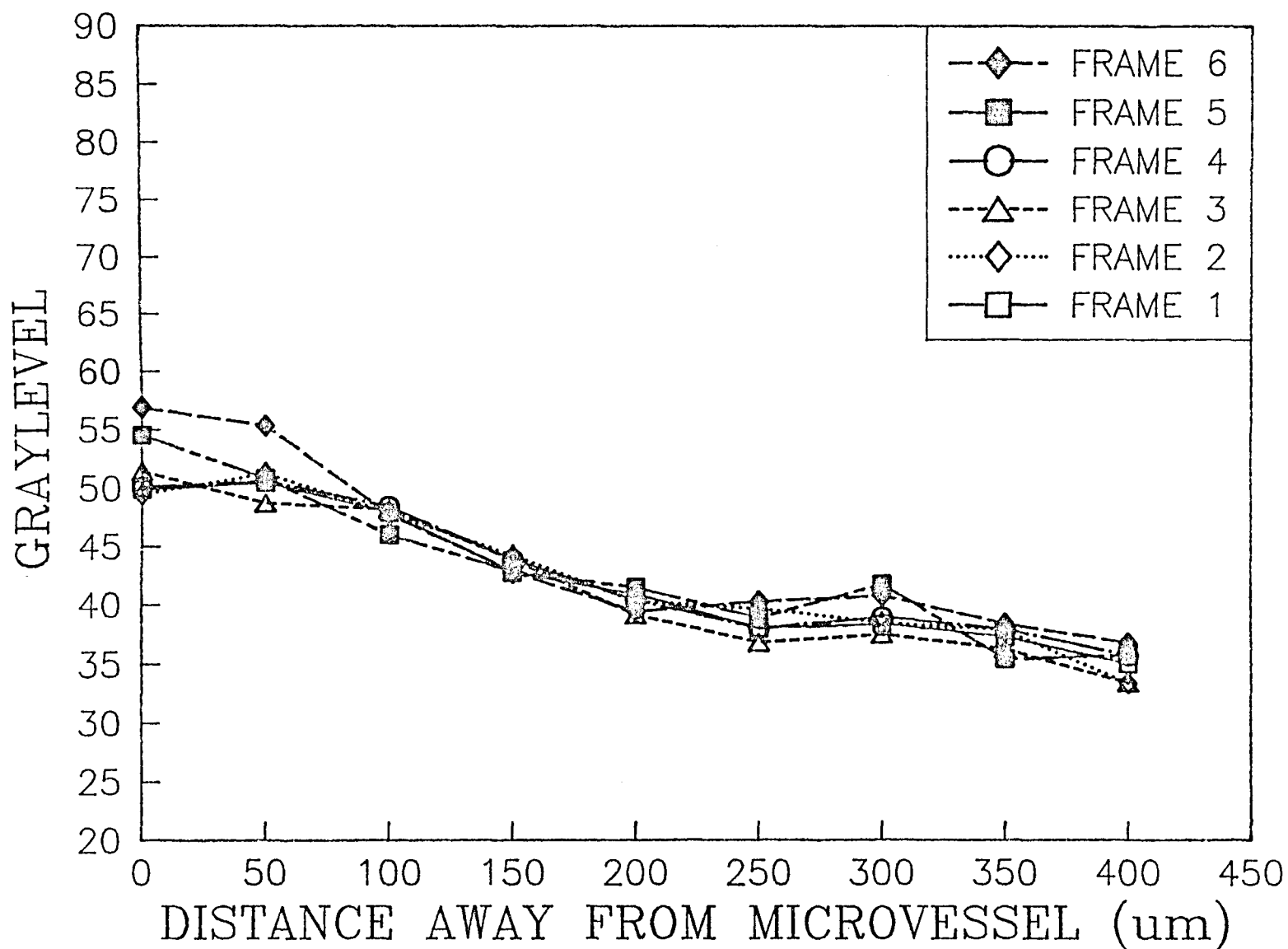


FIG.5.23 FITC-70 SECOND LEAKING SITE
TIME(sec)= 4320 PIXEL 10X10

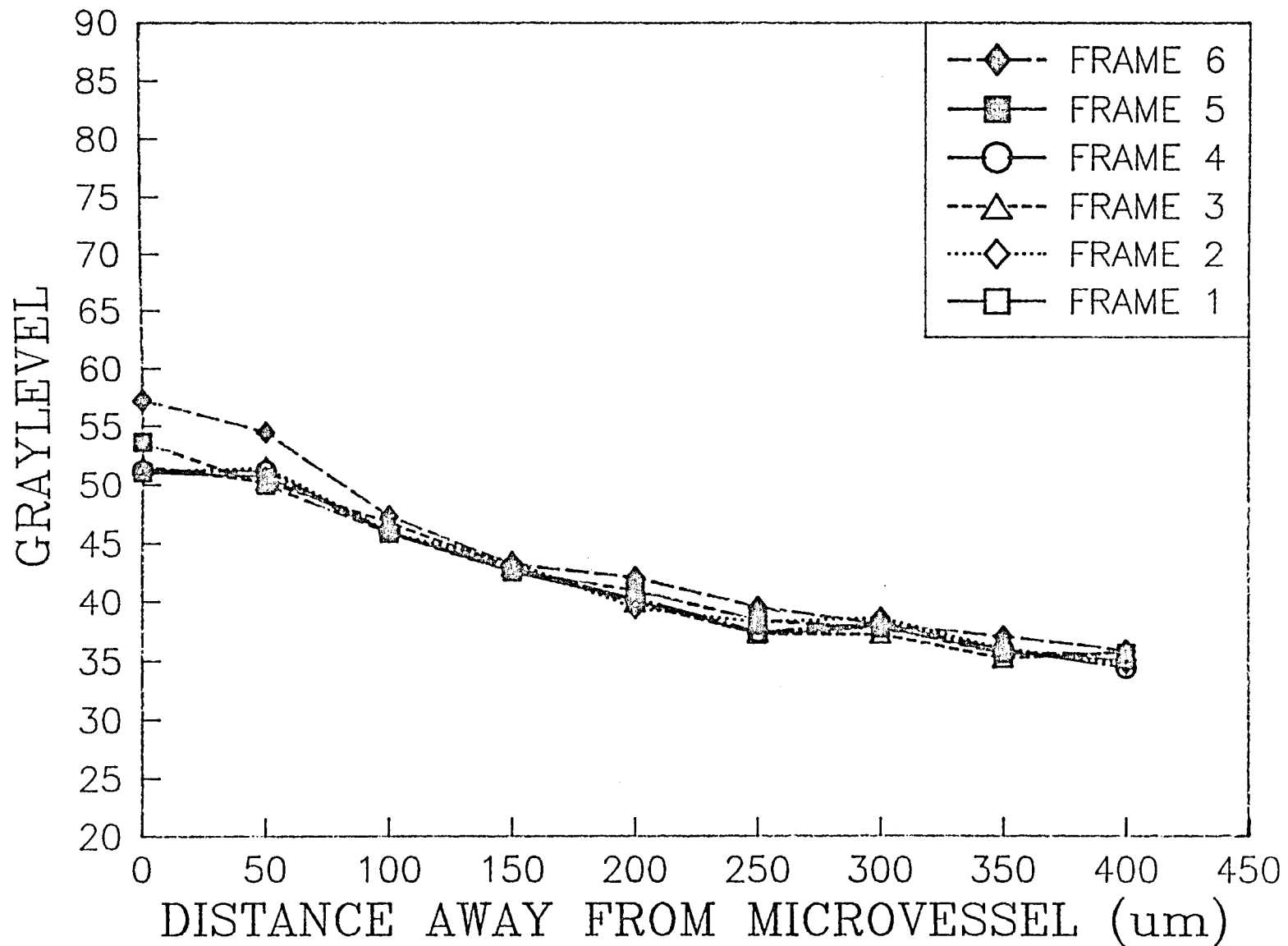


FIG.5.24 FITC-70 SECOND LEAKING SITE
TIME(sec)= 6675 PIXEL 1X1

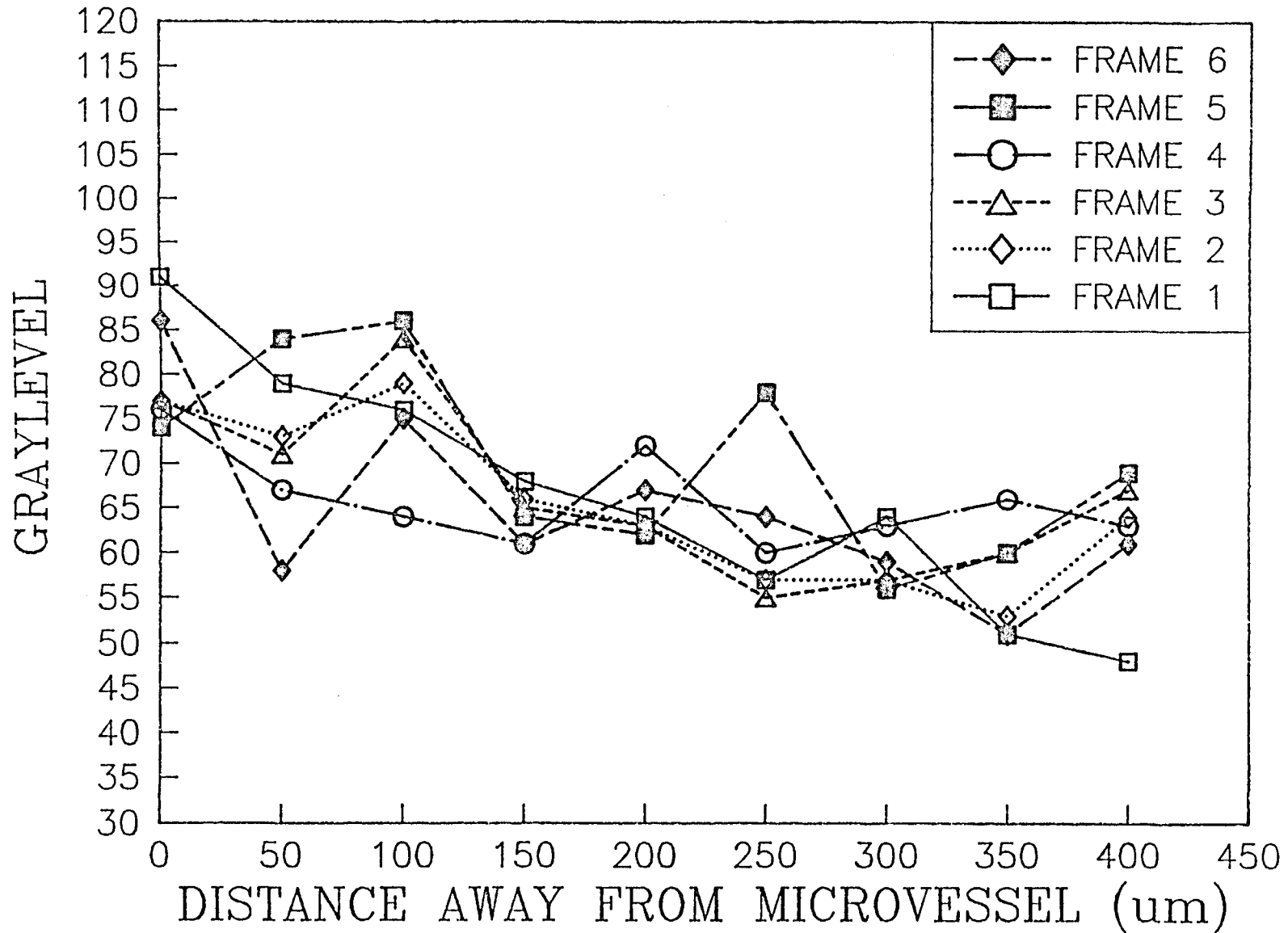


FIG.5.25 FITC-70 SECOND LEAKING SITE
TIME(sec)= 6675 PIXEL 5X5

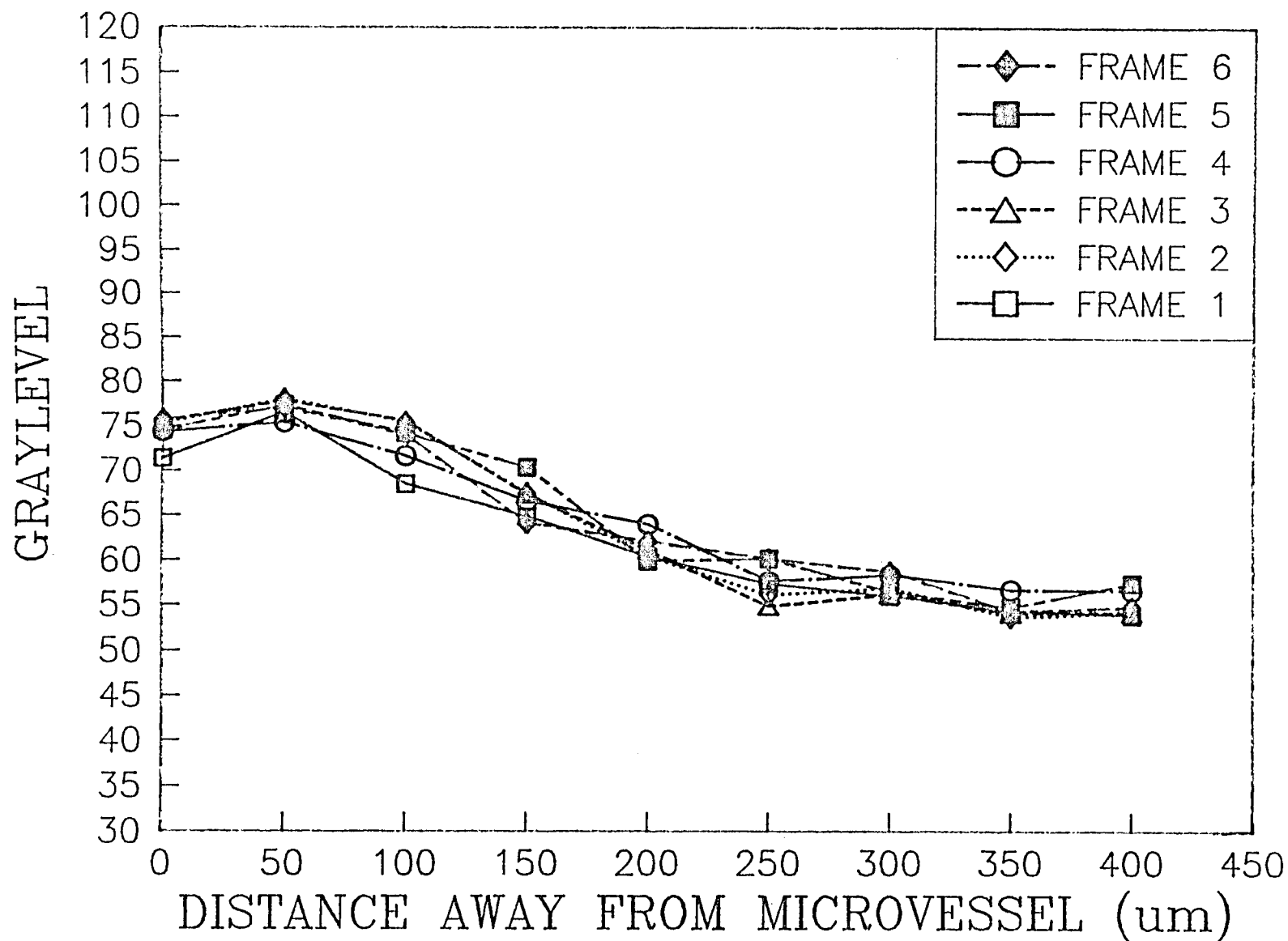


FIG.5.26 FITC-70 SECOND LEAKING SITE
TIME(sec)= 6675 PIXEL 10X10

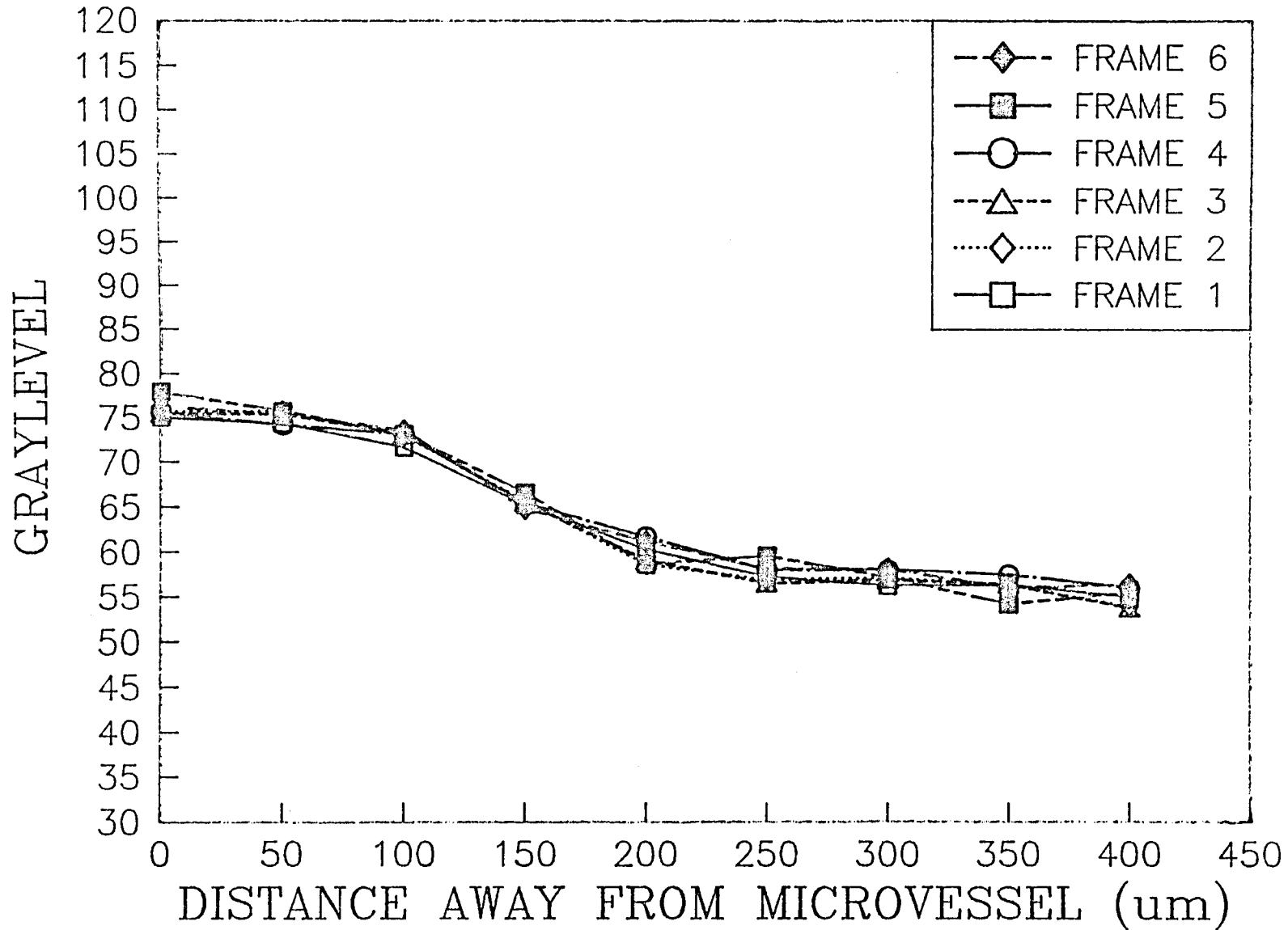


FIG.5.27 FITC-20 FIRST LEAKING SITE
TIME(sec)= 2711 PIXEL 1 X 1

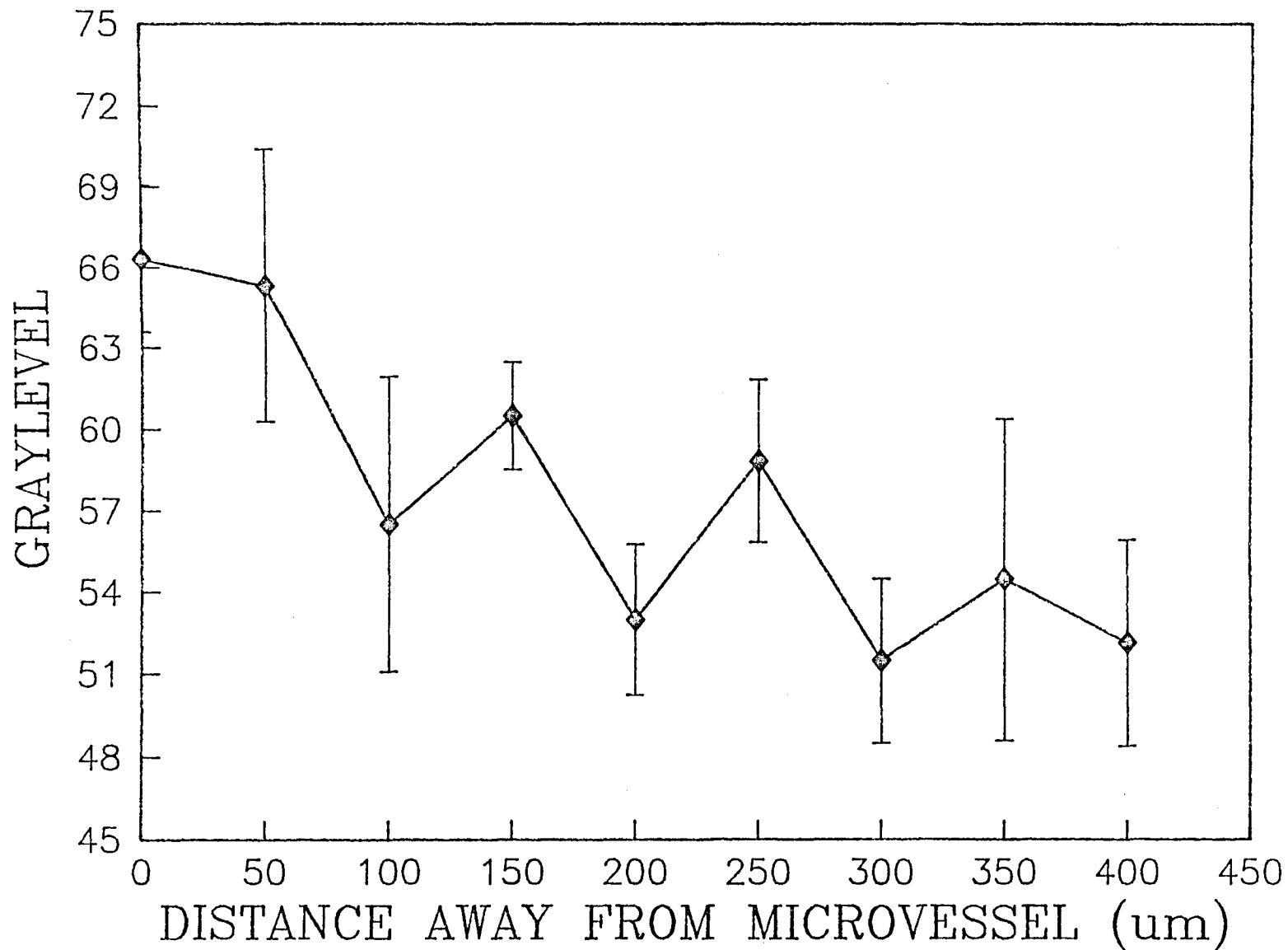


FIG.5.28 FITC-20 FIRST LEAKING SITE
TIME(sec)= 2711 PIXEL 5 X 5

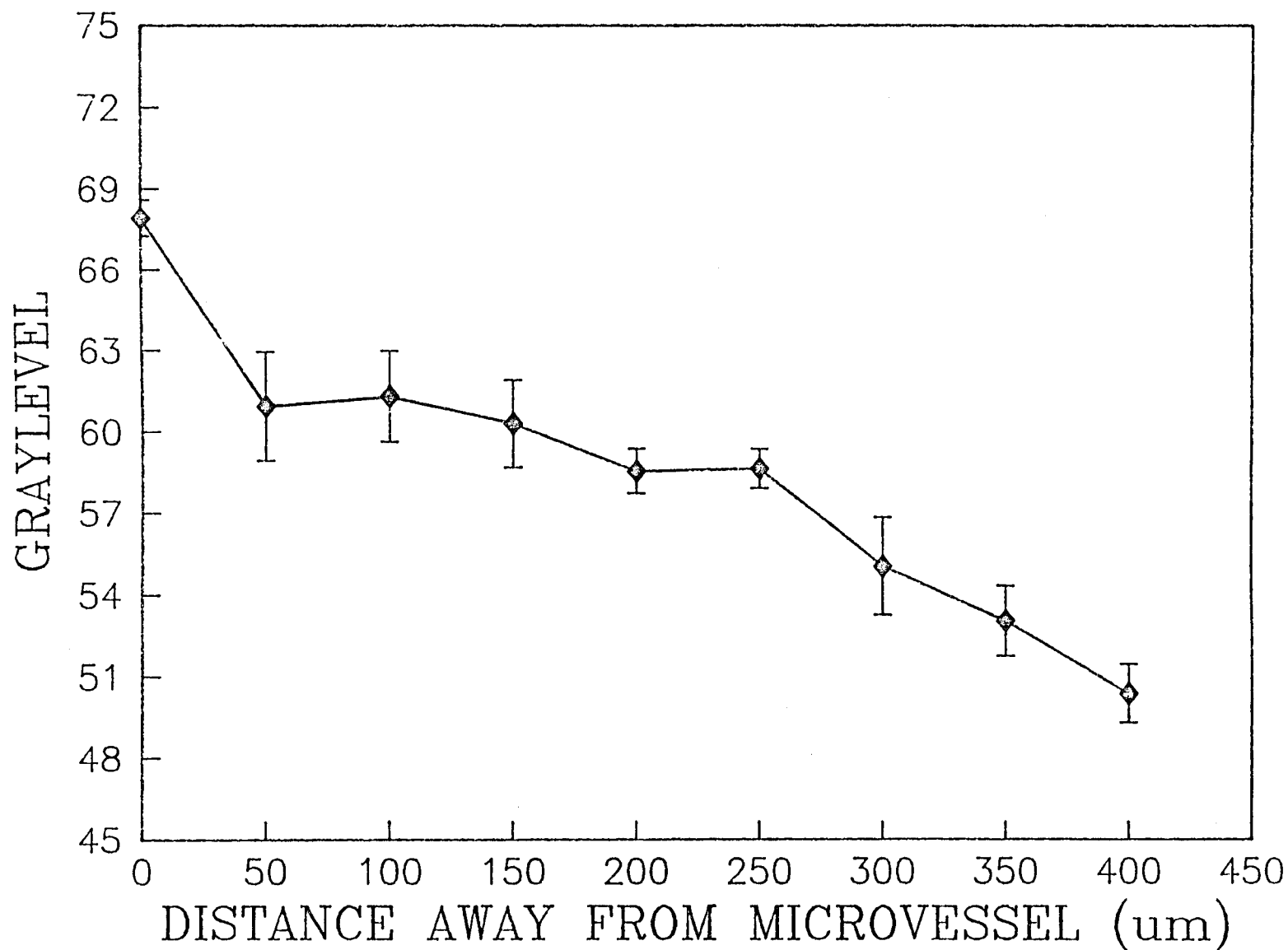


FIG.5.29 FITC-20 FIRST LEAKING SITE
TIME(sec)= 2711 PIXEL 10 X10

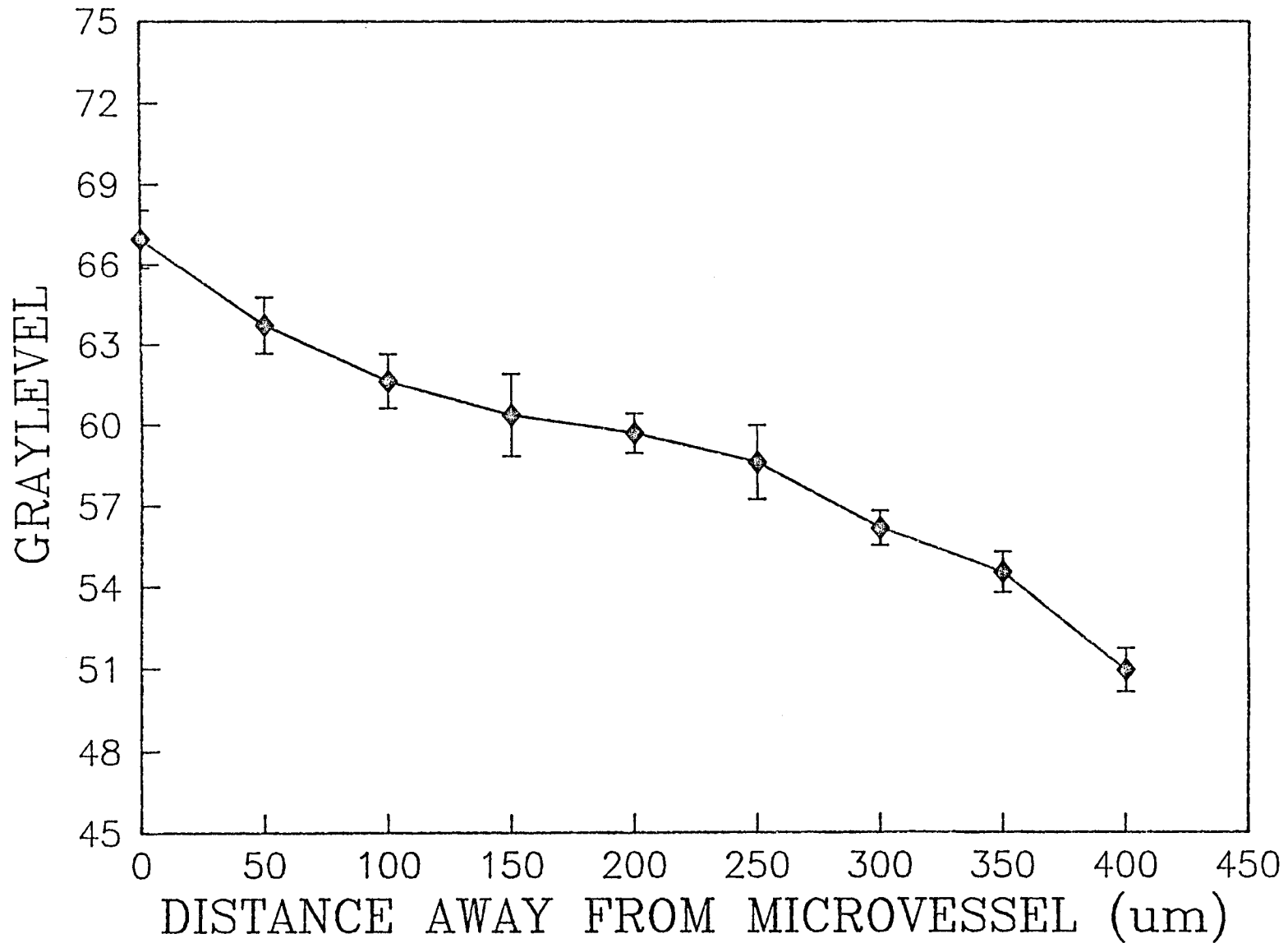


FIG.5.30 FITC-20 FIRST LEAKING SITE
TIME(sec)= 4401 PIXEL 1 X 1

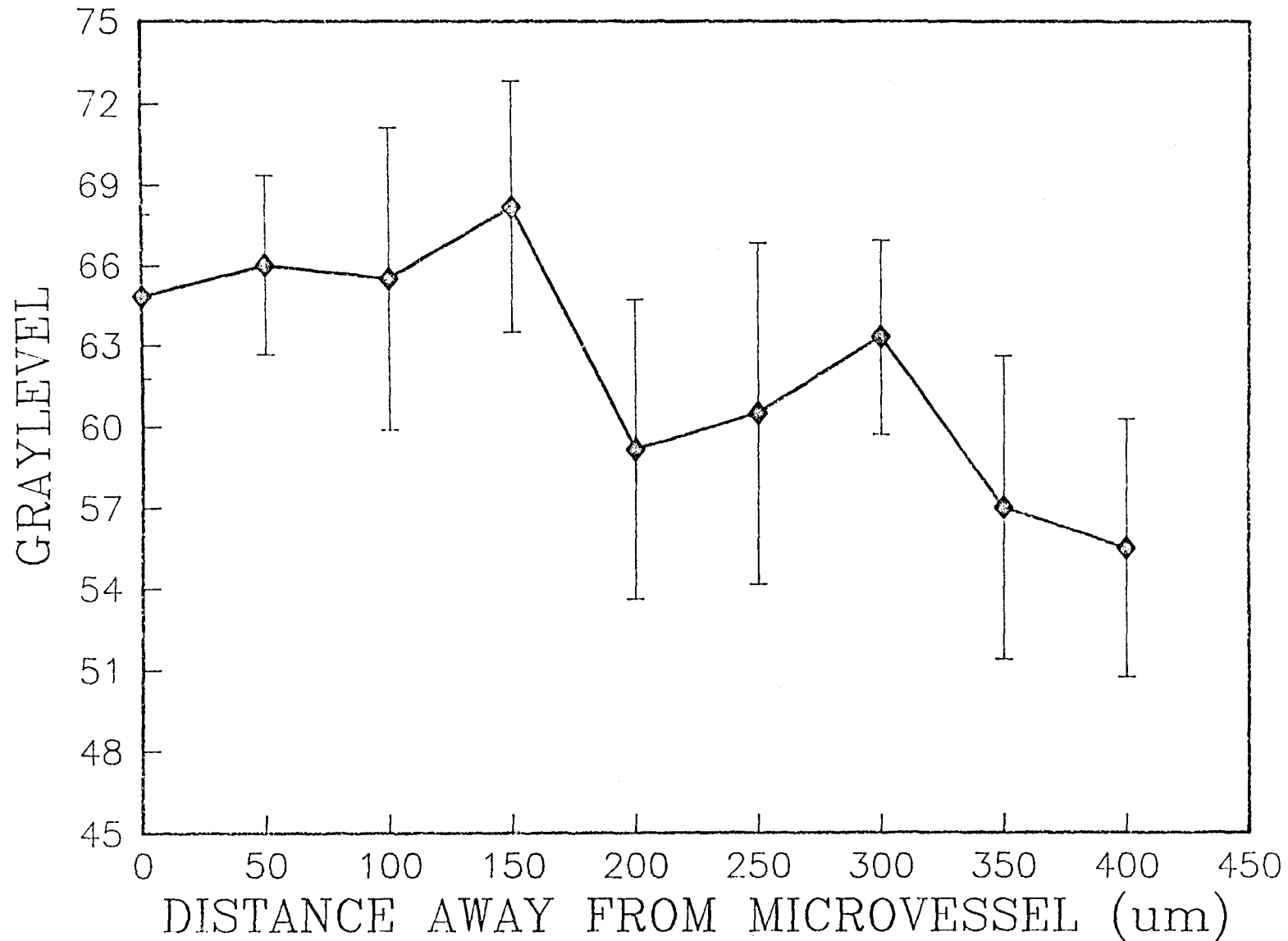


FIG.5.31 FITC-20 FIRST LEAKING SITE
TIME(sec)=4401 PIXEL 5 X 5

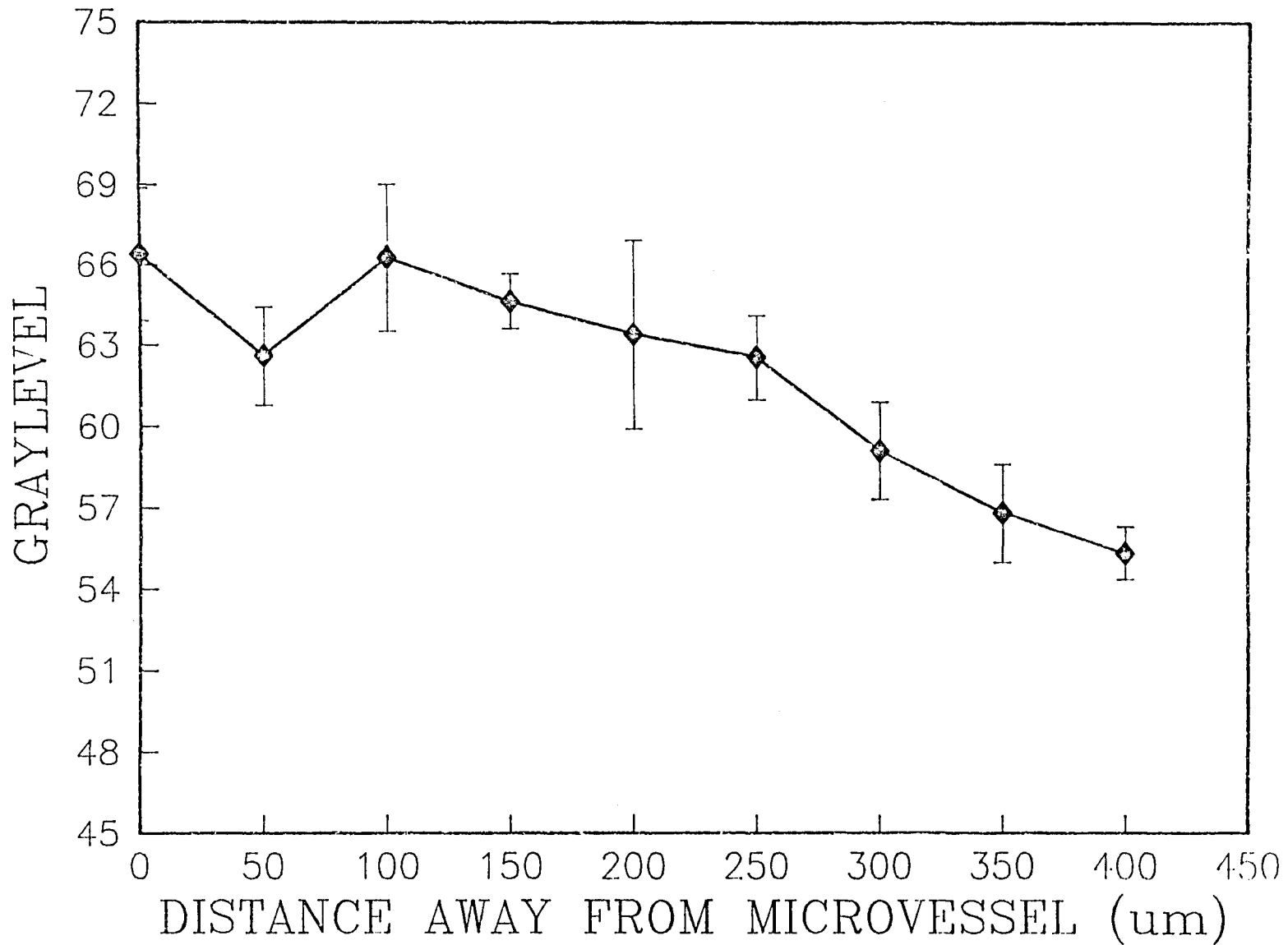


FIG.5.32 FITC-20 FIRST LEAKING SITE
TIME(sec)=4401 PIXEL 10 X 10

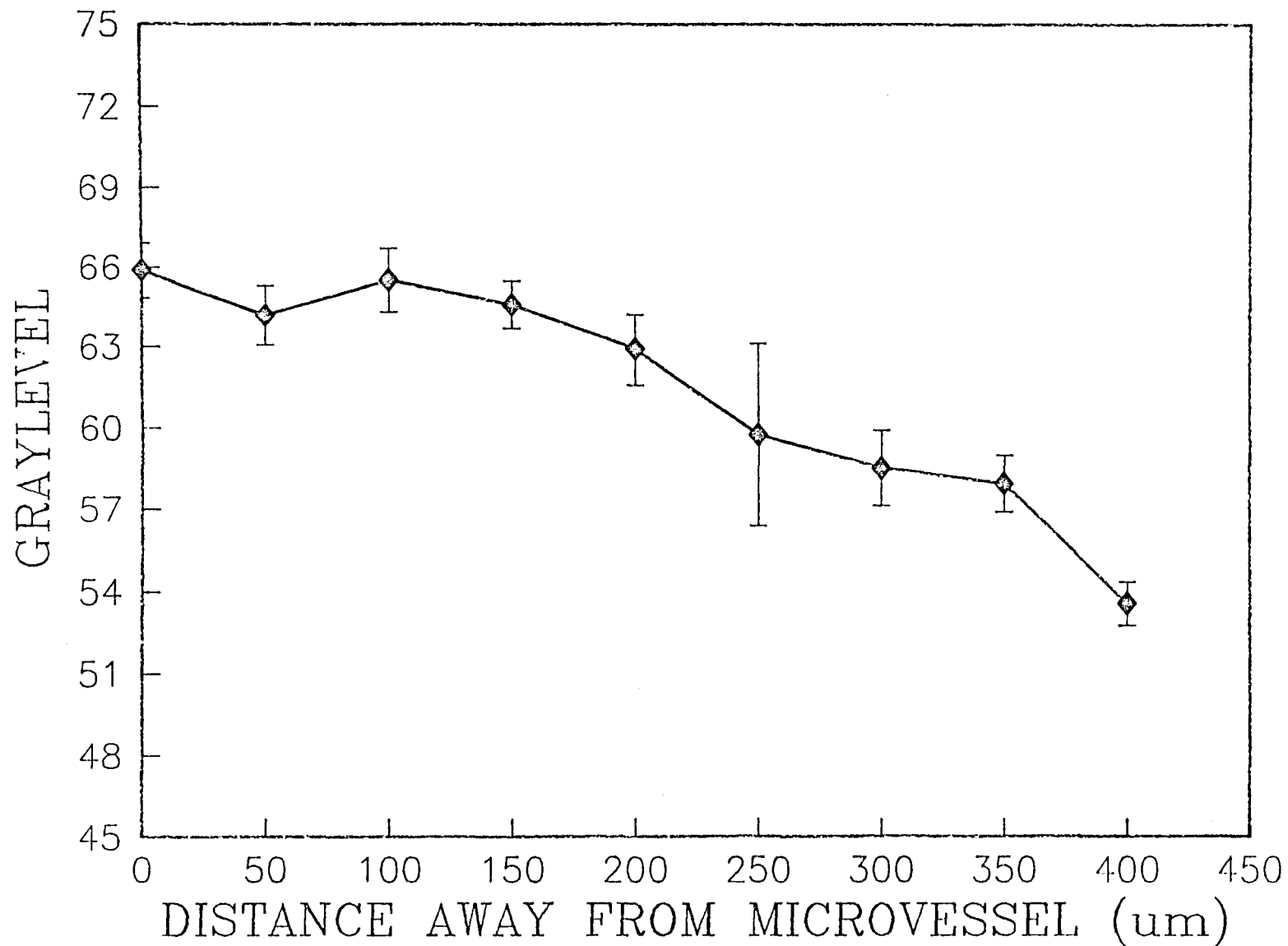


FIG.5.33 FITC-20 SECOND LEAKING SITE
TIME(sec)=4446 PIXEL 1 X 1

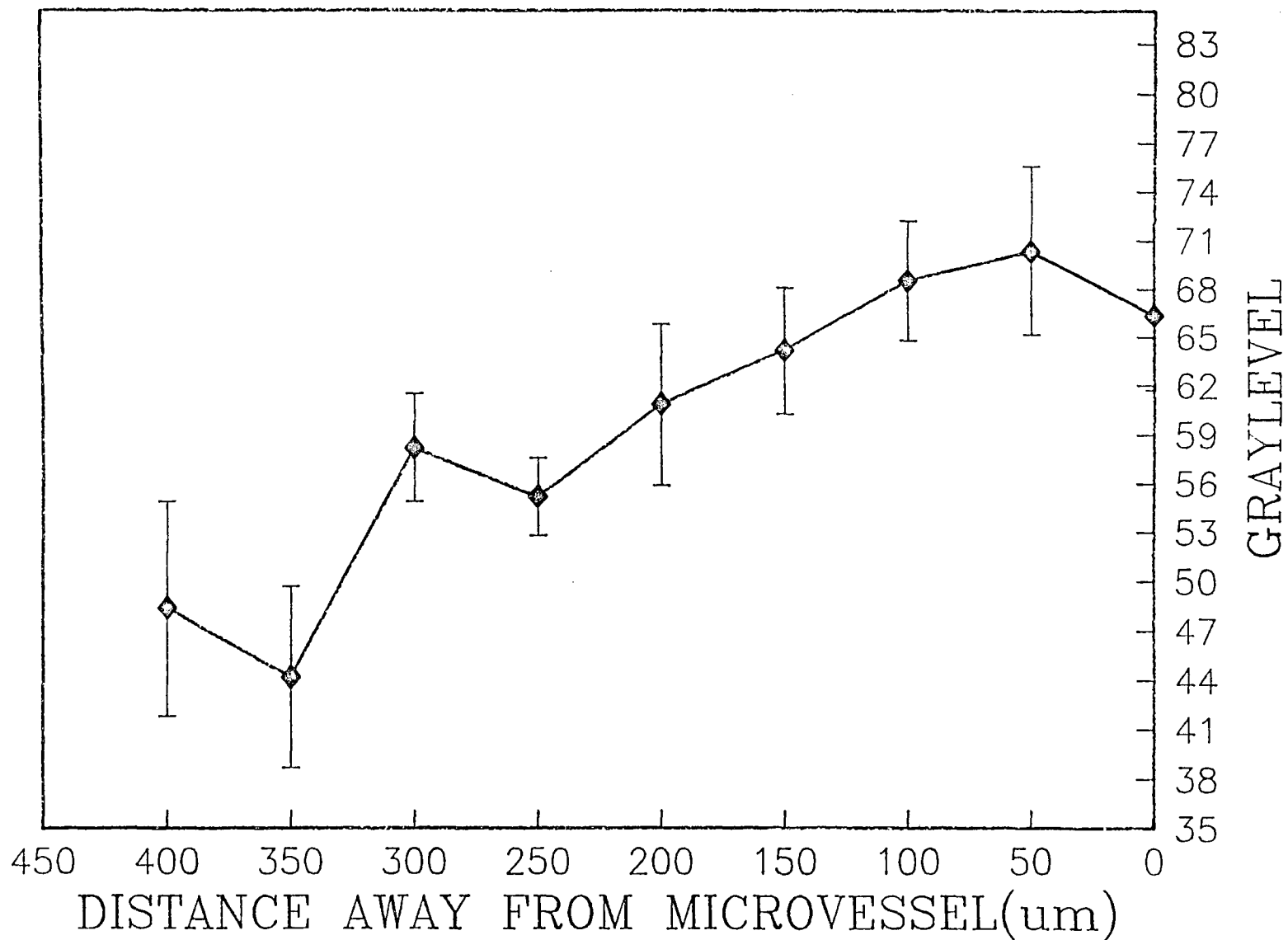


FIG.5.34 FITC-20 SECOND LEAKING SITE
TIME(sec)=4446 PIXEL 5 X 5

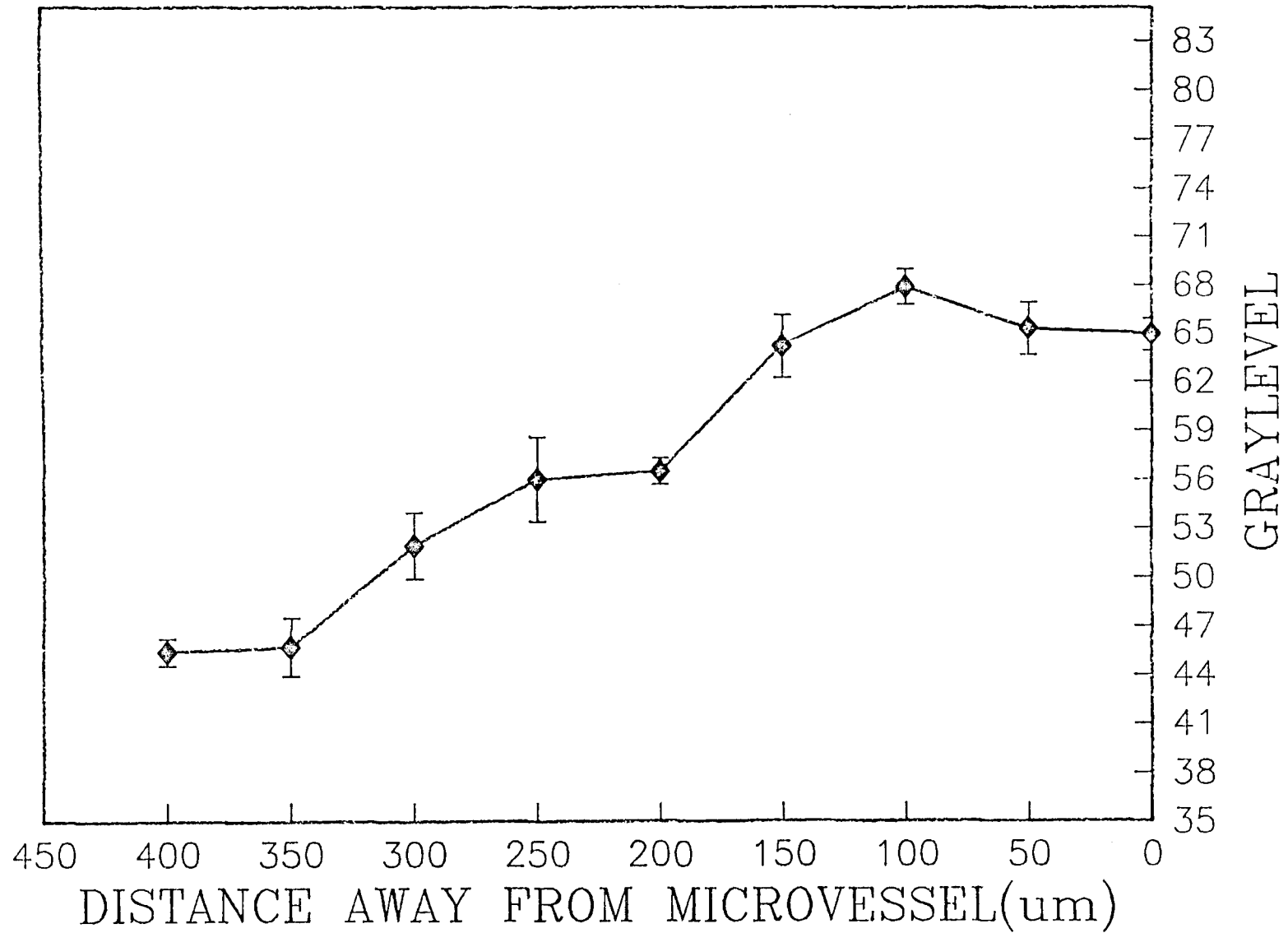


FIG.5.35 FITC-20 SECOND LEAKING SITE
TIME(sec)=4446 PIXEL 10 X 10

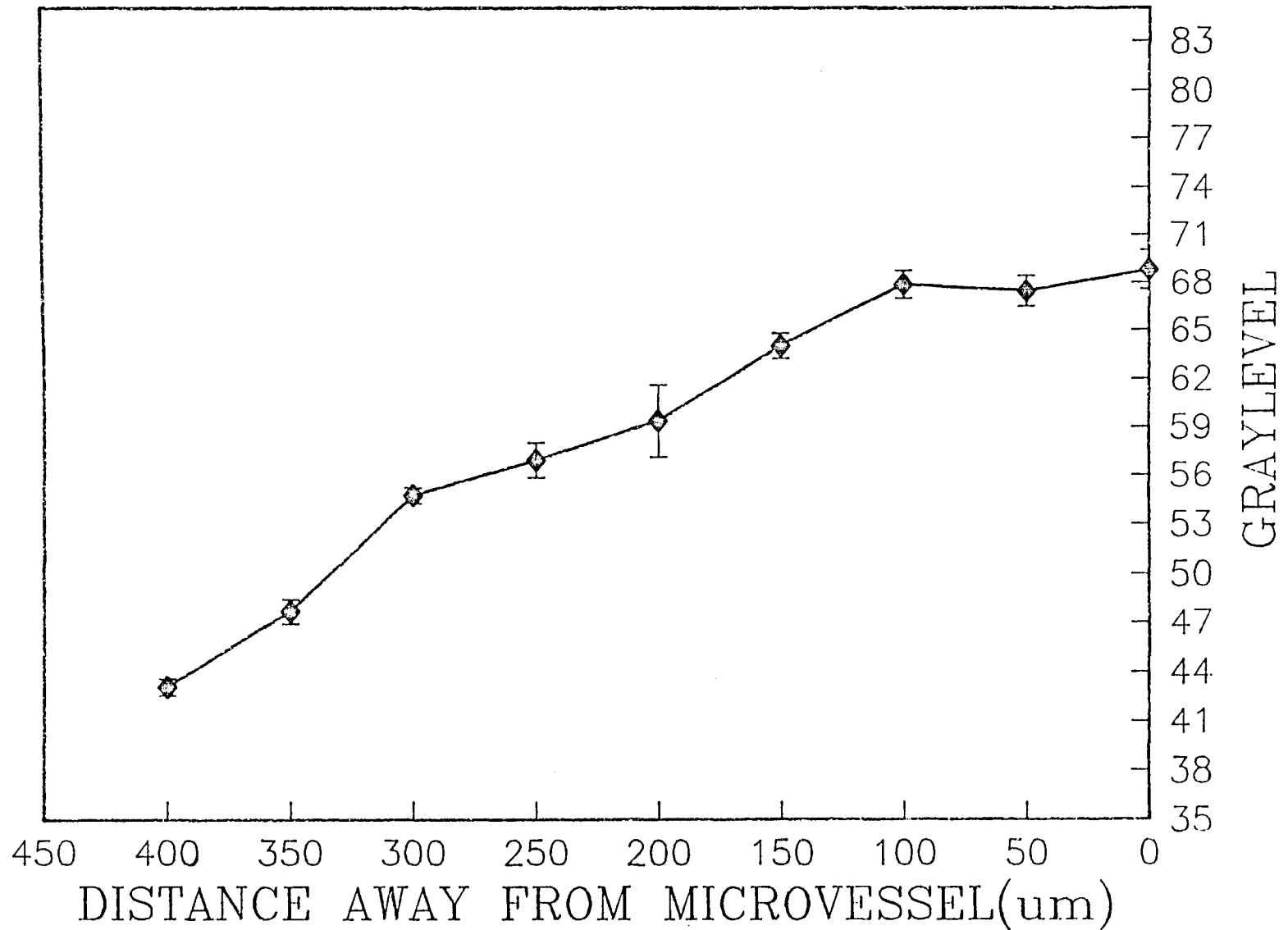


FIG.5.36 FITC-20 SECOND LEAKING SITE
TIME(sec)=5591 PIXEL 1 X 1

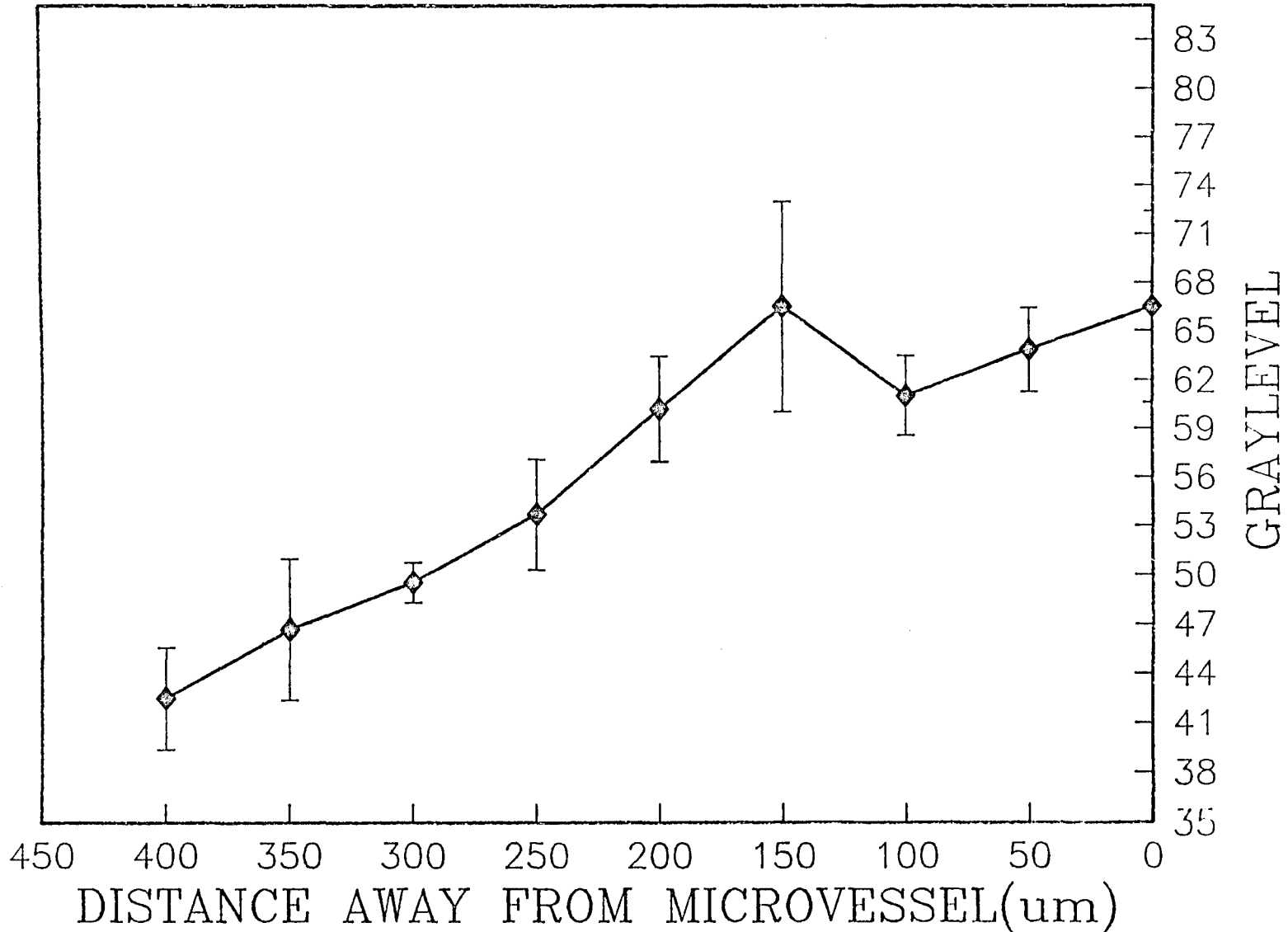


FIG.5.37 FITC-20 SECOND LEAKING SITE
TIME(sec)=5591 PIXEL 5 X 5

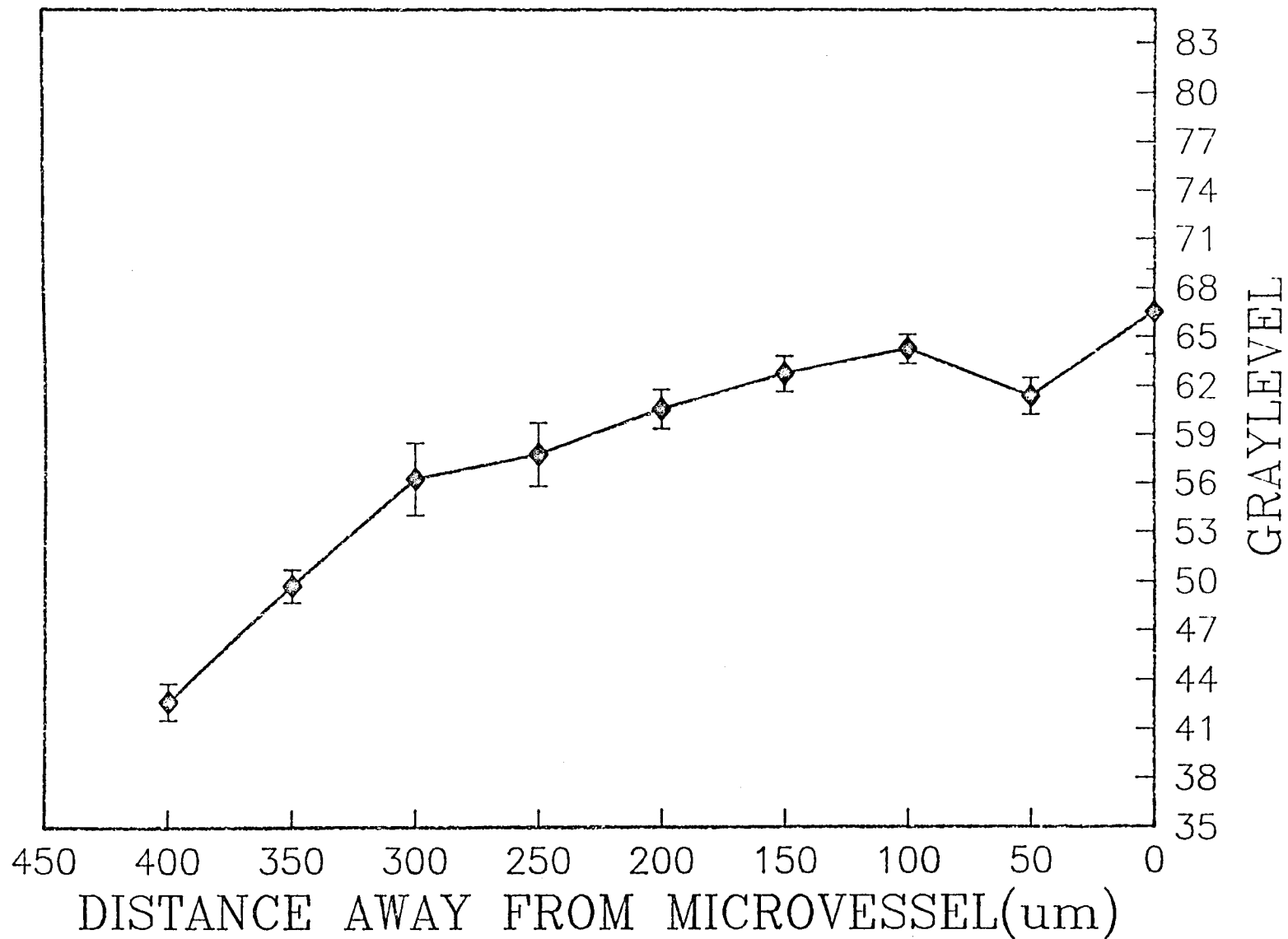


FIG.5.38 FITC-20 SECOND LEAKING SITE
TIME(sec)=5591 PIXEL 10 X 10

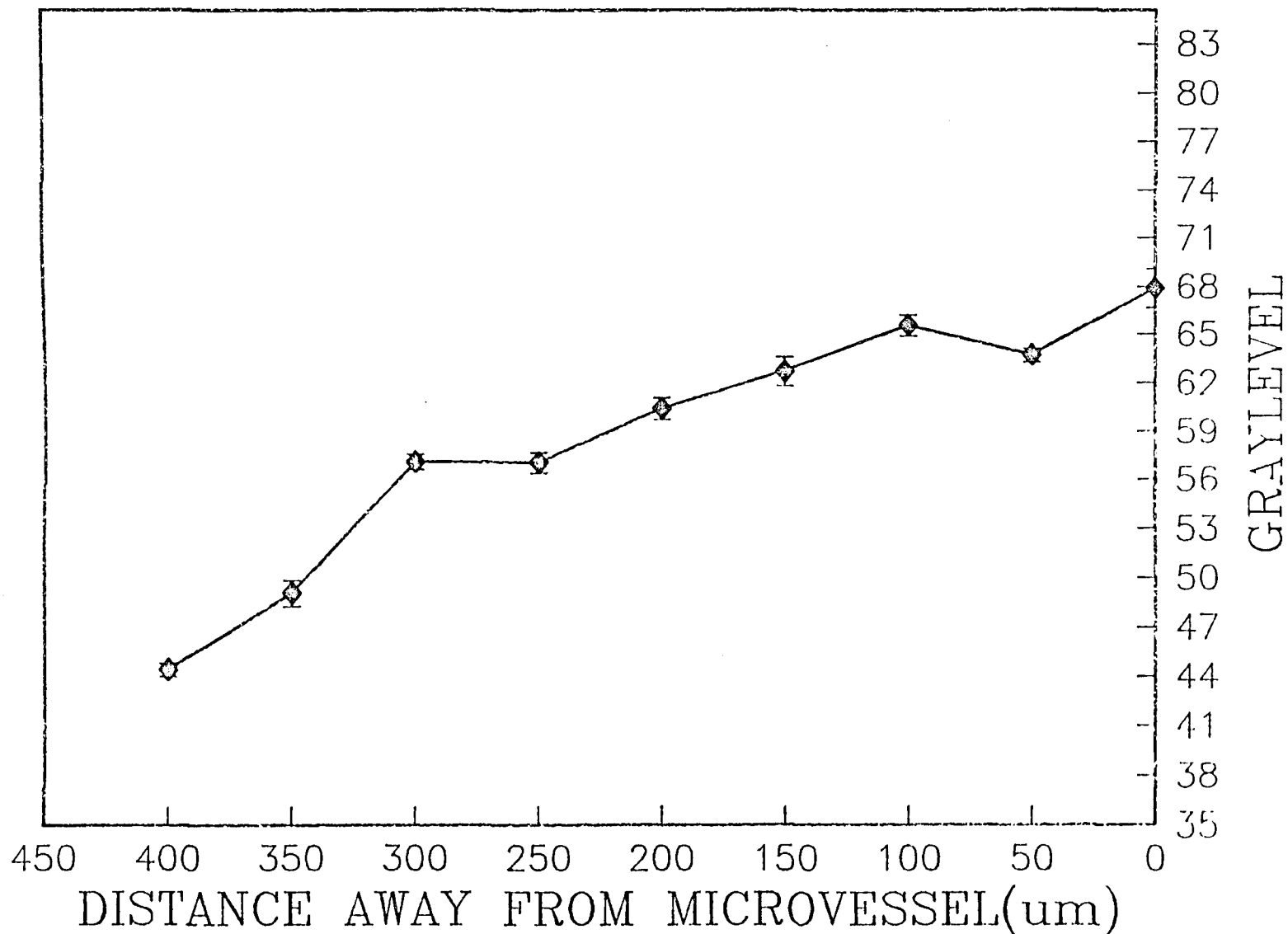


FIG.5.39 FITC-70 FIRST LEAKING SITE
TIME(sec)=5895 PIXEL 1 X 1

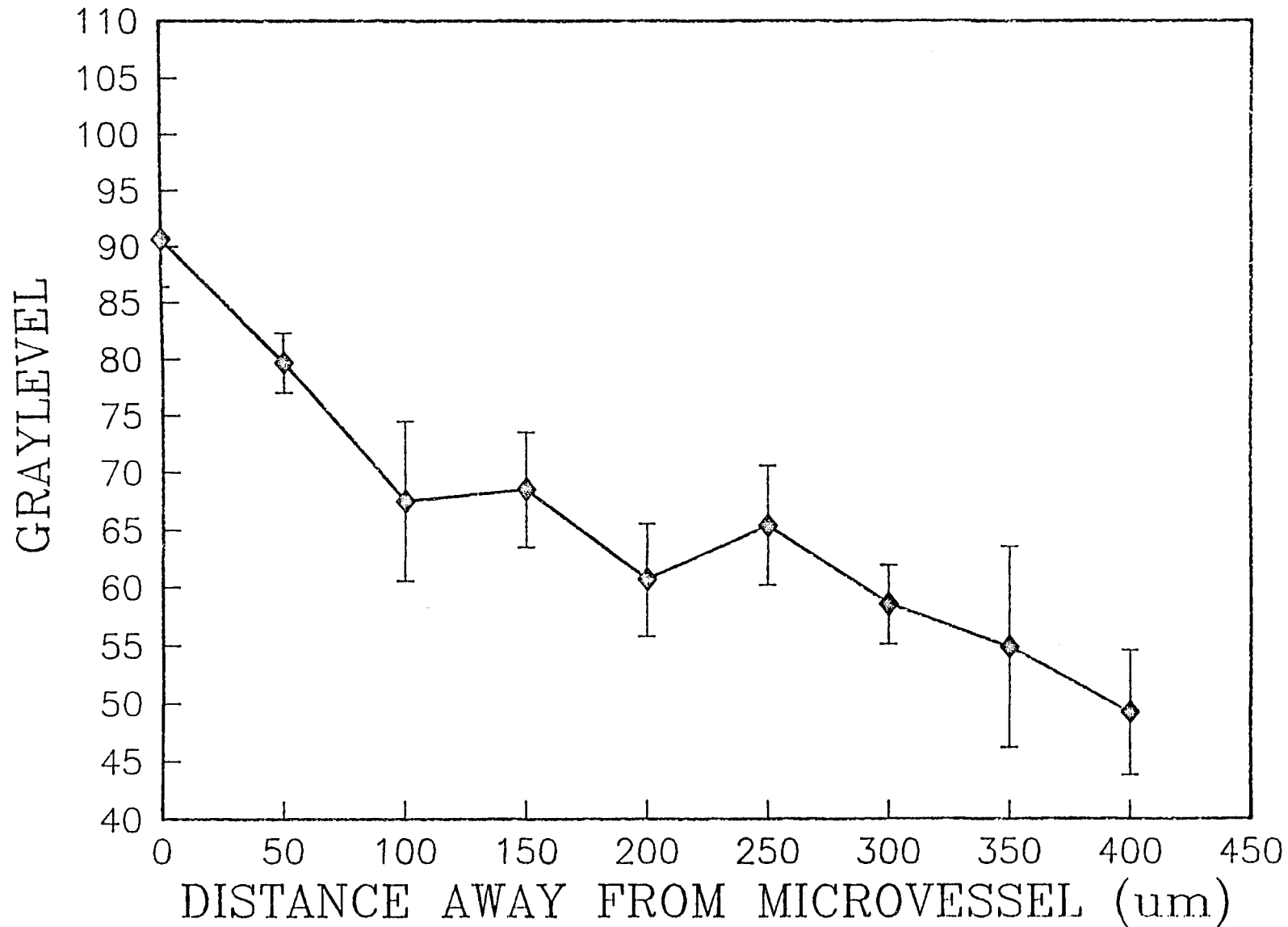


FIG.5.40 FITC-70 FIRST LEAKING SITE
TIME(sec)=5895 PIXEL 5 X 5

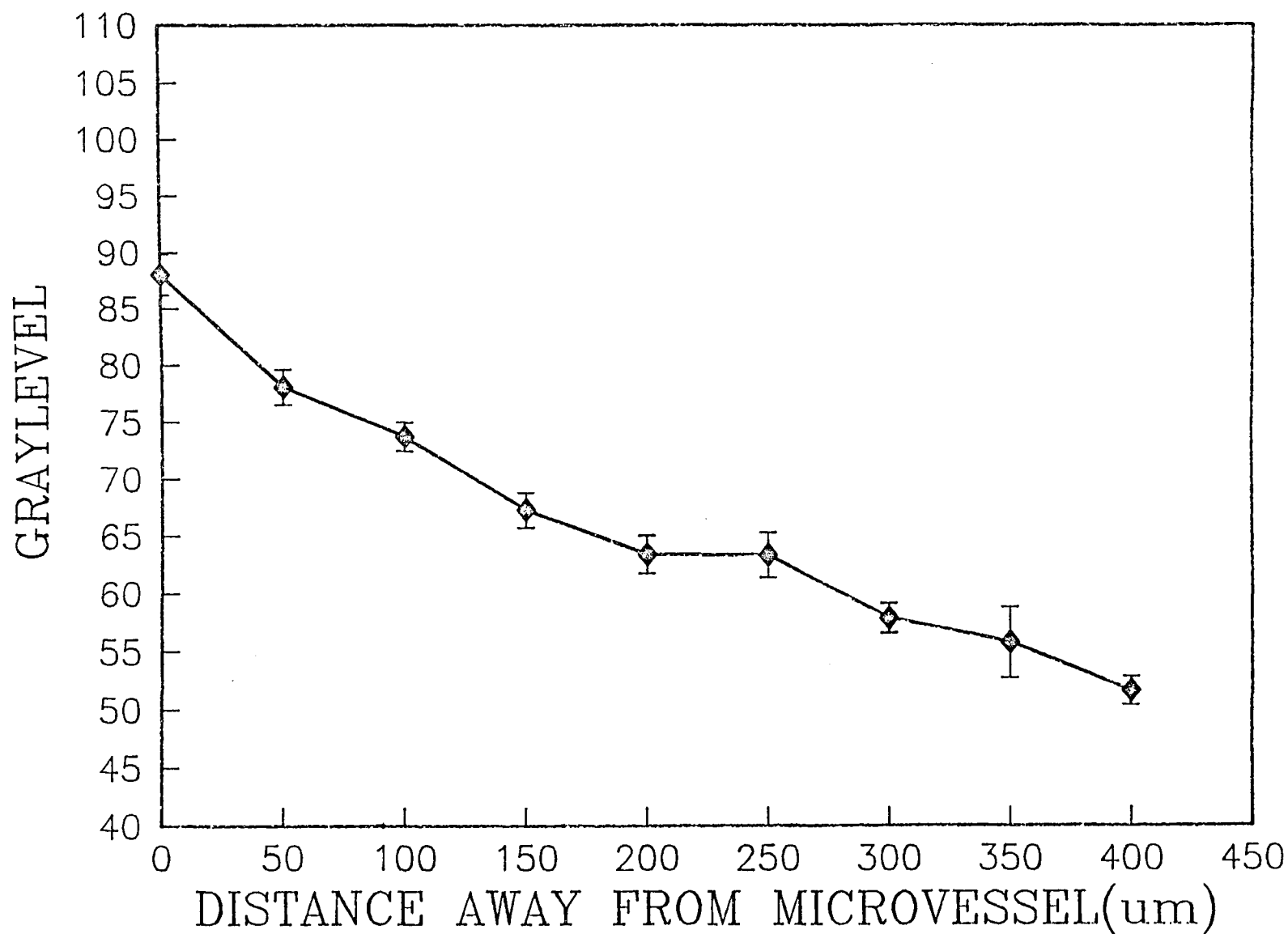


FIG.5.41 FITC-70 FIRST LEAKING SITE
TIME(sec)=5895 PIXEL 10 X 10

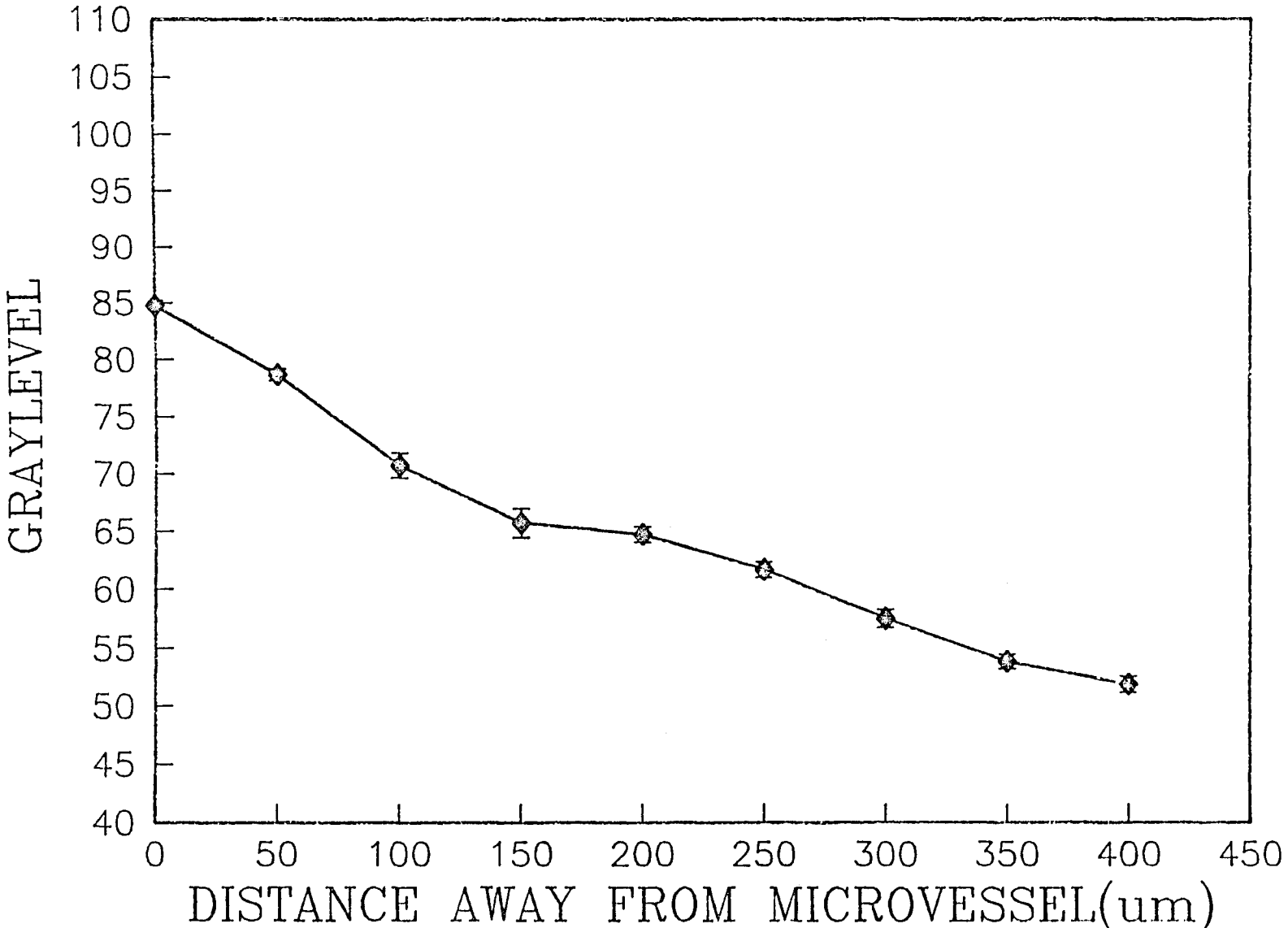


FIG.5.42 FITC-70 FIRST LEAKING SITE
TIME(sec)=7950 PIXEL 1 X 1

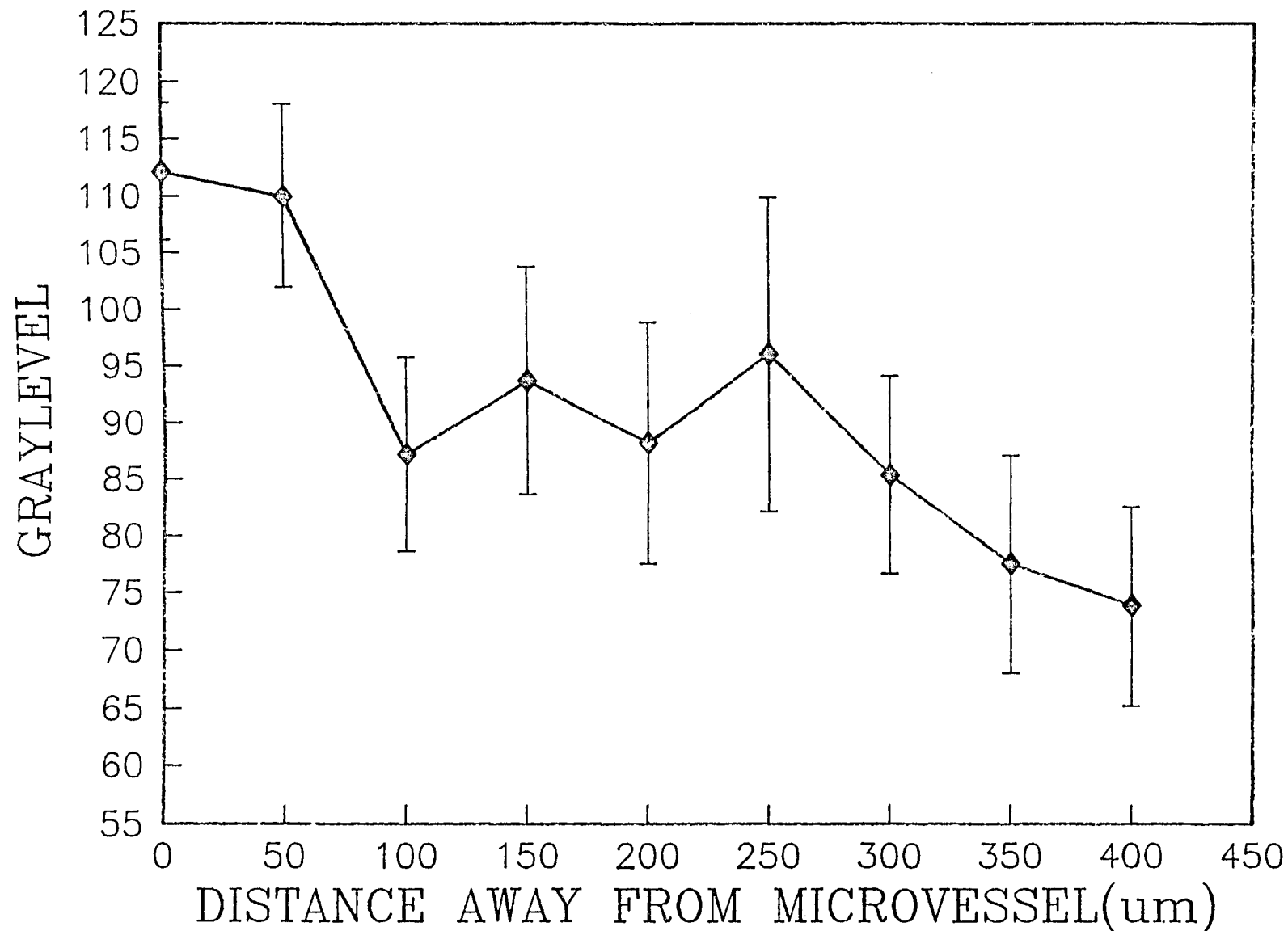


FIG.5.43 FITC-70 FIRST LEAKING SITE
TIME(sec)=7950 PIXEL 5 X 5

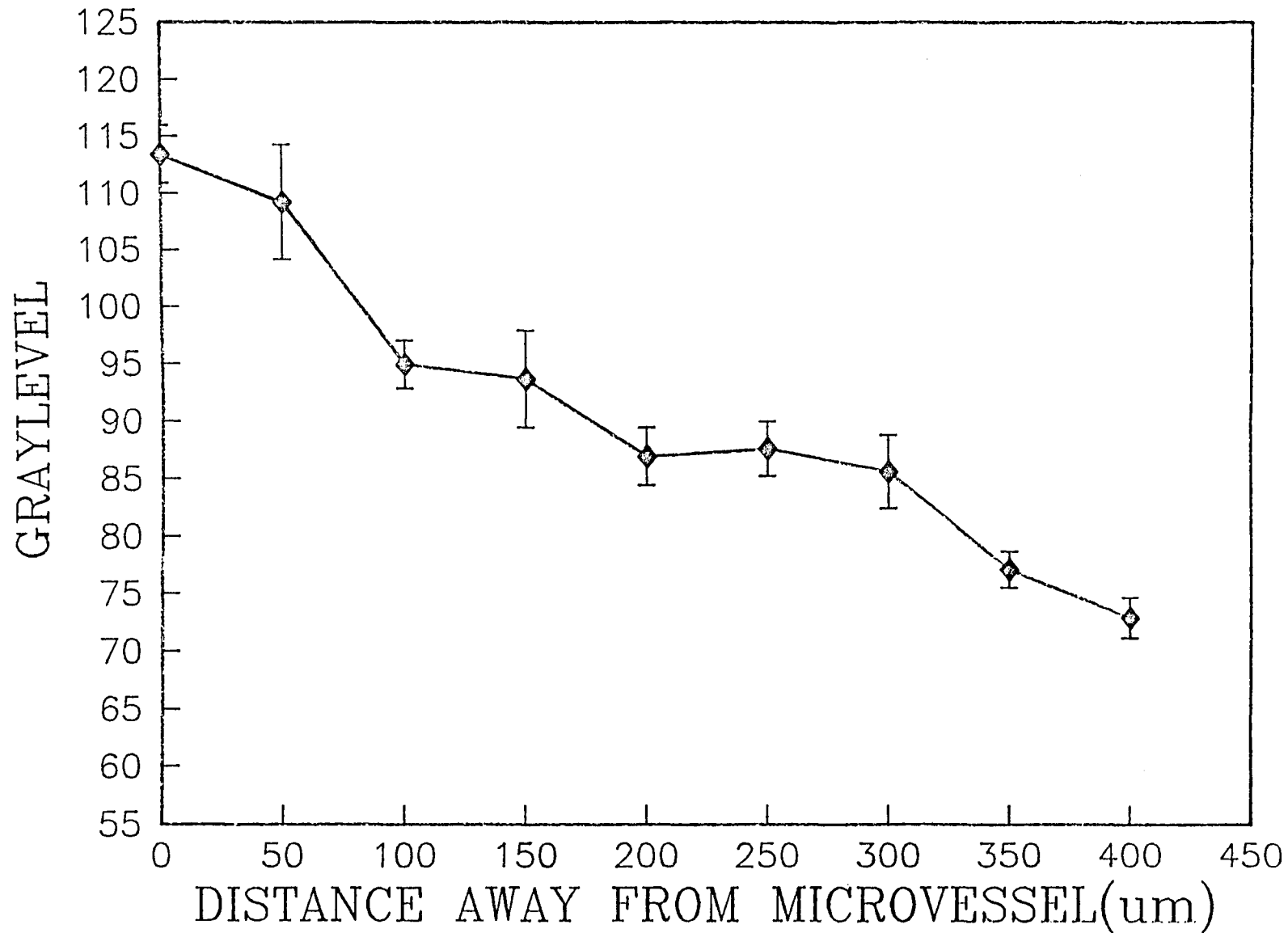


FIG.5.44 FITC-70 FIRST LEAKING SITE
TIME(sec)=7950 PIXEL 10 X 10

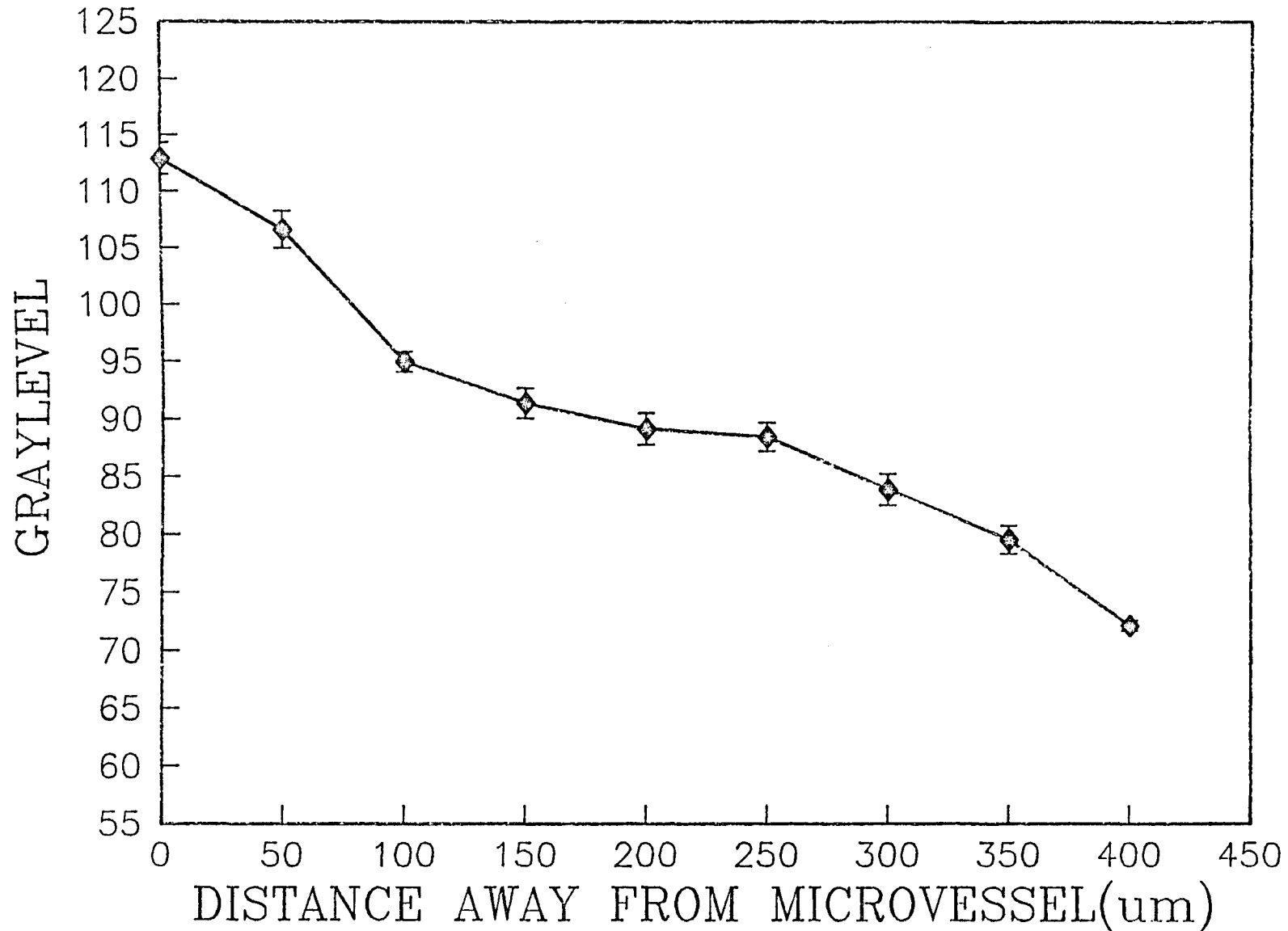


FIG.5.45 FITC-70 SECOND LEAKING SITE
TIME(sec)=4320 PIXEL 1 X 1

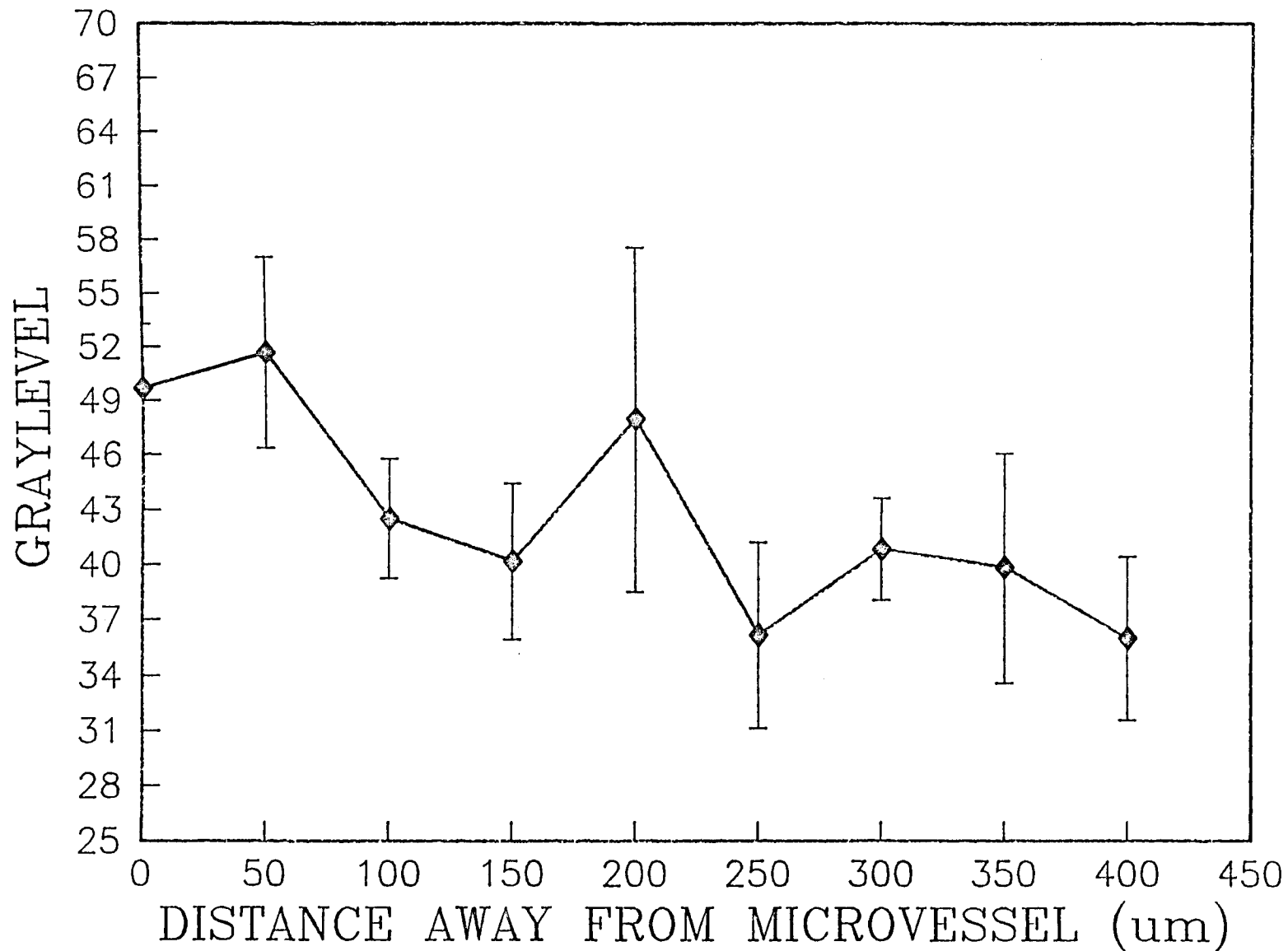


FIG.5.46 FITC-70 SECOND LEAKING SITE
TIME(sec)=4320 PIXEL 5 X 5

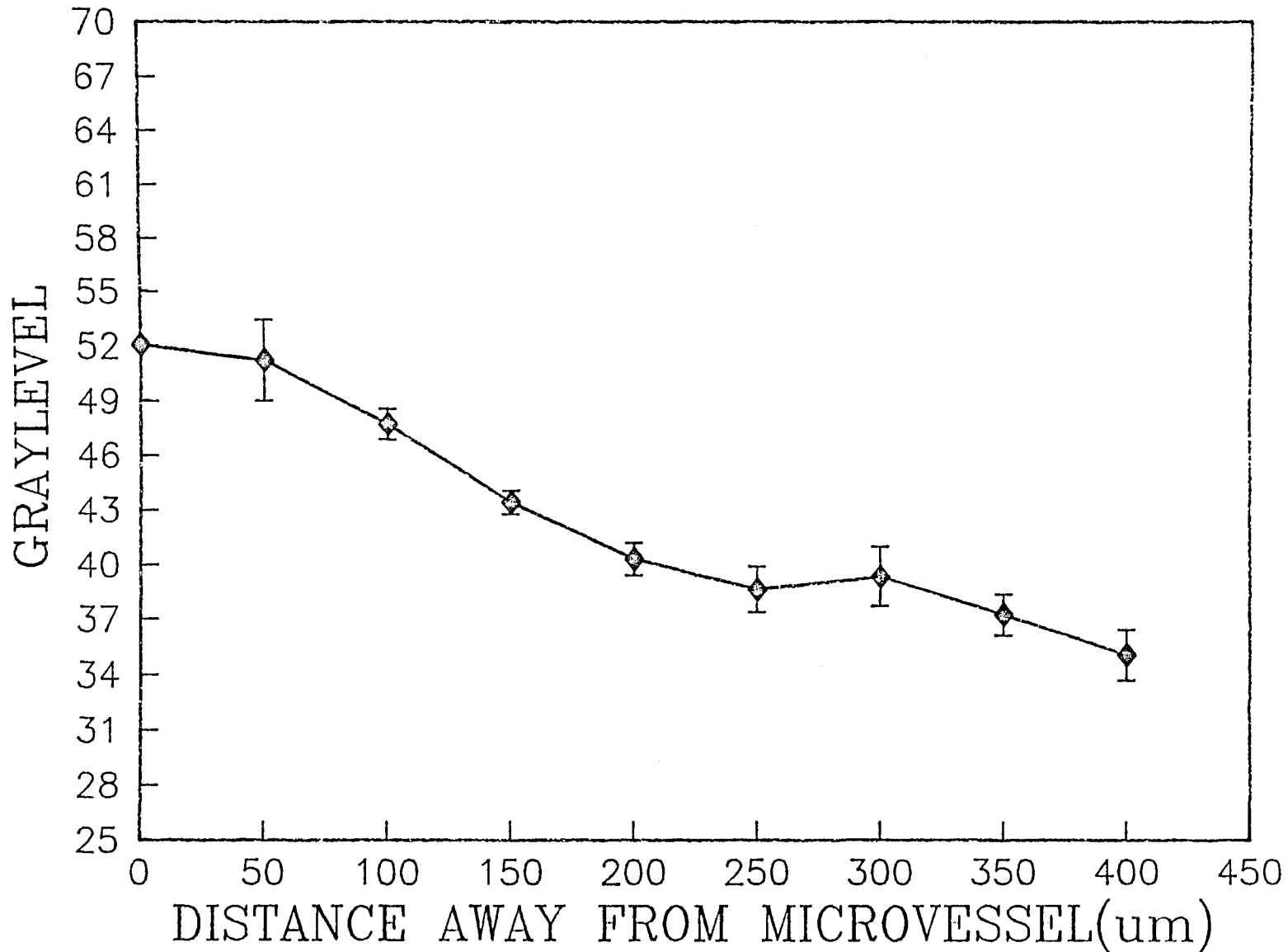


FIG.5.47 FITC-70 SECOND LEAKING SITE
TIME(sec)=4320 PIXEL 10 X 10

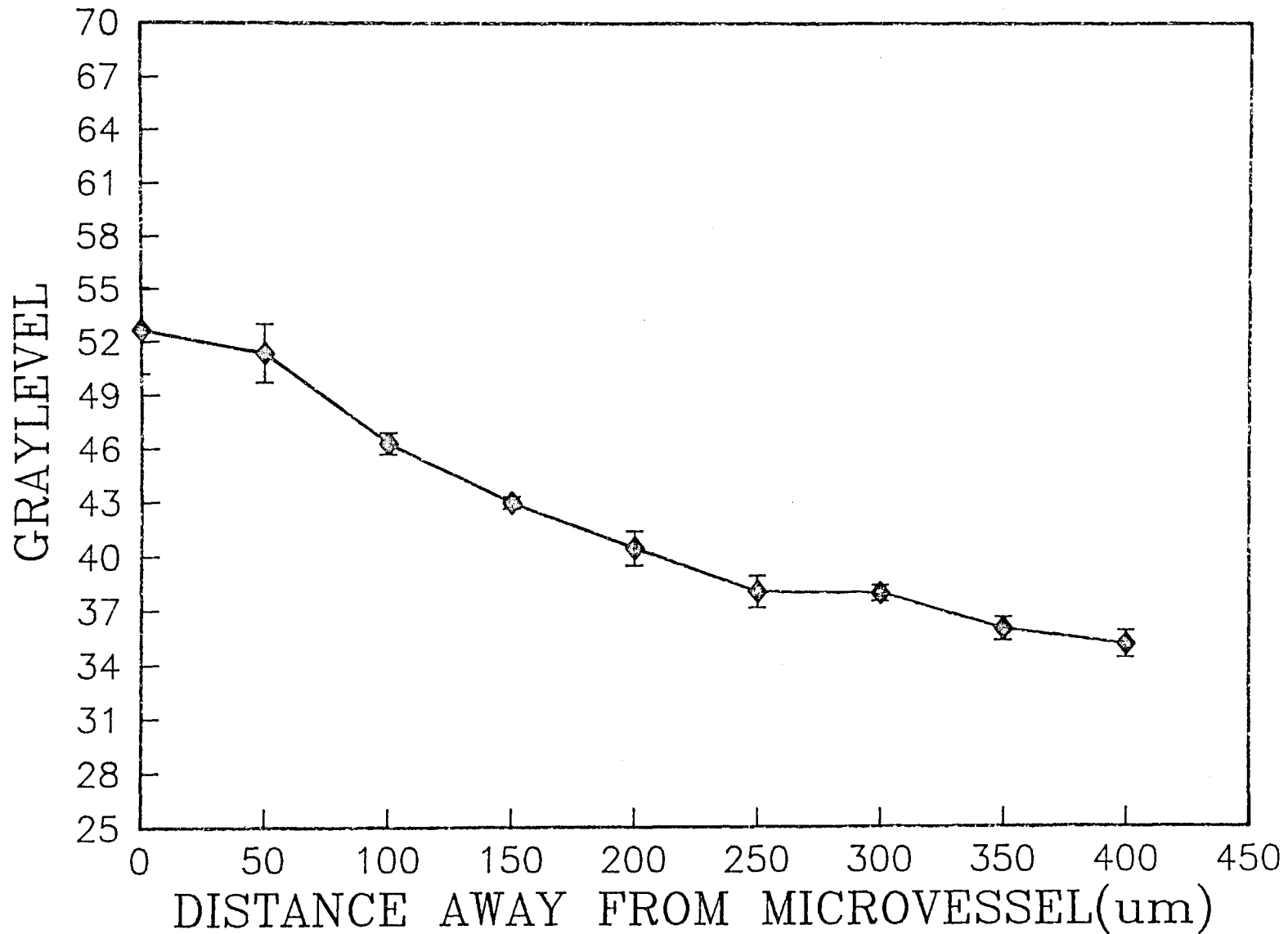


FIG.5.48 FITC-70 SECOND LEAKING SITE
TIME(sec)=6675 PIXEL 1 X 1

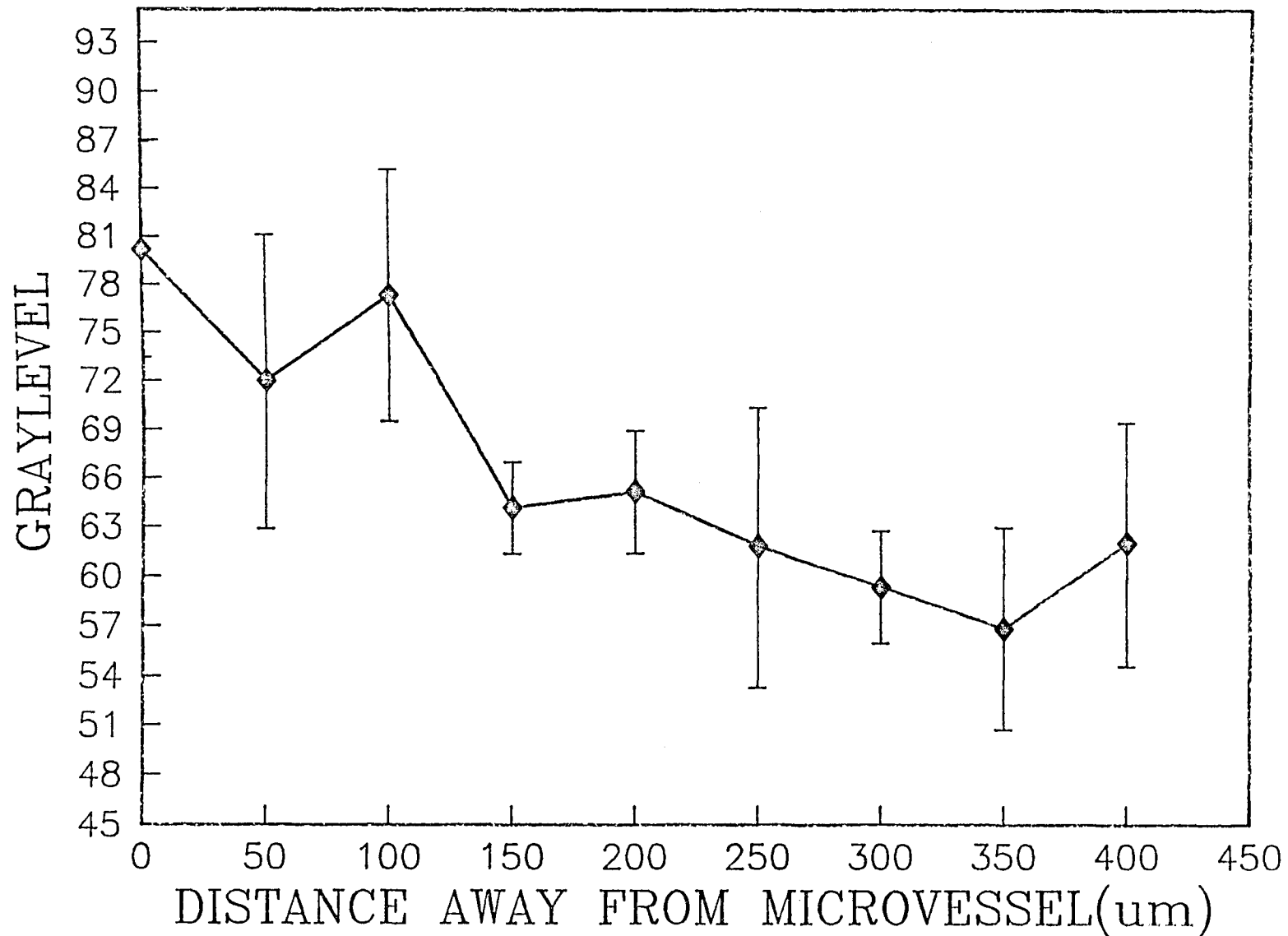


FIG.5.49 FITC-70 SECOND LEAKING SITE
TIME(sec)=6675 PIXEL 5 X 5

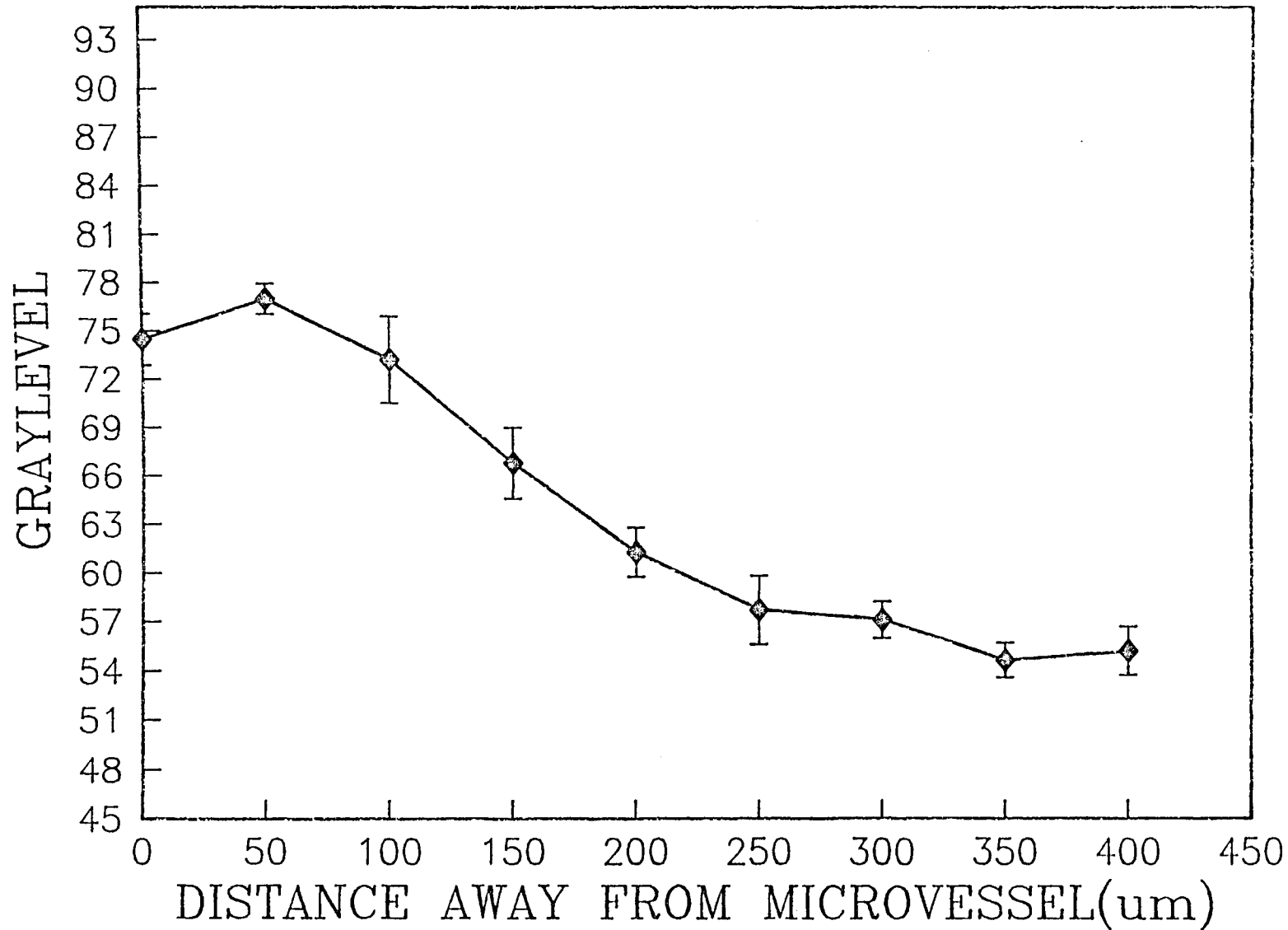


FIG.5.50 FITC-70 SECOND LEAKING SITE
TIME(sec)=6675 PIXEL 10 X 10

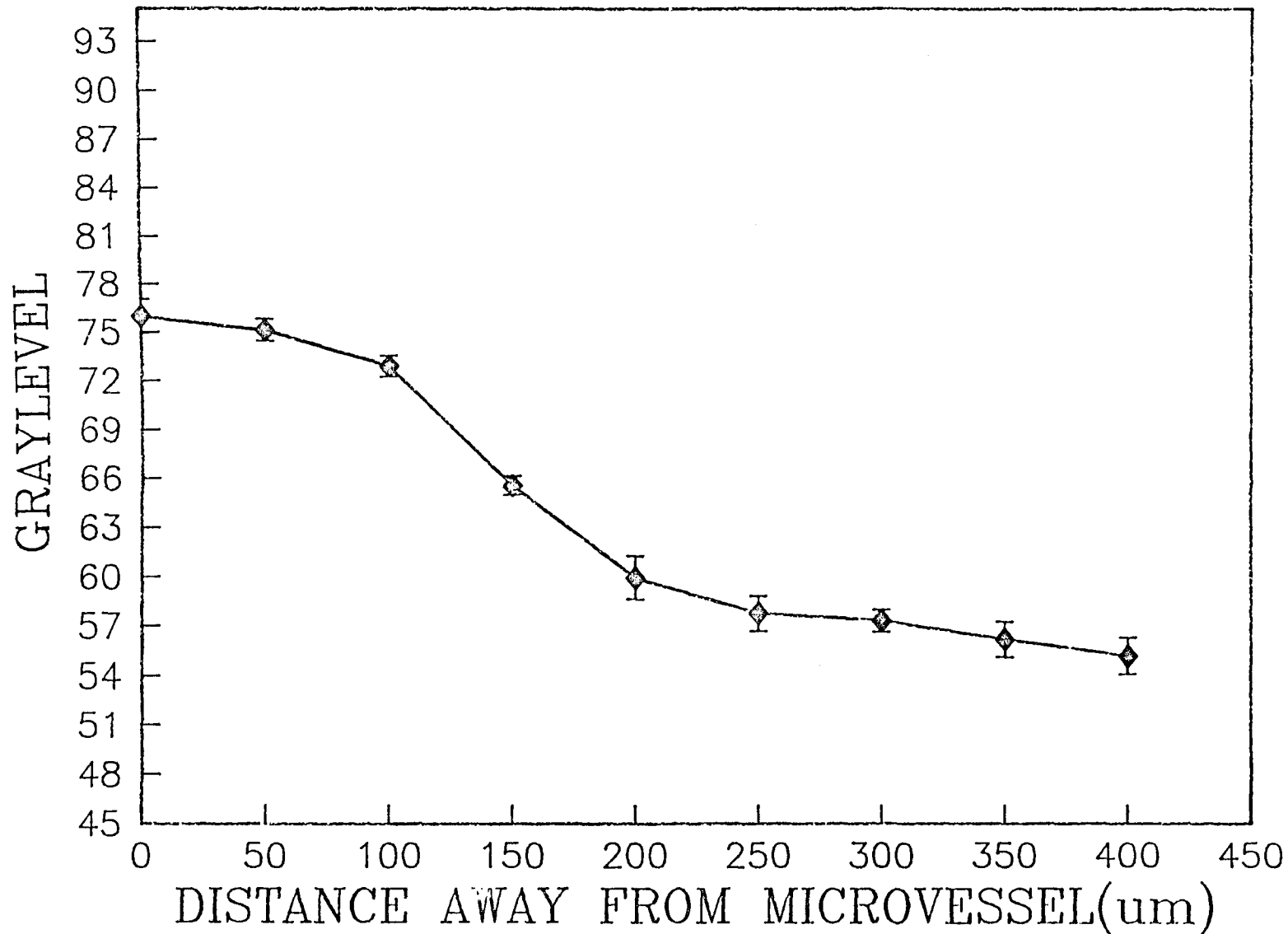


FIG.5.51 FITC-20 FIRST LEAKING SITE
TIME(sec)= 2711 PIXEL 1X1,5X5,10X10

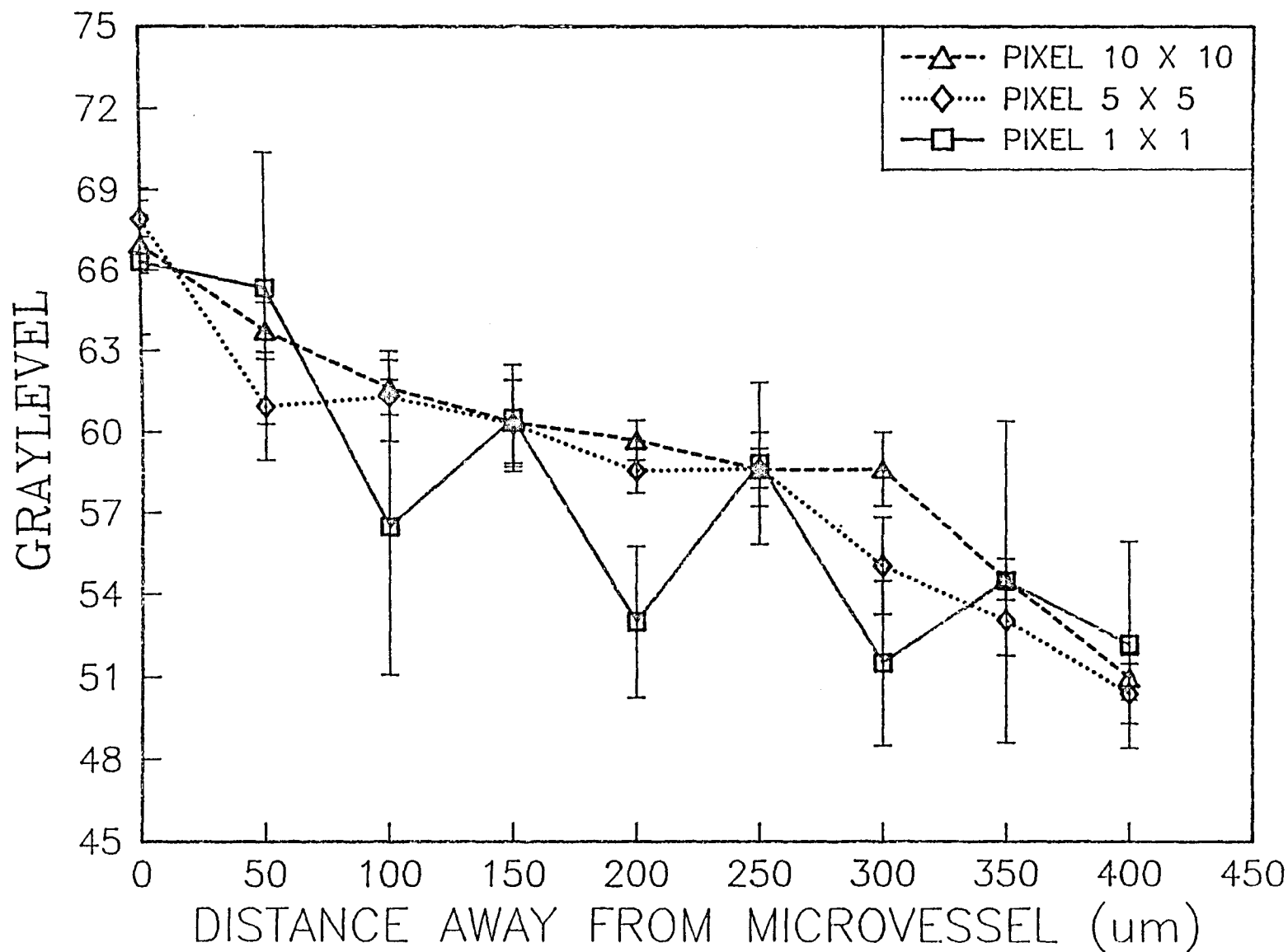


FIG.5.52 FITC-20 FIRST LEAKING SITE
TIME(sec)= 4401 PIXEL 1X1,5X5,10X10

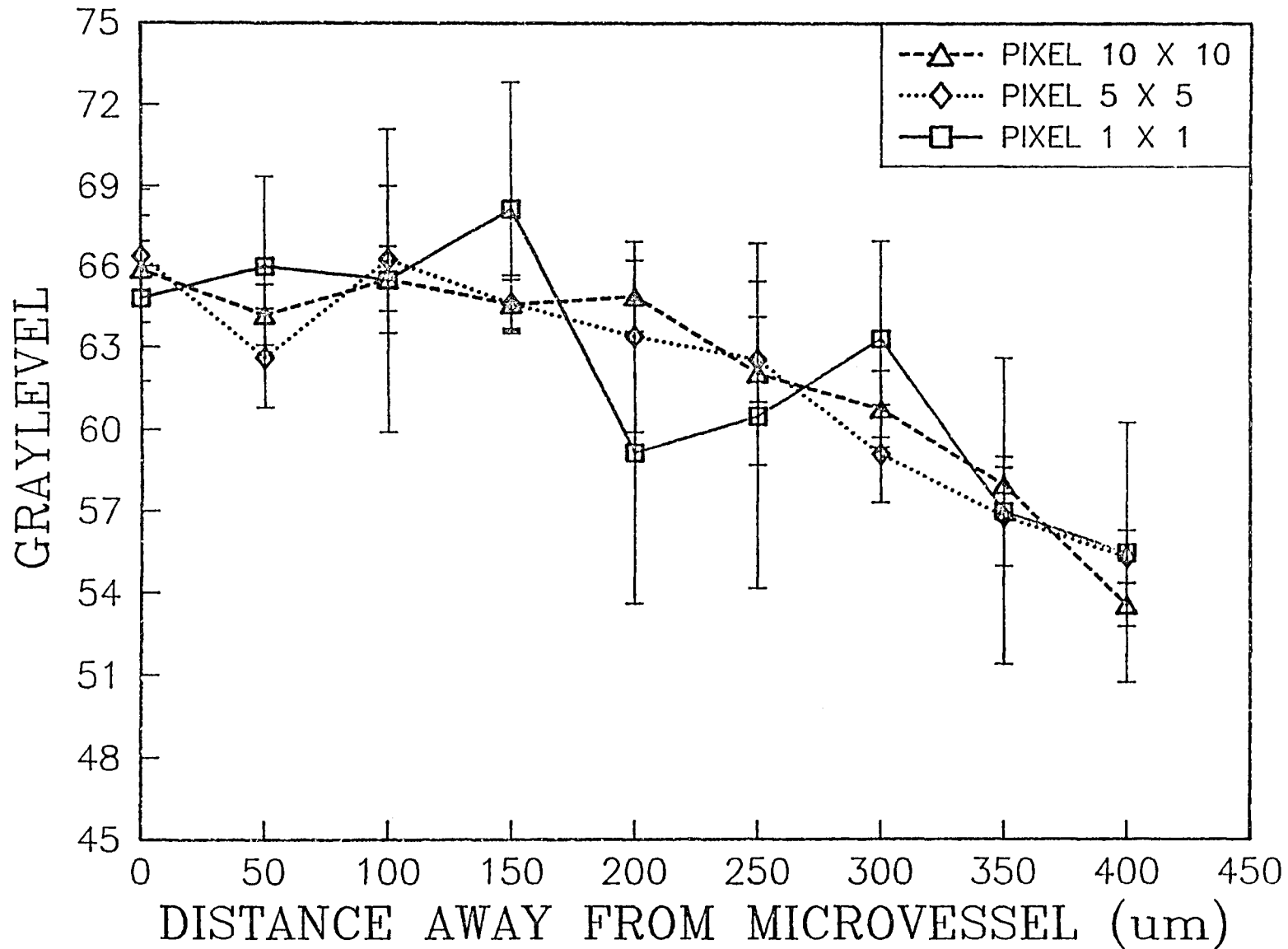


FIG.5.53 FITC-20 SECOND LEAKING SITE
TIME(sec)= 4446 PIXEL 1X1,5X5,10X10

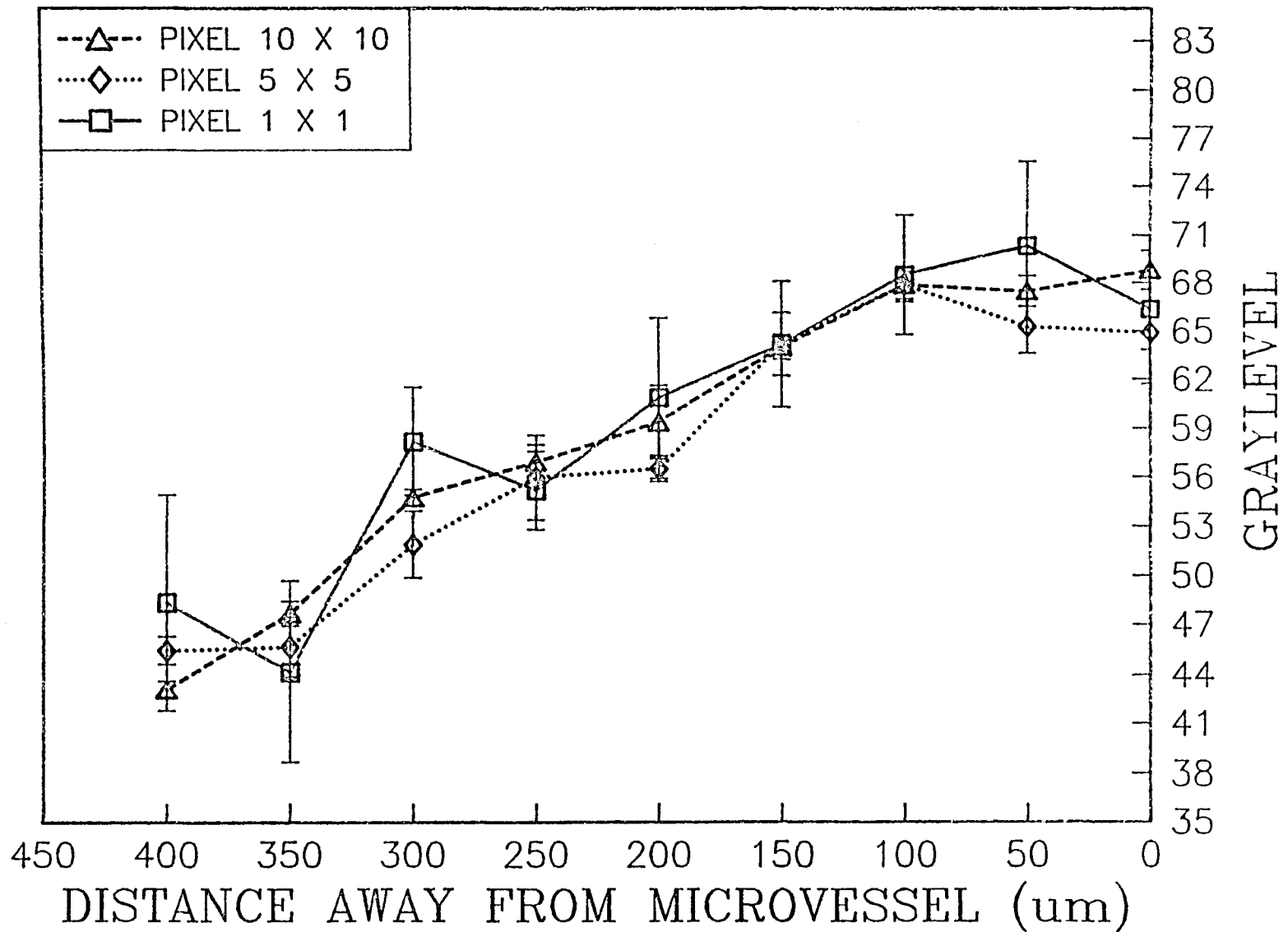


FIG.5.54 FITC-20 SECOND LEAKING SITE
TIME(sec)= 5591 PIXEL 1X1,5X5,10X10

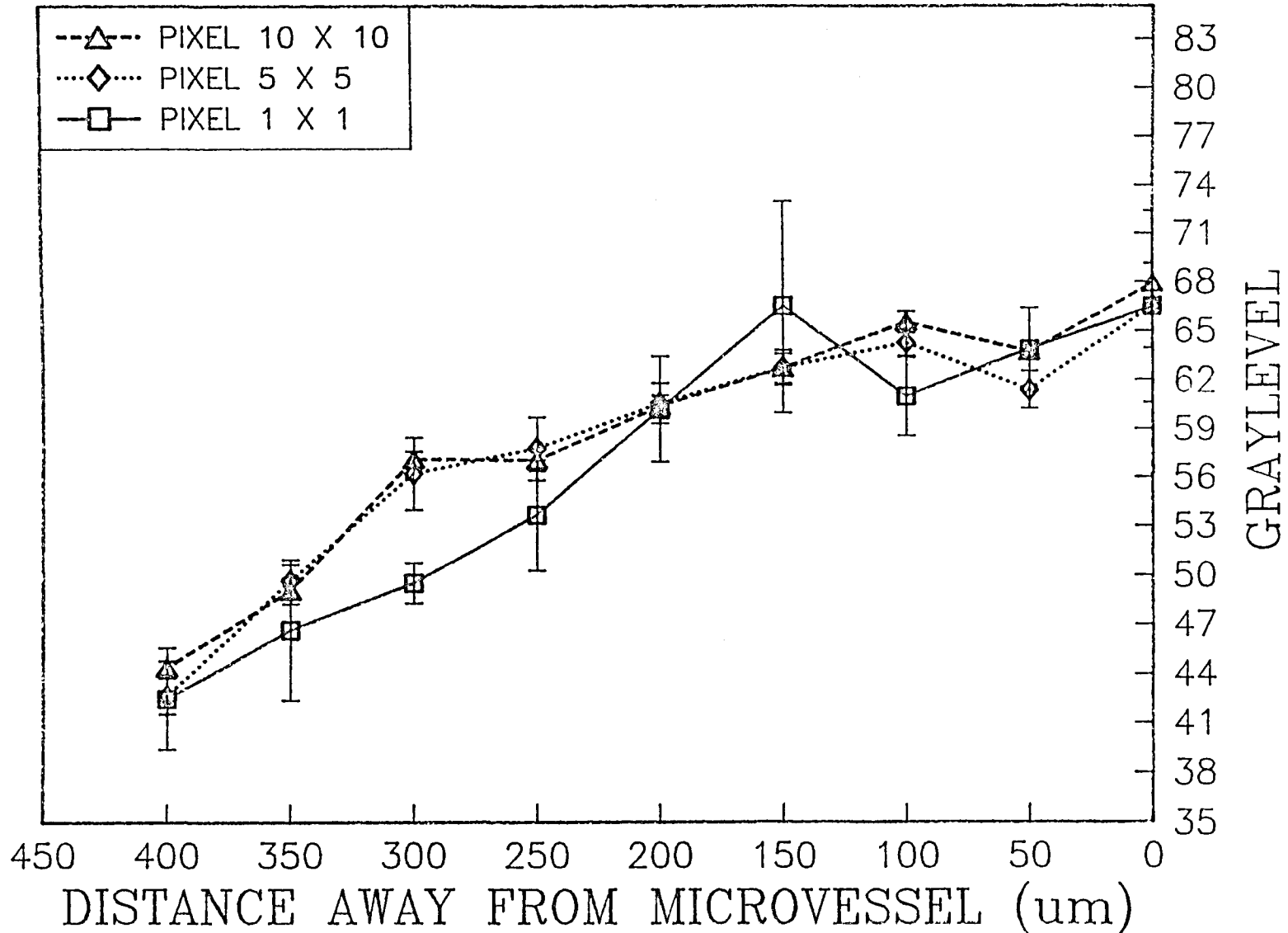


FIG.5.55 FITC-70 FIRST LEAKING SITE
TIME(sec)= 5895 PIXEL 1X1,5X5,10X10

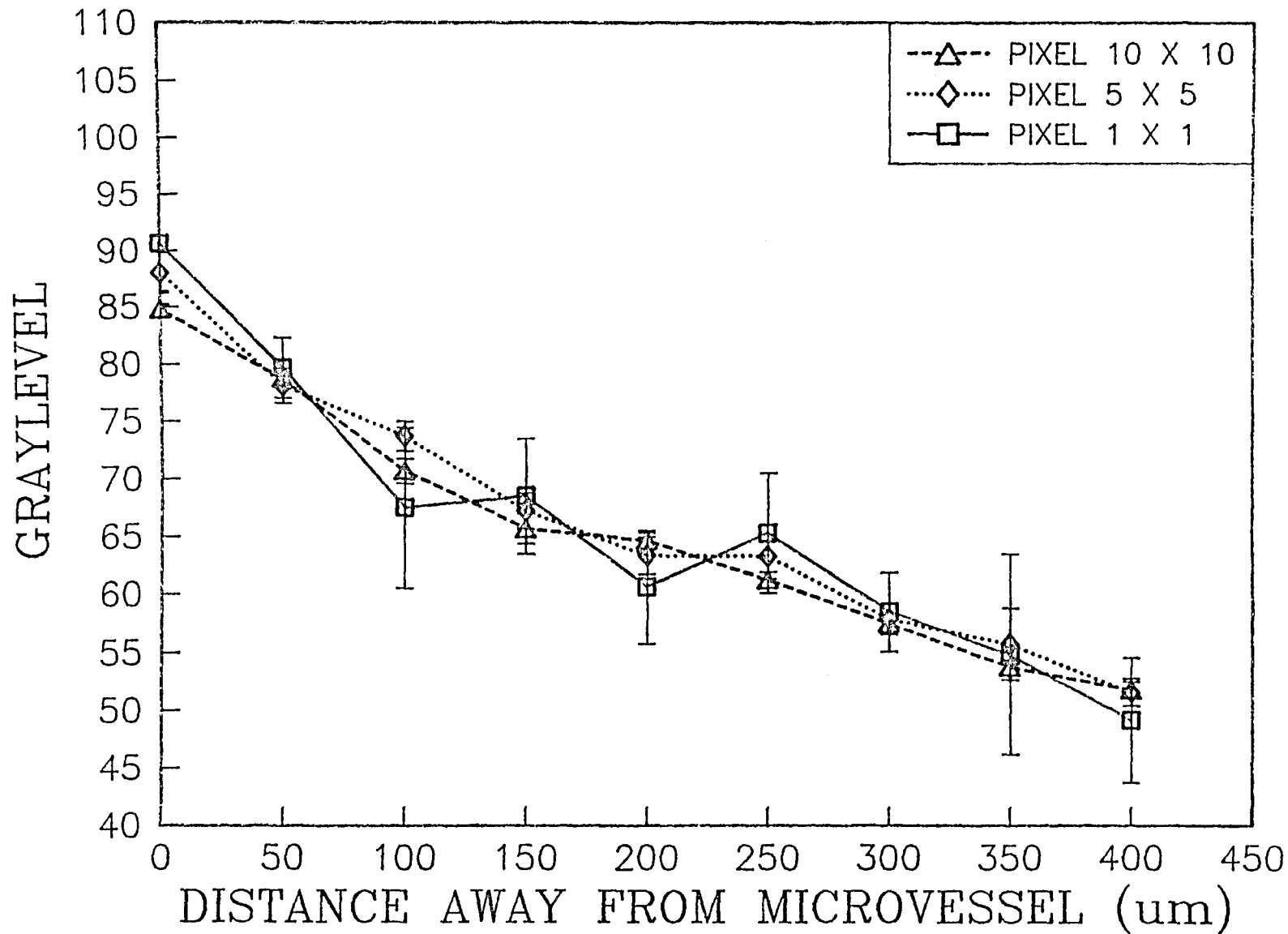


FIG.5.56 FITC-70 FIRST LEAKING SITE
TIME(sec)= 7950 PIXEL 1X1,5X5,10X10

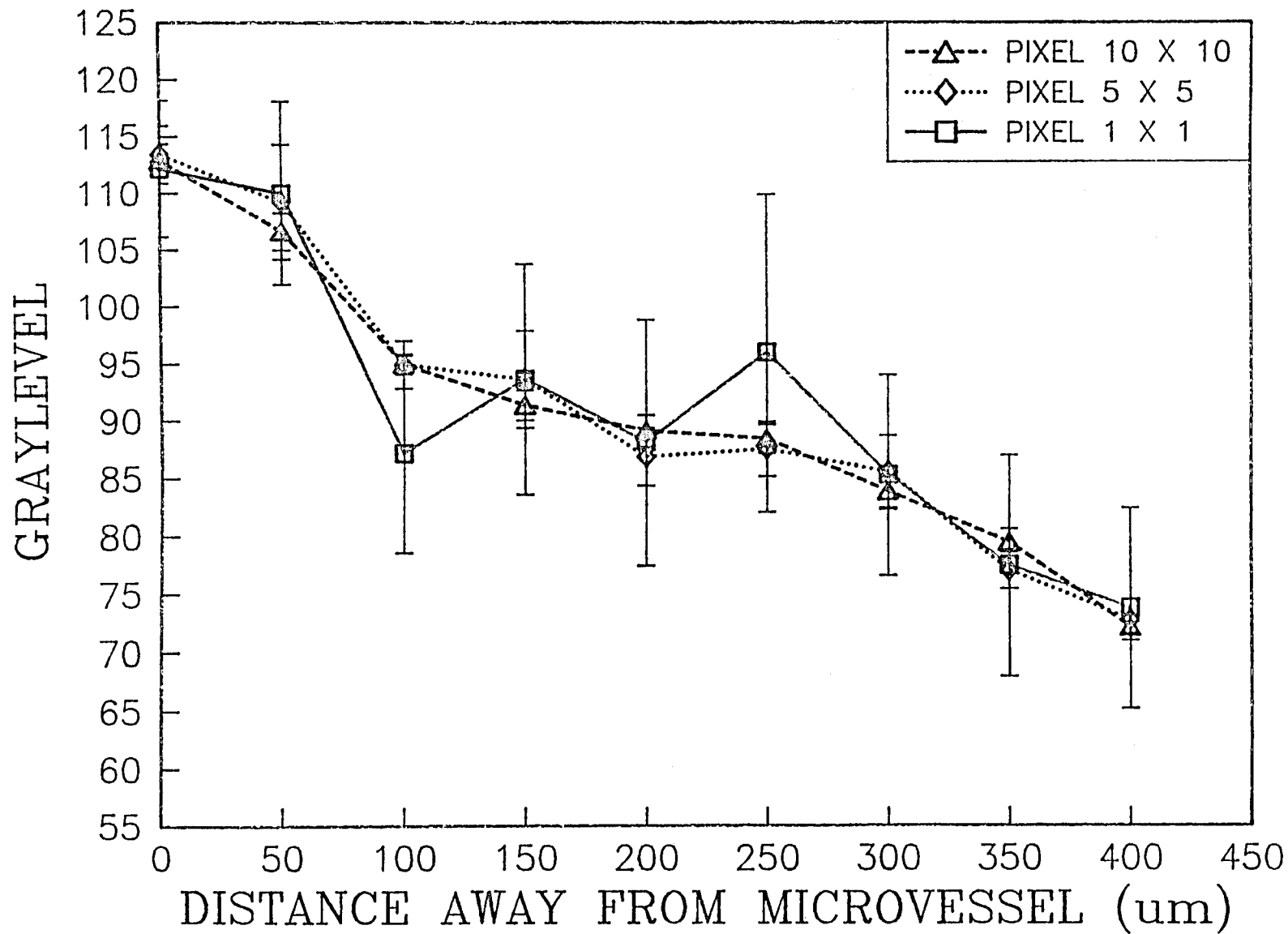


FIG.5.57 FITC-70 SECOND LEAKING SITE
TIME(sec)= 4320 PIXEL 1X1,5X5,10X10

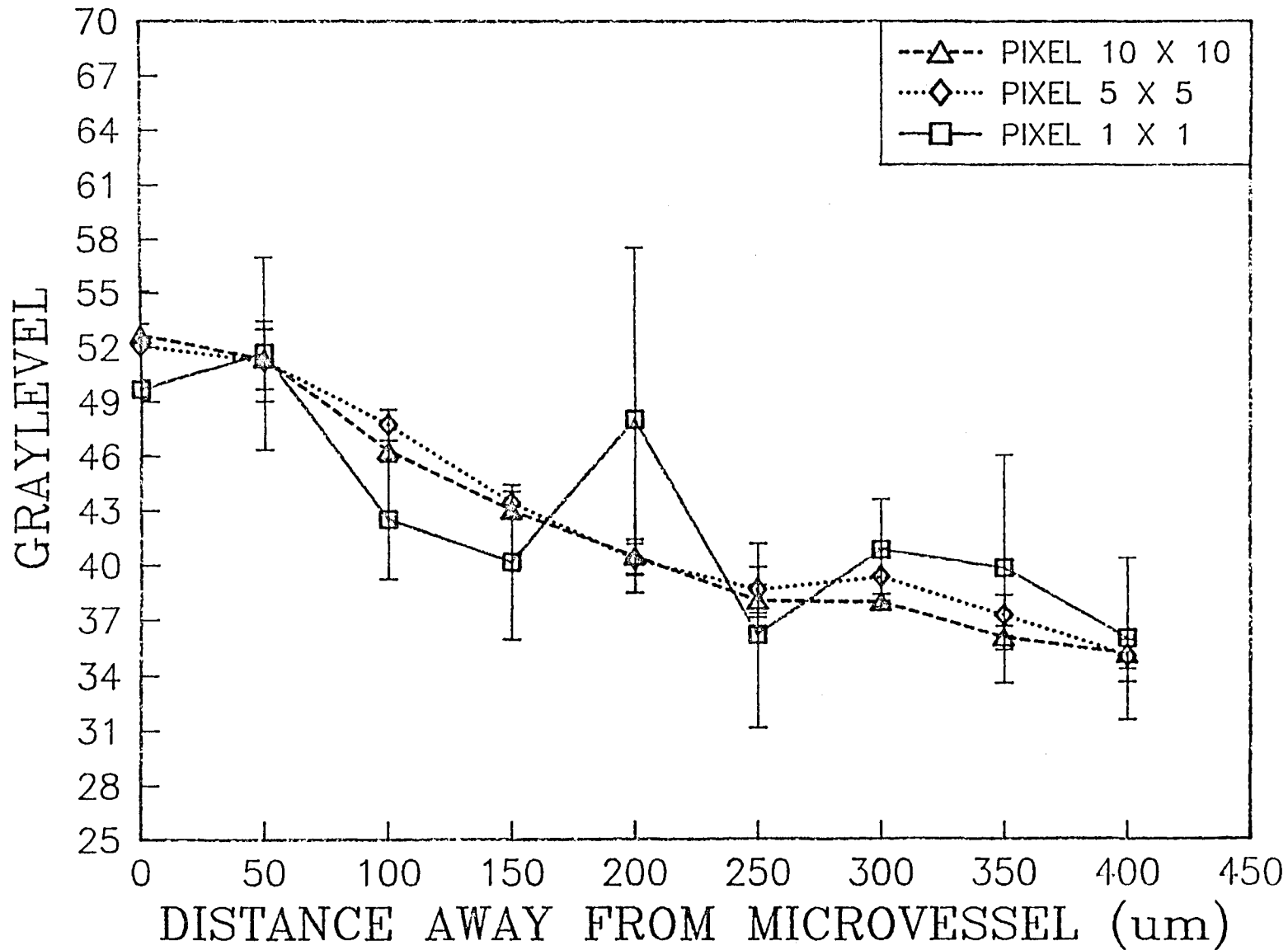
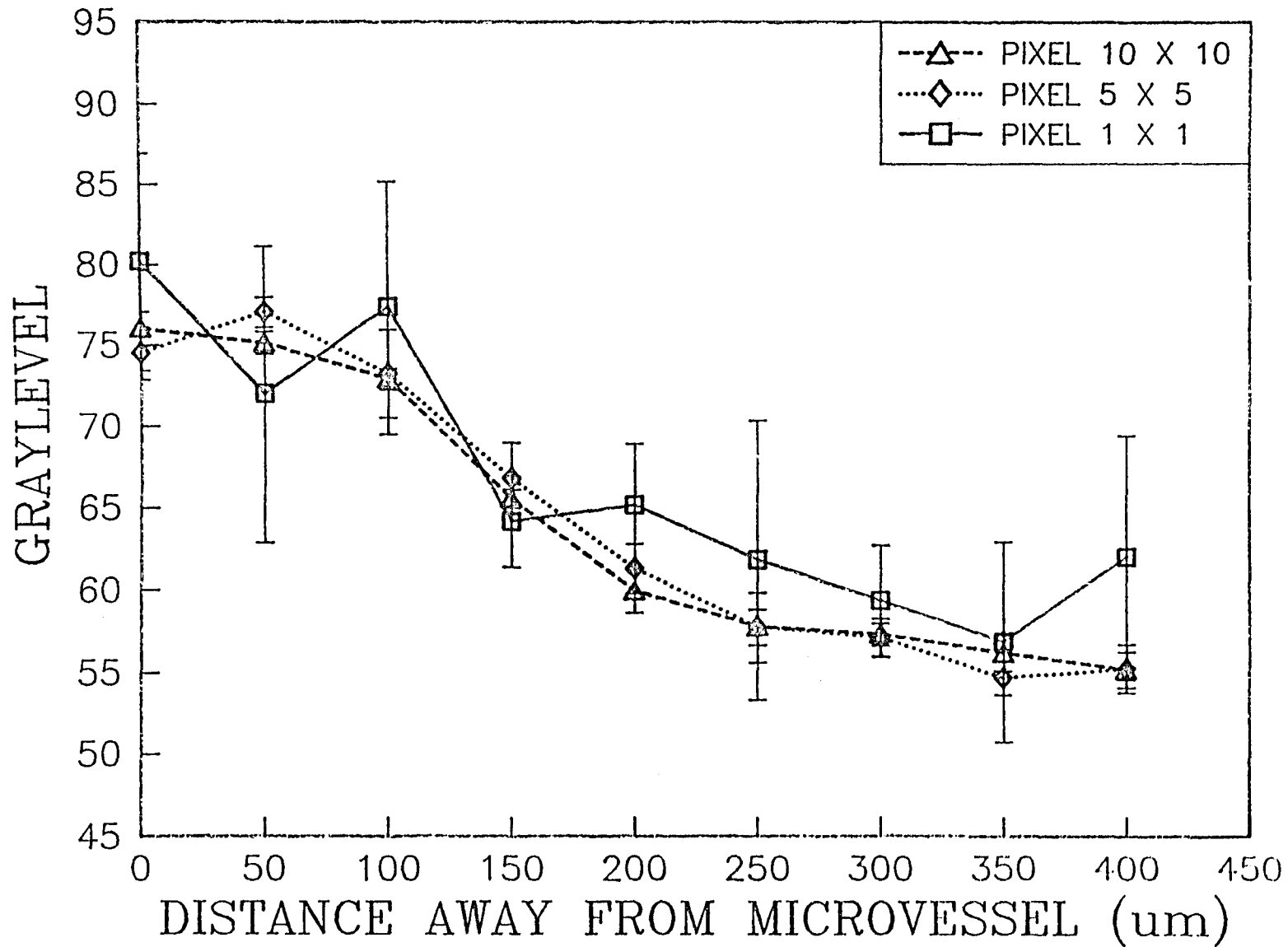


FIG.5.58 FITC-70 SECOND LEAKING SITE
TIME(sec)= 6675 PIXEL 1X1,5X5,10X10



CHAPTER 6

DISCUSSION

The goal of this study is to compare the variation in point estimates of concentration (intensity) with a single spatial filter (spatial average) to assess the improvement possible in estimation of the transport parameters.

1. From figures 5.51 through 5.58 the graylevel values of a single pixel in the middle of the window was compared with the average graylevel of 5 X 5 and 10 X 10 pixel windows. We found that the larger the window area, the less the variation is in the graycolor values.

2. The data in tables 5.1 through 5.24 allows a comparison of the standard deviations of intensity profiles constructed from single pixel values with intensity profiles constructed from 5 X 5 and 10 X 10 pixels spatial averages. We found that the larger the window areas, the

smaller the standard deviation values.

3. Figures 5.27 through 5.50, show that the spatial averaging of pixel intensities produces more stable intensity profiles than intensity profiles constructed from single pixel graylevel values. Standard deviations for single pixels values are in the range 3.38 to 9.35. In 5 X 5 and 10 X 10 pixel windows, the spatial average standard deviations were in the ranges 1.29 to 2.46 (5 X 5 window area) and 0.69 to 1.36 (10 X 10 window area).

4. Figures 5.4 through 5.26, show that the longer the time after injecting FITC-DXs tracer, the larger the graylevel values in the interstitial space. All figures show that the further away from the leaking microvessel, the smaller the graylevel value is.

5. It was also observed that the larger the size of the macromolecule, the larger is its standard deviation. Following table shows this.

Table 2. Average standard deviations (n=9) for 3 different window sizes at several time points for FITC-DX20 and FITC-DX 70

FITC-DX 20 ^a		Average Standard Deviation (n=9)			
Time	2711 secs	4401 secs	4446 secs	5591 secs	
1X1	3.38	4.62	4.05	3.63	
5X5	1.29	1.97	1.54	1.48	
10X10	1.01	1.36	0.99	0.69	

FITC-DX 70 ^b		Average Standard Deviation (n=9)			
Time	5895 secs	7950 secs	4320 secs	6675 secs	
1X1	5.17	9.35	4.94	6.19	
5X5	1.50	2.46	1.44	1.64	
10X10	0.76	1.21	0.97	0.92	

a. FITC-DX 20, Average molecular weight 19,400 daltons,
Average molecular size 31.2 A.

b. FITC-DX 70, Average molecular weight 71,600 daltons,
Average molecular size 56.8 A.

CHAPTER 7

CONCLUSIONS

AND

RECOMMENDATIONS

Conclusion:

The following are the conclusions drawn from this study:

(1) Graylevel values in single pixels show large experimental variations (1x1-pixel), whereas spatial averages of 5 X 5 or 10 X 10 pixel windows provided intensity profiles with much less variation as quantitated by the standard deviations.

(2) In single pixels, standard deviation (STDDEV) values are very large, indicating that graylevel values are very dispersed around the mean value. The STDDEV values get smaller as the window size increases. This indicates that the spatial average graylevel values are not as dispersed around their mean value.

We also showed that the intensity profiles constructed from spatial average graylevels are smoother than intensity profiles constructed from single pixel values.

(3) Graylevel values decreased, i.e. intensity decreased with increasing distance from the leaking vessel.

(4) Leakage takes place at more than one site. There are always nearby leaking sites with variable intensities. These contribute to the variation (noise) observed in single pixel measurements, spatial averaging improves the signal to noise ratio and improves the experimentally measured graycolor value.

Recommendations:

The present study is the first of its kind to analyze fluorescent intensity data in terms of point and spatial average estimates of intensity (graycolor). Hence, the conclusion drawn from this study is that 1x1-pixel graylevel values show much more variation than 10x10-pixel

averages. Since the effective vascular permeabilities and apparent interstitial diffusion coefficients are determined by a best-fit of the experimental data to a mathematical model, the use of spatial average intensity values or IOD values would yield more stable values (better estimates) of the transport parameters. Better estimates for these parameters and their changes with changing experimental conditions would aid in a better assessment of the roles of convection and diffusion in blood-tissue exchange of macromolecules.

Experimental Problems:

After completing the present study the following recommendations are made which might help in obtaining additional information necessary to understand the problem of dynamics of macromolecular transport.

(1) A reliable calibration for the determination of the relationship between the graylevel intensity and fluorescent tracer in the interstitium should be developed. The present work shows that the functional relationship between FITC-Dx and graylevel intensity is not

linear outside the microvessel. The smoothing process used in this study should help better establish the current functional relationship between fluorescent intensity and distance.

(2) Different tracers of variable molecular sizes should be tested in order to quantify the effect of size and shape of the tracer on the transport process.

(3) More sophisticated digitizing/recording equipment may help in reducing the error introduced while estimating the required parameters such as concentration. These errors are generally introduced because of a slight shift in the size and shape of the vessels in different frames. This shift is due to poor reference point locations. More accurate location of reference points can be achieved by more sophisticated digitizing equipment (e.g. Software IMAGE with a WINDOW function which can ZOOM IN/OUT of the picture. Also, the use of a mouse in order to help in locating a reference point, rather than conventional keyboard up and down arrows.) Sophistication can also be achieved by removing the background distortion/noise using

different types of filters in order to improve the sharpness of the picture.

(4) The mathematical model developed by S. Dumrongsiri may be employed in the future for providing better understanding of the roles of convection and diffusion in macromolecular transport. The model explicitly estimates both diffusion and velocity coefficients (convection) in any compartment from unsteady-state concentration profiles. In addition, spatial inhomogeneities can be evaluated since the model allows for different diffusion coefficients and velocities of the solute in the x and y directions.

APPENDIX A

PROGRAM SAGID

This program simulates a dot matrix picture of an original video image. A step by step procedure on how to use this program is given below:

(1) Have an IMAGE file ready (i.e. A digitized file which is created by program IMAGE). When the program prompts: Input File Name?-- Give this file name.

(2) It prompts you back to give a name to an output file, this file is created by running this program. Give an appropriate output filename. It is this file for which we are running this program. This file will have a graylevel intensity for each of the 27,950 addresses (215 by 130 pixels). By looking at the pseudo colored picture one can locate a leakage site. After locating an appropriate address one can then determine the intensity (orgraylevel) at that particular location or address, by looking at this output

file. Once the graylevels for a definite range of addresses are noted, it is a straightforward calculation to convert the graylevels to their corresponding concentrations.

(3) Next, SAGID will prompt you for the number of pen-colors to be used to make a picture. Our HP plotter has a maximum of four colors and hence we give four. However, you can always give less than that depending upon the requirement of the simulated picture.

(4) After specifying the number of pen-colors, it will ask you to define the range for each color. The word *range* here is important. The A/D converter which we employed was of 8 bits and hence the graylevel ranges from 0 to a maximum of 255 (i.e. $2^8 = 256$). The digitized picture is made up of 27,950 pixels (215 * 130; which is the uniform frame size we used throughout). By looking at the histogram of that particular digitized frame (Program IMAGE allows one to look at the histogram of a particular digitized frame), one can easily decide the four required ranges (or less than four, if one prefers) as to which ranges would fit a particular graylevel distribution. After specifying four ranges, stop

the program.

(5) SAGID has now created two files. A file called "GRF2" and a strange file called "%26%". The reason for a complicated filename is so as not to mistake this particular filename with any other file which is in the memory. One more important note: The file %26% must be removed from the present directory, otherwise the program SAGID will fail to run. The file GFR2 has the four graylevel ranges corresponding to addresses 0 to 27,950. Now call the GRAFIT software on the system and have GRAFIT read read the file %26% in accordance with the instructions in file GRF2. [The file %26% contains 27,950 graylevels (Between 0 to 255) and addresses, and file GRF2 dictates the graylevel range, which correspond to each color] Since we have, for example, four ranges we have to read file %26%, range by range, four times. After reading the file %26% if you wish, save it under an appropriate filename, which will have an extension as ".GRF" since it is created via the GRAFIT software.

(6) Once you are through reading the file %26% just punch in following:

```
G > CURVE 1 X C1 Y C2
G > CURVE 2 X C3 Y C4
G > CURVE 3 X C5 Y C6
G > CURVE 4 X C7 Y C8
G > DO FELT_7550(for color)
```

OR

```
Do BLACK_7550
```

That is it, in doing this you will have a pseudo-colorpicture of your original video image. The number of colors would, of course, depend on how many pen-colors you had specified at the beginning.

APPENDIX B

Experimental Data

Tables 5.1 through 5.24

Table 5-1 Leakage of FITC-Dx-20 from a leakage site on a
 18-20 um postcapillary venule. Measured Average Graylevel values,
 Mean and Standard Deviation at time = 2711 s.

Time = 2711 secs Pixel 1 X 1									
Position	Dist.	Avg. Graylevel						Mean	STDDEV
(X, Y)	(um)	F1	F2	F3	F4	F5	F6		±
140, 165	0	67	68	68	69	64	62	66.333	2.733
160, 165	50	56	66	71	66	65	68	65.333	5.046
180, 165	100	52	63	57	63	51	53	56.500	5.431
200, 165	150	60	62	62	62	57	60	60.500	1.975
220, 165	200	49	53	57	54	54	51	53.000	2.757
240, 165	250	53	61	60	61	59	59	58.833	2.994
260, 165	300	47	46	56	48	61	51	51.500	2.994
280, 165	350	56	52	53	53	59	54	54.500	5.891
300, 165	400	47	57	50	56	51	52	52.167	3.764

Table 5-2 Leakage of FITC-Dx-20 from a leakage site on a
 18-20 um postcapillary venule. Measured Average Graylevel values,
 Mean and Standard Deviation at time = 2711 s.

Time = 2711 secs Pixel 5 X 5									
Position Dist.		Avg. Graylevel						Mean	STDDEV
(X,Y)	(um)	F1	F2	F3	F4	F5	F6		±
140,165	0	68.24	67.68	67.04	68.04	67.56	69.00	67.927	0.670
160,165	50	58.32	61.28	59.96	61.88	64.16	60.08	60.947	1.997
180,165	100	58.72	61.68	62.16	62.20	63.20	59.92	61.313	1.665
200,165	150	58.96	58.84	62.1	59.24	62.44	60.24	60.307	1.609
220,165	200	57.76	57.80	59.52	58.16	58.48	59.64	58.560	0.833
240,165	250	57.64	58.36	58.88	58.16	59.32	59.56	58.653	0.731
260,165	300	52.88	54.60	56.00	55.08	57.96	53.76	55.047	1.786
280,165	350	51.80	53.80	53.88	54.16	51.04	53.56	53.040	1.292
300,165	400	48.56	50.80	50.12	51.08	51.64	50.16	50.393	1.066

Table 5-3 Leakage of FITC-Dx-20 from a leakage site on a 18-20 um postcapillary venule. Measured Average Graylevel values, Mean and Standard Deviation at time = 2711 s.

Time = 2711 secs Pixel 10 X 10									
Position	Dist.	Avg. Graylevel						Mean	STDDEV
(X, Y)	(um)	F1	F2	F3	F4	F5	F6		±
140, 165	0	65.49	67.63	67.45	68.10	65.70	67.41	66.963	1.090
160, 165	50	61.87	64.52	63.92	64.87	63.38	63.81	63.728	1.053
180, 165	100	60.56	62.13	62.28	62.42	60.15	62.29	61.638	1.007
200, 165	150	58.11	59.96	61.40	60.32	62.64	59.80	60.372	1.537
220, 165	200	58.89	59.27	59.19	59.60	60.61	60.59	59.692	0.739
240, 165	250	56.42	58.48	60.45	58.74	59.53	58.04	58.610	1.370
260, 165	300	54.94	56.49	56.61	56.71	56.18	56.13	56.177	0.648
280, 165	350	53.36	55.09	54.24	55.38	54.20	55.02	54.548	0.753
300, 165	400	50.22	50.65	50.21	50.87	52.29	51.50	50.957	0.890

Table 5-4 Leakage of FITC-Dx-20 from a leakage site on a 18-20 um postcapillary venule. Measured Average Graylevel values, Mean and Standard Deviation at time = 4401 s.

Time = 4401 secs Pixel 1 X 1									
Position	Dist.	Avg. Graylevel						Mean	STDDEV
(X, Y)	(um)	F1	F2	F3	F4	F5	F6		±
140, 165	0	68.00	64.00	63.00	60.00	67.00	67.00	64.833	3.061
160, 165	50	69.00	61.00	68.00	63.00	69.00	66.00	66.000	3.347
180, 165	100	70.00	64.00	55.00	67.00	70.00	67.00	65.500	5.612
200, 165	150	70.00	74.00	64.00	62.00	72.00	67.00	68.167	4.665
220, 165	200	60.00	57.00	52.00	69.00	59.00	58.00	59.167	5.565
240, 165	250	56.00	61.00	68.00	68.00	57.00	63.00	60.500	6.348
260, 165	300	67.00	60.00	63.00	59.00	68.00	63.00	63.333	3.615
280, 165	350	53.00	52.00	55.00	60.00	55.00	67.00	57.000	5.621
300, 165	400	52.00	54.00	65.00	55.00	54.00	53.00	55.500	4.764

Table 5-5 Leakage of FITC-Dx-20 from a leakage site on a
 18-20 um postcapillary venule. Measured Average Graylevel values,
 Mean and Standard Deviation at time = 4401 s.

Time = 4401 secs Pixel 5 X 5									
Position	Dist.	Avg. Graylevel						Mean	STDDEV
(X,Y)	(um)	F1	F2	F3	F4	F5	F6		±
140,165	0	67.16	64.12	63.00	66.08	68.88	69.08	66.387	2.481
160,165	50	59.76	62.84	62.28	64.60	61.68	64.48	62.607	1.822
180,165	100	64.44	63.96	65.20	71.56	66.36	66.00	66.253	2.753
200,165	150	64.20	63.28	64.68	64.00	66.00	65.64	64.633	1.030
220,165	200	69.96	64.04	62.68	60.56	60.36	62.84	63.407	3.509
240,165	250	60.08	63.48	64.32	63.32	61.36	62.80	62.560	1.560
260,165	300	56.64	58.84	59.28	61.84	57.88	60.16	59.107	1.804
280,165	350	54.04	56.76	58.08	58.04	55.28	58.64	56.807	1.816
300,165	400	54.88	53.64	55.64	55.60	56.48	55.72	55.327	0.970

Table 5-6 Leakage of FITC-Dx-20 from a leakage site on a 18-20 um postcapillary venule. Measured Average Graylevel values, Mean and Standard Deviation at time = 4401 s.

Time = 4401 secs Pixel 10 X 10									
Position	Dist.	Avg. Graylevel						Mean	STDDEV
(X, Y)	(um)	F1	F2	F3	F4	F5	F6		±
140, 165	0	65.33	65.06	65.12	65.45	66.96	67.42	65.890	1.027
160, 165	50	62.53	64.26	63.45	65.67	64.13	65.12	64.193	1.128
180, 165	100	64.38	64.02	65.12	66.92	66.02	66.66	65.520	1.202
200, 165	150	63.99	63.35	64.41	64.55	65.59	65.65	64.590	0.901
220, 165	200	60.96	64.90	63.29	62.78	62.20	63.38	62.918	1.315
240, 165	250	60.60	60.24	61.00	61.63	62.06	63.15	59.755	3.375
260, 165	300	56.58	58.30	58.88	60.75	57.72	58.97	58.533	1.397
280, 165	350	56.49	57.35	57.92	58.12	58.22	59.67	57.962	1.054
300, 165	400	52.62	52.49	53.95	54.03	54.15	54.22	53.577	0.798

Table 5-7 Leakage of FITC-Dx-20 from a left leakage site on a 18-20 um postcapillary venule. Measured Average Graylevel values, Mean and Standard Deviation at time = 4446 s.

Time = 4446 secs Pixel 1 X 1									
Position	Dist.	Avg. Graylevel						Mean	STDDEV
(X,Y)	(um)	F1	F2	F3	F4	F5	F6		±
278,165	0	62.00	59.00	69.00	69.00	70.00	69.00	66.333	4.633
258,165	50	77.00	64.00	65.00	75.00	70.00	71.00	70.333	5.203
238,165	100	71.00	64.00	64.00	73.00	70.00	69.00	68.500	3.728
218,165	150	58.00	66.00	63.00	62.00	68.00	68.00	64.167	3.920
198,165	200	66.00	65.00	60.00	52.00	61.00	61.00	60.833	4.956
178,165	250	58.00	58.00	55.00	52.00	54.00	54.00	55.167	2.401
158,165	300	57.00	55.00	60.00	54.00	61.00	62.00	58.167	3.312
138,165	350	45.00	46.00	49.00	50.00	38.00	37.00	44.167	5.492
118,165	400	53.00	47.00	36.00	54.00	50.00	50.00	48.333	6.532

Table 5-8 Leakage of FITC-Dx-20 from a left leakage site on a
 18-20 um postcapillary venule. Measured Average Graylevel values,
 Mean and Standard Deviation at time = 4446 s.

Time = 4446 secs Pixel 5 X 5									
Position	Dist.	Avg. Graylevel						Mean	STDDEV
(X, Y)	(um)	F1	F2	F3	F4	F5	F6		±
278, 165	0	64.80	64.04	64.08	64.12	65.96	66.36	64.893	1.028
258, 165	50	65.64	62.00	66.68	65.92	65.48	65.84	65.260	1.650
238, 165	100	67.52	66.00	68.60	67.56	68.56	69.00	67.873	1.096
218, 165	150	61.20	63.28	63.64	64.24	66.28	66.36	64.167	1.957
198, 165	200	57.00	55.04	56.88	57.36	56.44	56.20	56.487	0.820
178, 165	250	53.60	57.84	60.04	56.32	53.84	54.04	55.947	2.610
158, 165	300	54.20	50.28	50.64	54.76	50.44	50.92	51.873	2.038
138, 165	350	43.96	44.48	47.88	48.00	44.76	44.92	45.667	1.791
118, 165	400	45.60	45.28	44.40	46.84	44.88	45.08	45.347	0.835

Table 5-9 Leakage of FITC-Dx-20 from a left leakage site on a 18-20 um postcapillary venule. Measured Average Graylevel values, Mean and Standard Deviation at time = 4446 s.

Time = 4446 secs Pixel 10 X 10									
Position	Dist.	Avg. Graylevel						Mean	STDDEV
(X,Y)	(um)	F1	F2	F3	F4	F5	F6		±
278,165	0	68.54	69.06	70.85	67.08	68.41	66.36	68.795	1.221
258,165	50	68.04	65.94	66.92	68.76	67.32	67.75	67.455	0.973
238,165	100	68.04	66.53	67.03	68.82	68.26	68.46	67.857	0.887
218,165	150	63.22	63.71	64.72	63.02	64.50	64.77	63.990	0.776
198,165	200	59.25	58.94	63.80	58.38	57.89	57.85	59.352	2.250
178,165	250	56.17	57.26	58.87	56.89	55.94	56.21	56.890	1.090
158,165	300	55.23	53.82	54.67	54.99	54.67	54.94	54.720	0.489
138,165	350	47.70	47.26	49.11	47.64	47.00	47.26	47.662	0.756
118,165	400	42.75	42.82	43.13	44.09	42.80	42.96	43.092	0.508

Table 5-10 Leakage of FITC-Dx-20 from a left leakage site on a
 18-20 um postcapillary venule. Measured Average Graylevel values,
 Mean and Standard Deviation at time = 5591 s.

Time = 5591 secs Pixel 1 X 1									
Position	Dist.	Avg. Graylevel						Mean	STDDEV
(X, Y)	(um)	F1	F2	F3	F4	F5	F6		±
278, 165	0	56.00	69.00	68.00	73.00	64.00	69.00	66.500	5.891
258, 165	50	66.00	62.00	62.00	63.00	62.00	68.00	63.833	2.563
238, 165	100	60.00	60.00	65.00	59.00	63.00	59.00	61.000	2.449
218, 165	150	65.00	65.00	79.00	62.00	61.00	67.00	66.500	6.504
198, 165	200	58.00	64.00	64.00	59.00	56.00	60.00	60.167	3.251
178, 165	250	50.00	50.00	57.00	57.00	52.00	56.00	53.667	3.386
158, 165	300	50.00	50.00	50.00	50.00	50.00	47.00	49.500	1.225
138, 165	350	41.00	46.00	46.00	53.00	44.00	50.00	46.667	4.274
118, 165	400	43.00	41.00	43.00	39.00	48.00	41.00	42.500	3.082

Table 5-11 Leakage of FITC-Dx-20 from a left leakage site on a 18-20 um postcapillary venule. Measured Average Graylevel values, Mean and Standard Deviation at time = 5591 s.

Time = 5591 secs									
Pixel 5 X 5									
Position	Dist.	Avg. Graylevel						Mean	STDDEV
(X,Y)	(um)	F1	F2	F3	F4	F5	F6		±
278,165	0	68.48	61.92	66.04	69.40	66.08	67.20	66.520	2.615
258,165	50	62.00	59.20	61.56	61.68	62.40	61.36	61.367	1.122
238,165	100	63.92	65.00	63.96	63.52	63.40	65.64	64.240	0.888
218,165	150	62.48	62.76	61.84	62.20	64.44	61.60	62.720	1.080
198,165	200	60.52	59.88	59.76	61.72	62.32	59.16	60.560	1.225
178,165	250	56.76	56.52	57.08	58.28	57.24	57.20	57.753	1.963
158,165	300	54.60	57.00	58.04	58.20	52.48	57.00	56.220	2.239
138,165	350	48.32	48.96	50.88	50.00	50.64	49.08	49.647	1.108
118,165	400	44.04	41.84	41.56	41.72	43.80	43.08	42.673	1.109

Table 5-12 Leakage of FITC-Dx-20 from a left leakage site on a 18-20 um postcapillary venule. Measured Average Graylevel values, Mean and Standard Deviation at time = 5591 s.

Time = 5591 secs Pixel 10 X 10									
Position	Dist.	Avg. Graylevel						Mean	STDDEV
(X,Y)	(um)	F1	F2	F3	F4	F5	F6		±
278,165	0	67.54	66.72	66.74	69.99	68.06	68.29	67.890	1.218
258,165	50	63.65	63.12	63.41	64.37	63.58	63.95	62.680	0.435
238,165	100	65.32	66.08	64.80	64.86	65.80	66.40	65.543	0.657
218,165	150	62.51	62.05	61.55	64.07	63.21	62.72	62.685	0.885
198,165	200	59.98	60.76	60.31	61.37	60.61	59.36	60.398	0.690
178,165	250	57.13	56.04	56.87	58.08	57.16	56.82	57.017	0.660
158,165	300	57.92	57.28	56.75	56.97	56.48	57.13	57.088	0.496
138,165	350	48.65	48.07	49.26	50.40	48.65	49.18	49.035	0.795
118,165	400	43.95	44.94	44.04	44.23	44.75	44.58	44.415	0.402

Table 5-13 Leakage of FITC-Dx-70 from a leakage site on a
 18-20 um postcapillary venule. Measured Average Graylevel values,
 Mean and Standard Deviation at time = 5895 s.

Time = 5895 secs Pixel 1 X 1									
Position	Dist.	Avg. Graylevel						Mean	STDDEV
(X, Y)	(um)	F1	F2	F3	F4	F5	F6		±
135, 165	0	86.00	98.00	92.00	91.00	87.00	90.00	90.667	4.274
155, 165	50	78.00	78.00	83.00	83.00	77.00	79.00	79.667	2.658
175, 165	100	65.00	67.00	61.00	67.00	81.00	64.00	67.500	6.979
195, 165	150	65.00	60.00	71.00	70.00	73.00	72.00	68.500	5.010
215, 165	200	55.00	65.00	58.00	60.00	68.00	58.00	60.667	4.885
235, 165	250	60.00	65.00	64.00	66.00	75.00	62.00	65.333	5.203
255, 165	300	63.00	56.00	55.00	59.00	62.00	56.00	58.500	3.391
275, 165	350	48.00	72.00	54.00	52.00	53.00	50.00	54.833	8.681
295, 165	400	56.00	49.00	52.00	47.00	51.00	40.00	49.167	5.419

Table 5-14 Leakage of FITC-Dx-70 from a leakage site on a 18-20 um postcapillary venule. Measured Average Graylevel values, Mean and Standard Deviation at time = 5895 s.

Time = 5895 secs									
Pixel 5 X 5									
Position	Dist.	Avg. Graylevel						Mean	STDDEV
(X,Y)	(um)	F1	F2	F3	F4	F5	F6		±
135,165	0	85.56	87.60	89.40	88.52	86.56	90.56	88.033	1.842
155,165	50	80.04	75.48	77.44	78.92	78.48	78.20	78.093	1.542
175,165	100	71.88	72.68	75.40	74.24	73.76	74.44	73.733	1.271
195,165	150	67.04	65.96	68.68	68.56	64.92	68.16	67.220	1.531
215,165	200	63.52	61.00	62.12	63.96	65.68	64.00	63.380	1.630
235,165	250	63.88	63.80	61.04	63.80	66.20	61.16	63.313	1.946
255,165	300	58.96	59.16	56.08	56.76	58.76	57.28	57.833	1.298
275,165	350	54.32	59.88	58.84	53.96	51.92	55.56	55.747	3.052
295,165	400	52.44	49.60	51.92	53.00	51.92	50.84	51.620	1.220

Table 5-15 Leakage of FITC-Dx-70 from a leakage site on a 18-20 um postcapillary venule. Measured Average Graylevel values, Mean and Standard Deviation at time = 5895 s.

Time = 5895 secs Pixel 10 X 10									
Position	Dist.	Avg. Graylevel						Mean	STDDEV
(X,Y)	(um)	F1	F2	F3	F4	F5	F6		±
135,165	0	84.56	84.07	85.18	85.36	84.73	84.73	84.772	0.459
155,165	50	78.26	78.31	78.30	79.51	79.12	78.58	78.680	0.520
175,165	100	69.29	71.58	72.11	71.17	70.25	69.83	70.705	1.089
195,165	150	64.11	64.69	66.59	67.02	64.86	66.86	65.688	1.275
215,165	200	64.30	65.29	65.71	64.10	64.00	64.65	64.675	0.689
235,165	250	61.89	60.81	60.56	61.66	62.05	60.53	61.250	0.694
255,165	300	56.36	57.90	57.44	57.83	56.84	58.48	57.475	0.770
275,165	350	54.07	54.43	53.55	52.63	54.20	53.95	53.805	0.646
295,165	400	50.55	52.13	51.56	52.69	51.78	52.14	51.808	0.726

Table 5-16 Leakage of FITC-Dx-70 from a leakage site on a
 18-20 μm postcapillary venule. Measured Average Graylevel values,
 Mean and Standard Deviation at time = 7950 s.

Time = 7950 secs Pixel 1 X 1									
Position Dist.		Avg. Graylevel						Mean	STDDEV
(X,Y)	(μm)	F1	F2	F3	F4	F5	F6		\pm
135,165	0	117.0	112.0	111.0	101.0	115.0	117.0	112.167	6.014
155,165	50	100.0	103.0	107.0	120.0	118.0	112.0	110.000	8.075
175,165	100	101.0	78.00	92.00	79.00	86.00	87.00	87.167	8.565
195,165	150	98.00	91.00	104.0	98.00	96.00	75.00	93.667	10.053
215,165	200	99.00	87.00	96.00	74.00	77.00	96.00	88.167	10.647
235,165	250	74.00	91.00	117.0	99.00	98.00	97.00	96.000	13.885
255,165	300	77.00	100.0	84.00	84.00	77.00	90.00	85.333	8.710
275,165	350	86.00	70.00	66.00	74.00	78.00	91.00	77.500	9.545
295,165	400	77.00	80.00	57.00	80.00	73.00	76.00	73.833	8.658

Table 5-17 Leakage of FITC-Dx-70 from a leakage site on a 18-20 um postcapillary venule. Measured Average Graylevel values, Mean and Standard Deviation at time = 7950 s.

Time = 7950 secs Pixel 5 X 5									
Position	Dist.	Avg. Graylevel						Mean	STDDEV
(X, Y)	(um)	F1	F2	F3	F4	F5	F6		±
135, 165	0	110.6	115.4	114.2	115.8	114.6	109.9	113.427	2.523
155, 165	50	102.7	110.2	103.8	111.5	116.2	110.7	109.200	5.067
175, 165	100	96.68	92.44	95.20	97.04	92.28	95.84	94.913	2.080
195, 165	150	86.04	92.44	95.20	97.04	92.28	95.84	93.620	4.231
215, 165	200	88.40	83.64	85.44	88.36	85.24	90.32	86.900	2.514
235, 165	250	83.48	89.12	86.88	89.24	86.76	89.84	87.553	2.375
255, 165	300	89.80	83.52	85.12	88.12	85.92	80.84	85.553	3.203
275, 165	350	78.72	78.36	76.24	75.40	75.24	78.36	77.053	1.605
295, 165	400	75.32	74.04	72.80	70.16	72.76	71.80	72.813	1.781

Table 5-18 Leakage of FITC-Dx-70 from a leakage site on a 18-20 μm postcapillary venule. Measured Average Graylevel values, Mean and Standard Deviation at time = 7950 s.

Time = 7950 secs Pixel 10 X 10									
Position Dist.		Avg. Graylevel						Mean	STDDEV
(X, Y)	(μm)	F1	F2	F3	F4	F5	F6		\pm
135, 165	0	111.1	113.6	112.8	113.7	114.8	111.5	112.917	1.414
155, 165	50	103.8	107.5	105.4	107.7	107.5	107.8	106.607	1.642
175, 165	100	93.55	94.68	95.18	95.03	95.06	96.28	94.963	0.880
195, 165	150	89.20	93.11	91.35	91.07	92.25	91.17	91.358	1.315
215, 165	200	88.55	87.72	87.50	90.30	90.65	90.06	89.130	1.380
235, 165	250	87.34	89.15	87.26	89.57	87.35	89.95	88.437	1.253
255, 165	300	84.79	81.43	84.80	84.92	84.07	83.21	83.870	1.360
275, 165	350	79.96	81.39	79.61	79.70	78.29	78.17	79.520	1.189
295, 165	400	72.64	72.07	72.32	71.46	72.62	71.81	72.153	0.446

Table 5-19 Leakage of FITC-Dx-70 from a leakage site on a
 18-20 um postcapillary venule. Measured Average Graylevel values,
 Mean and Standard Deviation at time = 4320 s.

Time = 4320 secs Pixel 1 X 1									
Position	Dist.	Avg. Graylevel						Mean	STDDEV
(X,Y)	(um)	F1	F2	F3	F4	F5	F6		±
144,165	0	52.00	43.00	48.00	51.00	52.00	52.00	49.667	3.615
164,165	50	51.00	49.00	46.00	56.00	48.00	60.00	51.667	5.317
184,165	100	44.00	39.00	41.00	43.00	40.00	48.00	42.500	3.271
204,165	150	35.00	38.00	40.00	38.00	43.00	47.00	40.167	4.262
224,165	200	59.00	50.00	39.00	59.00	43.00	38.00	48.000	9.508
244,165	250	33.00	30.00	37.00	33.00	42.00	42.00	36.167	5.037
264,165	300	43.00	39.00	38.00	43.00	44.00	38.00	40.833	2.787
284,165	350	44.00	47.00	32.00	44.00	33.00	39.00	39.833	6.242
304,165	400	33.00	35.00	32.00	34.00	44.00	38.00	36.000	4.427

Table 5-20 Leakage of FITC-Dx-70 from a leakage site on a 18-20 um postcapillary venule. Measured Average Graylevel values, Mean and Standard Deviation at time = 4320 s.

Time = 4320 secs Pixel 5 X 5									
Position Dist.		Avg. Graylevel						Mean	STDDEV
(X, Y)	(um)	F1	F2	F3	F4	F5	F6		±
144, 165	0	49.92	49.48	51.44	50.12	54.52	56.92	52.067	3.002
164, 165	50	50.52	51.28	48.72	50.64	50.84	55.36	51.227	2.207
184, 165	100	47.96	47.88	48.20	48.44	46.04	47.80	47.720	0.856
204, 165	150	42.80	44.24	43.88	43.88	42.84	42.84	43.413	0.656
224, 165	200	40.96	40.32	39.16	40.44	41.52	39.48	40.313	0.885
244, 165	250	38.04	39.72	36.84	38.04	38.92	40.32	38.647	1.267
264, 165	300	38.40	38.52	37.52	39.00	41.80	40.84	39.347	1.630
284, 165	350	37.32	37.88	36.32	37.96	35.48	38.44	37.233	1.124
304, 165	400	35.08	33.44	33.44	35.80	35.80	36.80	35.060	1.369

Table 5-21 Leakag of FITC-Dx-70 from a leakage site on a
 18-20 um postcapillary venule. Measured Average Graylevel values,
 Mean and Standard Deviation at time = 4320 s.

Time = 4320 secs Pixel 10 X 10									
Position	Dist.	Avg. Graylevel						Mean	STDDEV
(X, Y)	(um)	F1	F2	F3	F4	F5	F6		±
144, 165	0	51.09	51.09	51.62	51.25	53.66	57.24	52.658	2.449
164, 165	50	50.76	51.49	50.23	51.20	49.95	54.50	51.355	1.645
184, 165	100	45.86	45.94	46.76	45.98	45.88	47.32	46.290	0.609
204, 165	150	42.62	43.46	43.02	42.88	42.63	43.28	42.982	0.342
224, 165	200	40.11	39.45	39.88	40.29	40.98	42.12	40.472	0.952
244, 165	250	37.26	38.27	37.30	37.47	38.41	39.55	38.043	0.889
264, 165	300	37.87	38.64	37.26	38.17	37.76	38.09	37.965	0.461
284, 165	350	35.69	36.40	35.25	35.97	35.66	37.07	36.007	0.645
304, 165	400	34.15	34.86	35.80	34.47	35.70	35.95	35.155	0.763

Table 5-22 Leakage of FITC-Dx-70 from a leakage site on a 18-20 um postcapillary venule. Measured Average Graylevel values, Mean and Standard Deviation at time = 6675 s.

Time = 6675 secs Pixel 1 X 1									
Position	Dist.	Avg. Graylevel						Mean	STDDEV
(X, Y)	(um)	F1	F2	F3	F4	F5	F6		±
144, 165	0	91.00	77.00	77.00	76.00	74.00	86.00	80.167	6.735
164, 165	50	79.00	73.00	71.00	67.00	84.00	58.00	72.000	9.121
184, 165	100	76.00	79.00	84.00	64.00	86.00	75.00	77.333	7.840
204, 165	150	68.00	66.00	65.00	61.00	64.00	61.00	64.167	2.787
224, 165	200	64.00	63.00	63.00	72.00	62.00	67.00	65.167	3.764
244, 165	250	57.00	57.00	55.00	60.00	78.00	64.00	61.833	8.519
264, 165	300	64.00	57.00	57.00	63.00	56.00	59.00	59.333	3.386
284, 165	350	51.00	53.00	60.00	66.00	60.00	51.00	56.833	6.113
304, 165	400	48.00	64.00	67.00	63.00	69.00	61.00	62.000	7.430

Table 5-23 Leakage of FITC-Dx-70 from a leakage site on a 18-20 um postcapillary venule. Measured Average Graylevel values, Mean and Standard Deviation at time = 6675 s.

Time = 6675 secs Pixel 5 X 5									
Position	Dist.	Avg. Graylevel						Mean	STDDEV
(X, Y)	(um)	F1	F2	F3	F4	F5	F6		±
144, 165	0	71.40	75.28	75.56	74.36	74.56	75.72	74.480	1.603
164, 165	50	76.56	78.00	77.76	75.40	77.28	77.00	77.000	0.939
184, 165	100	68.52	75.44	75.56	71.64	74.20	74.00	73.227	2.704
204, 165	150	64.88	67.48	67.32	66.60	70.36	64.08	66.787	2.215
224, 165	200	60.36	60.40	61.08	64.00	59.88	62.04	61.293	1.523
244, 165	250	57.40	56.16	54.88	57.68	60.16	60.12	57.733	2.113
264, 165	300	56.00	56.92	56.24	58.36	56.48	58.68	57.113	1.136
284, 165	350	54.40	53.68	54.12	56.72	54.76	54.32	54.667	1.067
304, 165	400	53.92	54.24	54.24	56.68	57.48	54.84	55.233	1.483

Table 5-24 Leakage of FITC-Dx-70 from a leakage site on a 18-20 um postcapillary venule. Measured Average Graylevel values, Mean and Standard Deviation at time = 6675 s.

Time = 6675 secs										Pixel 10 X 10									
Position		Dist.	Avg. Graylevel						Mean	STDDEV									
(X,Y)	(um)		F1	F2	F3	F4	F5	F6		±									
144,165	0		75.00	75.71	75.47	75.57	77.93	76.30	75.997	1.036									
164,165	50		74.34	75.75	75.42	74.17	75.72	75.35	75.125	0.694									
184,165	100		71.62	72.92	73.06	73.10	73.13	73.59	72.903	0.668									
204,165	150		65.25	65.69	65.52	65.44	66.58	64.80	65.547	0.591									
224,165	200		60.29	58.65	59.06	61.69	58.69	61.19	59.928	1.323									
244,165	250		57.25	56.94	56.57	58.02	59.58	58.15	57.752	1.084									
264,165	300		56.30	57.17	56.97	58.02	57.19	58.14	57.298	0.687									
284,165	350		56.39	56.35	56.44	57.51	54.23	56.07	56.165	1.070									
304,165	400		55.09	53.97	53.80	56.10	55.56	56.50	55.170	1.105									

BIBLIOGRAPHY

- Adair, T.H., Moffatt, D.S., and Guyton, A.C., "Lymph Flow and Composition is Modified by the Lymph Node", Microvasc. Res., vol. 21, 1981, p.234
- Alvarez, O.A., and Yudilevich, D., "Heart Capillary Permeability to Lipid-Insoluble Molecules", J. Physiol. (London), vol. 202, 1969, pp. 45-48.
- Arfors, K.E., Rutili, G., and Svensjo, E., "Microvascular Transport of Macromolecules in Normal and Inflammatory Conditions", Acta. Physiol. Scand., vol. 463, 1979, pp. 93-103.
- Arturson, G., Arescog, N.A., Arfors, K.-E., Grotte, G., and Malmberg, P., "The Transport of Macromolecules across the Blood-Lymph Barrier", Bibl. Anat., vol 10, 1969, pp. 228-233
- Arturson, G., Groth, T., and Grotte, G., "The Functional Ultra-structure of the Blood-Lymph Barrier. Computer Analysis of Data from Dog Heart-Lymph Experiments Using Theoretical Models", Acta Physiol. Scand. (Suppl.), vol.377, 1979, pp. 1-29
- Baxter, L.T., and Jain, R.K., "Vascular Permeability and Interstitial diffusion in Perfused Tissues: A Two Dimensional Model", Microvasc. Res., 36, 1988, pp. 108-115.
- Bekker, A.Y., "Transient Analysis of Macromolecular Blood-Tissue Exchange In Microvascular Bed", Ph.D. Dissertation, NJIT, Dept. Chemical Engineering, 1987

- Bekker, A.Y., Ritter, A.B., Durán, W.N. "Reduction of Pressure in Postcapillary Venules Induced by EPI-Fluorescent Illumination of FITC-Dextrans", Microcirc. Endoth. Lymphatics, 3, 1987, pp. 411-423
- Bekker, A.Y., Ritter, A.B., Durán, W.N. "Analysis of Microvascular Permeability to Macromolecules by Video Image Digital Processing", Microvas. Res., 38, 1989, pp. 200-216
- Blake, L., and Staub, N., "Pulmonary Vascular Transport In Sheep: A Mathematical Model", Microvasc. Res., vol. 12, 1976, pp. 197-220
- Brigham, K.L., Harris, T.R., Bowers, R.E., and Roselli, R.J., "Lung Vascular Permeability: Inferences from Measurement of Plasma to Lung Lymph Protein Transport", Lymphology, vol. 12, 1979, pp. 177-190
- Dillon, P., "Microvascular Effects of Platelet Activating Factor: Characterization of the Dose-Response Relationships and Elucidation of its Pathways of Action", Ph.D. Dissertation, UMDNJ, Dept. Physiology, 1986
- Drake, R., Adair, T., Traber, D., and Gabel, J., "Contamination of Caudal Mediastinal Node Efferent Lymph in Sheep", Am. J. Physiol., vol. 241, 1981, pp. H354-H357
- Duling, B.R., and Staples, E., "A Comparison of the Performance of Microvessels in the Hamster Cheek Pouch During Exposure to Tris and Bicarbonate Buffers", Microvasc. Res., vol. 7, 1974, pp. 277-279
- Durán, W.N., and Yudilevich, D.L., "Estimate of Capillary Permeability Coefficients of Canine Heart to Sodium and Glucose", Microvasc. Res., vol. 15, 1978, pp. 195-205.

- Dumrongsiri, S., "Mathematical And Experimental Model of Coronary Macromolecular Transportation in Diabetes Mellitus", Ph.D Dissertation, UMDNJ, 1990
- Fox, I.R., and Wayland, H., "Interstitial Diffusion of Macromolecules in the Rat Mesentery", Microvasc. Res., vol. 18, 1979, pp. 255-276.
- Ganrot, K., Jacobsson, S., and Rothman, U., "Transcapillary Passage of Plasma Proteins in Experimental Burns", Acta Physiol. Scand., vol. 91, 1974, pp. 497-501.
- Garlick, D.G., and Renkin, E.M., "Transport of Large Molecules from Plasma to Interstitial Fluid and Lymph in Dog", Am. J. Physiol., vol. 219, 1970, pp. H1596-H1605.
- Gawlowski, D.M., "Influence of Vasodilating Agents on Microvascular Permeability in the Hamster Cheek Pouch", Ph.D. Dissertation, UMDNJ, Dept. Physiology, 1984.
- Gawlowski, D.M., and Duran, W.N., "Dose-Related Effects of Adenosine and Bradykinin on Microvascular Permeability to Macromolecules in the Hamster Cheek Pouch" Circ. Res., vol. 55, 1986, pp. 348-355.
- Gawlowski, D.M., and Granger, N.J., "Dextran-Induced Leukocytes Activation in Hamster Cheek Pouch Microcirculation", Fed. Proc., vol. 46, 1987, p. 1529.
- Gawlowski, D.M., Ritter, A.B., and Duran, W.N., "Reproducibility of Microvascular Permeability Responses to Successive Topical Applications of Bradikinin in the Hamster Cheek Pouch", Microvasc. Res., vol. 24, 1982, pp. 354-363.
- Granger, D.N., Miller, T., Allen, R., Parker, R.E., Parker J.C., and Taylor, A.E., "Permeability of the Liver Blood-Lymph Barrier to Endogeneous Macromolecules", Gastroenterology, vol. 77, 1979, pp. 103-109.

- Grotte, G., "Passage of Dextran Molecules Across the Blood-Lymph Barrier", Acta Chir. Scand. (Suppl.), vol. 211, 1956, pp. 1-84
- Haddy, F.J., Scott, J.B., and Grega, G.J., "Effects of Histamine on Lymph Protein Concentration and Flow in the Dog Forelimb", Am. J. Physiol., vol. 223, 1972, pp. H1172-H1177.
- Joyner, W.L., "Effects of Prostaglandins on Macromolecular Transport from Blood to Tissue in the Dog", Am. J. Physiol., vol. 236, 1977, pp. H690-H696.
- Joyner, W.L., Svensjo, E., and Arfors, K.-E., "Simultaneous Measurement of Macromolecular Leakage and Arteriolar fBlood Flow as Altered by PGE, and -receptor Stimulant in the Hamster Cheek Pouch", Microvasc. Res., vol. 18, 1979, pp. 301-310.
- Kedem, O., and Katchalsky, A., "Thermodynamic Analysis of the Permeability of Biological Membranes to Non-electrolytes", Biochim. Biophys. Acta, vol. 27, 1958, pp. 1229-1246.
- Khimani, N.V., "Three Dimensional Study of Macromolecular Leakage Patterns Using Video Image Analysis", NJIT Coll., 1988.
- Lee, K., and Arfors, K.-E., "Segmental Differences of Microvascular Permeability for FITC-Dextran Measured in fthe Hamster Cheek Pouch", Microvasc. Res., vol. 31, 1986, pp.84-99.
- Marquardt, D.W., "An Algorithm for Least Squares estimation of Nonlinear Parameters", SIAM J., vol. 11, 1963, pp. 431-440.

- Mayhan, W.G., and Joyner, W.L., "The Effect of Altering the External Calcium Concentration and Calcium Channel Blocker, Verapamil, on Microvascular Leaky Sites and Dextran Clearance in the Hamster Cheek Pouch", Microvasc. Res., vol. 28, 1984, pp. 143-158.
- McNamee, J.E., and Staub, N.C., "Pore Model of Sheep Lung Microvascular Barrier Using New Data on Protein racers" Microvasc. Res., vol. 18, 1979, pp. 229-244.
- Nugent, L.J., and Jain, R.K., "Two-Compartmental Model for Plasma Pharmacokinetics in Individual Blood Vessels", J. Pharmacokin. Biopharm., vol. 12, 1984, pp. 270-274.
- Nugent, L.J., and Jain, R.K., "Plasma Pharmacokinetics and Interstitial Diffusion of Macromolecules in a Capillary Bed", Am. J. Physiol., vol. 246, 1984, pp. H129-H137.
- Paaske, W.P., "Microvascular Exchange of Albumin", Microvasc. Res., vol. 25, 1982, pp. 101-107.
- Pappenheimer, J.R., Renkin, E.M., and Borrero, L.M., "Filtration, Diffusion and Molecular Sieving Through Peripheral Capillary Membranes. A Contribution to the Pore Theory of Capillary Permeability", Am. J. Physiol., vol. 167, 1951, pp. 13-46.
- Parving, H.-H., Nielsen, S.L., and Lassen, N.A., "Increased Transcapillary Escape Rate of Albumin, IgG, and IgM During Angiotensin-ii Induced Hypertension in Man", Scand. J. Clin. Lab. Invest., vol. 34, 1974, pp. 111-118.
- Perry, M.A., Crook, W.J., and Granger, D.N., "Permeability of Gastric Capillaries to Small and Large Molecules", Am. J. Physiol., vol. 241, 1981, pp. G478-G486.
- Renkin, E.M., "Transport of Large Molecules Across Capillary Walls", Physiologist, vol. 7, 1964, pp. 13-28.

- Renkin, E.M., Watson, P.D., Sloop, C.H., Joyner, W.L., and Curry, F.E., "Transport Pathways for Fluid and Large Molecules in Microvascular Endothelium of the Dog's Paw", Microvasc. Res., vol. 14, 1977, pp. 205-214.
- Richardson, P.D.I., Granger, D.N., Mailman, D., and Kvietys, P.R., "Permeability Characteristics of Colonic Capillaries", Am. J. Physiol., vol. 239, 1980, pp. G300-G305.
- Ritter, A.B., Braun, W., Stein, A., and Durán, W.N., "Visualisation of the coronary Microcirculation Using Digital Image Processing", Comput. Biol. Med., vol. 15, 1985, pp. 361-374
- Rutili, G., Granger, D.N., Taylor, A.E., Parker, J.C., and Mortillaro, N.A., "Analysis of Lymphatic Protein Data. IV. Comparison of the different Methods used to Estimate Reflection Coefficient and Permeability-Surface Area Products", Microvasc. Res., vol. 23, 1982, pp. 346-360.360.
- Rutili, G., and Hagander, P., "Transport of Macromolecules in Subcutaneous Tissue", Acta Univ. Ups. (Suppl), vol. 306, 1979, pp. 1-51 .
- Sejrsen, P., Paaske, W.P., and Henriksen, O., "Capillary Permeability of I-Albumin in Skeletal Muscle", Microvasc. Res., vol. 29, 1985, pp. 265-281.
- Taylor, A.E., and Granger, D.N., "Exchange of Macromolecules Across the Circulation", Handbook of Physiology, vol. 4, E.M. Renkin and C.C. Michel (eds), Bethesda: Amer. Physiol. Soc., 1983.
- Taylor, A.E., Perry, M.A., Shin, D.W., Granger, D.N., and Parker, J.C., "Calculation of the Effective Pore Radii in Dog Hind Paw Capillaries Using Lymph Endogenous Proteins", Microvasc. Res., vol. 23, 1982, pp. 276-290.

Vargas, F., and Johnson, J.A., "An Estimate of Reflection Coefficient from Rabbit Heart Capillaries", J. Gen. Physiol., vol. 47, 1964, pp. 667-677.

Yablonski, M.E., and Lifson, N., "Mechanism of Production of Intestinal Secretion by Elevated Venous Pressure", J. Clin. Invest., vol. 57, 1976, pp. 904-915.

Youlten, L.J.F., "Permeability to Human Serum Albumin (HSA) and Polyvinylpyrrolidone (PVP) of Skeletal Muscle (Rat Cremaster) Blood Vessel Walls", J. Physiol. (London), vol. 204, 1969, pp. 112-113.